Norwegian University
of Life Sciences

Master's Thesis 2020 30 ECTS
Faculty of Chemistry, Biotechnology and Food Science

The effect of lignin in light-driven photobiocatalytic LPMO reactions

Camilla Fløien Angeltveit
Chemistry and biotechnology

Acknowledgments

The research for this thesis was completed at the Protein Engineering and Proteomics group at the Faculty of Chemistry, Biotechnology and Food Science at the Norwegian University of Life Sciences, with Professor Vincent G. H. Eijsink as a supervisor and Eirik Kommedal as a co-supervisor.

First and foremost, I would like to express my gratitude to my supervisor Professor Vincent G. H. Eijsink for giving me this opportunity. I really appreciate all your support, encouragement, and that you have used your valuable time to educate me. A particularly big thanks to Eirik Kommedal for your practical advice in the lab, and for being so dedicated and eager to help me explore this exciting research field.

I would also like to thank the rest of the PEP groups and fellow master students for a very good professional and social environment. Finally, a special thanks to my friends, family, and boyfriend for believing in me and giving me the determination to strive towards my goals and to fulfill this five-year-long education.

Thanks for five rich, memorable, educational, and fun years here at NMBU.

Ås, May 2020

Camilla Fløien Angeltveit

Abstract

Our understanding of enzymatic hydrolysis of recalcitrant polysaccharides was revolutionized when lytic polysaccharide monooxygenases (LPMOs) were discovered by Vaaje-Kolstad et al. in 2010. LPMOs are copper-dependent redox enzymes, which after a priming reduction of the copper ion, uses the co-substrate, H_2O_2, to hydroxylate glycosidic bonds. A characteristic solvent-exposed active site and a flat surface enable LPMOs to interact directly with crystalline surfaces. Previous studies have demonstrated that photobiocatalytic systems, using, i.e., chlorophyllin as a photosensitizer, can provide LPMOs with reducing equivalence and H_2O_2. Lignin has been shown to both function as a reductant and to produce H_2O_2 in light-driven reactions. The research described in this study aimed to investigate LPMOs activity in light-driven reactions using lignin as a photosensitizer. Various parameters, including lignin concentration, light intensity, enzyme concentration, and superoxide's role in the system, have been studied using the cellulose-active AA10C from *Streptomyces coelicolor* as model enzyme.

The results from this study show that lignin can promote *Sc*AA10C activity on Avicel, in the 1-10 g/L range. Light exposed reactions using a low lignin concentration show a 10-fold increase in activity compared to similar reactions performed in the absence of visible light. In contrast, the highest activity was observed in reactions with high concentrations of lignin performed in the dark. This can be explained by enzyme inactivation due to accumulation of H_2O_2, causing oxidative damage of *Sc*AA10C's catalytic site when combining high lignin concentration and light exposure. Adding low amounts of reductant led to minor differences in activity, suggesting that lignin provided *Sc*AA10C with reducing equivalents and co-substrate. On the other hand, increasing the concentration of lignin, AscA, or light intensity led to an increase in LPMO activity. Interestingly, the addition of SOD and Mn(II) both improved the generation of H_2O_2 from lignin. This confirms that superoxide formation occurs, and that the boost in LPMO activity comes from the accelerated H_2O_2 formation. Taken together, these results show that lignin can provide *Sc*AA10C, both with reducing power and H_2O_2 in aerobic conditions and that the production of reactive oxygen species must be carefully controlled to avoid enzyme inactivation.

The observation that visible light-exposed lignin increases the LPMO activity, points to lignin functioning as a photosensitizer. Light exposure leads to oxidation of lignin, which results in the reduction of molecular oxygen to superoxide. Superoxide act both as a reductant for the LPMO and as an intermediate in the generation of hydrogen peroxide, the co-substrate of LPMOs. By using lignin as a photosensitizer, reducing equivalents and co-substrate are produced *in situ,* and enable oxidative

cleavage of cellulose by LPMOs. Further work should focus on determining the limiting factor(s), investigate lignin modifications induced by light exposure, and include anaerobic control reactions.

Sammendrag

Vår forståelse av den enzymatiske nedbrytningen av polysakkarider ble revolusjonert i 2010, da Vaaje-Kolstad et al. oppdaget lytisk polysakkarid monooksygenaser (LPMOer). LPMOer er kobberavhengige redoksenzymer, som krever reduksjon av kobberatomet i det aktive setet for å bli aktivert, og bruker deretter kosubsratet H_2O_2 til å hydroksylere glykosidbinger. Et karakteristisk flatt substrateksponert bindingssete gjør LPMOene spesielt godt egent for interaksjoner med krystallinske overflater. I tidligere studier har det blitt vist at fotobiokatalytiske systemer kan bruke blant annet klorofyllin som et fotosensibiliserende stoff, for å både redusere og tilføre H_2O_2 til LPMOer. Lignin fungerer som et reduksjonsmiddel, men har også vist en evne til å produsere H_2O_2 i lysdrevne reaksjoner. Målet med forskningen beskrevet i dette studiet var å undersøke LPMO-aktivitet i lysdrevne reaksjoner ved bruk av lignin som et fotosensibiliserende stoff. Ulike parametere som ligninkonsentrasjon, lysintensitet og enzymkonsentrasjon, i tillegg til superoksidets rolle i systemet ble undersøkt i reaksjoner ved bruk av en celluloseaktiv AA10 LPMO fra *Streptomyces coelicolor*.

Resultatene fra dette studiet viste at tilstedeværelsen av mellom 1 og 10 g/L lignin kan fremme *Sc*AA10C sin nedbrytning av Avicel. Lyseksponerte reaksjoner med lav lignin konsentrasjon viste 10 ganger høyere aktivitet sammenlignet med like reaksjoner utført uten lyseksponering. Til tross for dette, ble den høyeste aktiviteten observert i reaksjonene med høy ligninkonsentrasjon uten lyseksponering. Dette kommer av at lyseksponering av reaksjoner med høy ligninkonsentrasjon fører til økt produksjon av H_2O_2 som kan gi oksidativ skade på *Sc*AA10C sitt katalytiske sete og inaktivere enzymet. Reaksjoner tilført lave mengder reduksjonsmiddel, AscA, førte ikke til noe nevneverdig endring i aktivitet, som tyder på at lignin selv kan redusere *Sc*AA10C. Derimot viste det seg at høye konsentrasjoner av AscA eller lignin, og høy lysintensitet førte til økt LPMO-aktivitet. Reaksjoner tilført SOD eller Mn(II) økte aktiviteten betraktelig under disse forholdene, som viser at superoksid ble dannet og videre omdannet til H_2O_2. Alt i alt, viser disse resultatene at lignin kan redusere og tilføre *Sc*AA10C H_2O_2 under aerobe forhold og at produksjonen av reaktive oksygenforbindelser må strengt kontrolleres for å unngå enzyminaktivering.

Observasjonene viser at lyseksponert lignin øker LPMO-aktiviteten betraktelig. Dette tyder på at lignin fungerer som et fotosensibiliserende stoff. Lyseksponering av lignin fører til elektronoverføring fra lignin til oksygen som danner superoksid. Superoksid vil både redusere LPMOene og fungere som intermediat i produksjonen av hydrogenperoksid, som er LPMO sitt kosubstrat. Dette viser at LPMOer kan utføre oksidativ nedbrytning av Avicel i lyseksponerte reaksjon med lignin som et fotosensibiliserende stoff. Videre arbeid burde undersøke begrensende faktor(er), studere strukturelle

modifiseringer av lignin som følge av lyseksponering, i tillegg til å utføre anaerobe kontrollreaksjoner for å avgjøre om dette kun er et aerobt fenomen.

Table of contents

Abbreviations

2-NAP	2-naphthol
A_{280}	Absorbance of ultraviolet light at 280 nanometers
AA	Auxiliary Activities
AscA	Ascorbic acid
Avicel	Microcrystalline cellulose
CAZy	Carbohydrate-active enzyme
CBM	Carbohydrate-binding module
CBM2	Family 2, carbohydrate-binding module
CBM33	Family 33, carbohydrate-binding module
CBP21	Chitin-binding protein
CelS2	*Sc*AA10C
Chl	Chlorophyllin
CV	Column volume
dH_2O	Milli-Q® Sterile Water
DTT	Dithiothreitol
E. coli	*Escherichia coli*
EDTA	Ethylenediaminetetraacetic acid
G	Guaiacyl
GH	Glycoside hydrolase
GH5	Family 5, glycoside hydrolase
GH6	Family 6, glycoside hydrolase
H	P-hydroxyl phenol
His-tag	Polyhistidine tag
HPAEC	High-Performance Anion-Exchange Chromatography
HRP	Horseradish peroxidase
IEX	Ion-Exchange Chromatography
IMAC	Immobilized Metal Ion Affinity Chromatography
kDa	Kilo Dalton
LDS	Lithium dodecyl sulfate
LPMO	Lytic polysaccharide monooxygenase

Mn-SOD	Manganese dependent superoxide dismutase
NaOAc	Sodium acetate, CH_3COONa
PAD	Pulsed Amperometric Detection
pI	Isoelectric point
ROS	Reactive oxygen species
S	Syringyl
Sc	*Streptomyces coelicolor*
LDS-PAGE	Lithium Dodecyl Sulfate - Polyacrylamide Gel Electrophoresis
SE	Steam-exploded
SEC	Size-Exclusion Chromatography
SOD	Superoxide dismutase
Tf	*Thermobifida fusca*
TGS	Tris-Glycine-SDS
tsH_2O	Trace select sterile water
w/v	Weight/Volume

1. Introduction

1.1. Lignocellulosic biomass

Lignocellulosic biomass is a sustainable source for production of green energy and fuel (Isikgor & Becer, 2015; Weng et al., 2008). Bioethanol is one of the most important types of biofuel consumed worldwide and is obtained by conversion of lignocellulosic biomass (Fatma et al., 2018). Earth's biomass represents approximately five gigatons of carbon (Bar-On et al., 2018), most of which are contained in lignocellulosic biomass (Isikgor & Becer, 2015). The term lignocellulosic biomass refers to plant dry matter, and the main components of lignocellulosic biomass are cellulose (40 - 50 %), hemicellulose (20 - 40 %), and lignin (20 - 30 %). Minor components include pectin, minerals, proteins, lipids, and soluble sugars. The composition of these main constituents makes up the complex matrix of plant cell walls (Pauly & Keegstra, 2008). Plant cell walls have developed a robust structure to resist degradation (Chundawat et al., 2011). This robustness makes the utilization of lignocellulosic biomass in the production of energy and fuel demanding (Isikgor & Becer, 2015).

1.1.1. Cellulose

Cellulose is the most abundant polysaccharide in lignocellulosic biomass, and because of its crystalline structure, it is highly resistant to depolymerization. Despite cellulose's recalcitrance, its homogeneity is an immense advantage, as depolymerization of glucose yields just one product, glucose. Cellulose is a linear polymer of β-1,4-linked D-glucose units. The repeating unit in cellulose is cellobiose, which contains two monomers that are rotated 180° relative to each other (**Figure 1**) (Horn et al., 2012; Imai & Sugiyama, 1998). The polysaccharide chains associate to form an insoluble material, including both crystalline and amorphous regions. Aggregation of parallel microfibril chains makes up the native crystalline cellulose structure (Imai & Sugiyama, 1998), strengthen by van der Waals interaction and intra- and intermolecular hydrogen bonds (**Figure 1**) (Horn et al., 2012). The breakdown of cellulose is particularly demanding since only the surface-exposed cellulose chains are available for degradation, and because of the strong interactions between polymer chains (Lee et al., 2014).

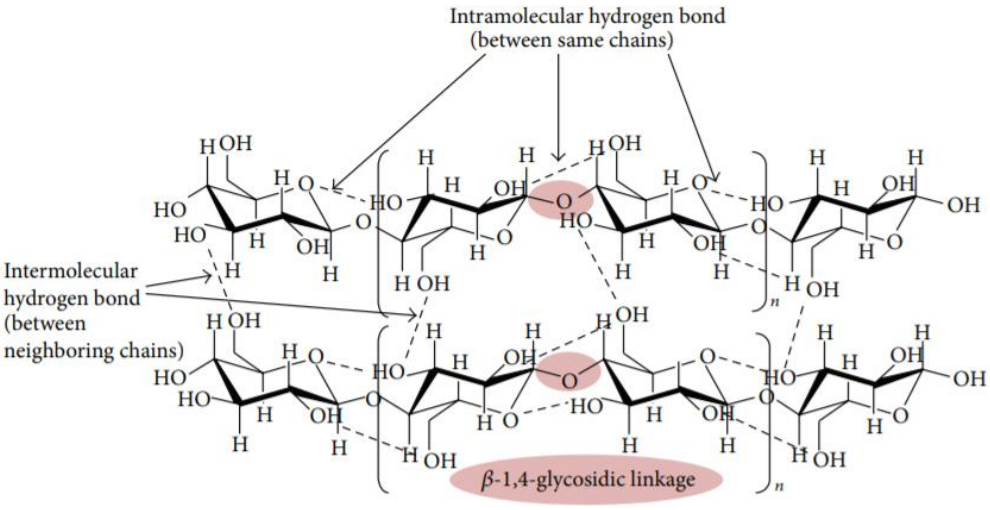

Figure 1. Chemical structure of cellulose. The figure shows two chains of D-glucose connected by β(1→4) glycosidic bonds. The crystalline cellulose structure is strengthened by hydrogen bonds and van der Waals interactions, both within single cellulose chains (intramolecular) and in between neighboring chains (intermolecular). The repeating unit in the cellulose polymer is cellobiose, as indicated. The figure was taken from (Lee et al., 2014).

1.1.2. Hemicellulose

The biological role of hemicellulose is to strengthen the cell wall, in part by interconnecting cellulose and lignin (Scheller & Ulvskov, 2010). Hemicellulose is a term used to describe multiple non-cellulosic polysaccharides in the plant cell wall. Hemicelluloses include xylans, xyloglucans, glucomannans, mannans, and β-(1→3,1→4)-glucans. Degradation of hemicelluloses generates a mix of different sugars (Horn et al., 2012), and is often more accessible than the degradation of cellulose. The strength of the cell walls is due to the high recalcitrance of some oligomeric structures, partly caused by acetylation patterns (Agger et al., 2010) and intricate branching patterns between hemicellulose, lignin, and cellulose (Silveira et al., 2013).

1.1.3. Lignin

Lignin is the richest aromatic biopolymer found on Earth. In plant cell walls, lignin confers structural rigidity and protection against chemical and biological attack (Lu et al., 2017). Lignin is a hydrophobic polymer with a complex chemical structure. The complex structure consists of cross-linked phenol polymers, so-called monolignols. The difference between the monolignols is their degree of methoxylation (**Figure 2**). Coniferyl alcohol, p-coumaryl alcohol, and sinapyl alcohol make up the basic

building blocks of lignin. These units are connected by ether or ester bonds and integrated into lignin in the form of guaiacyl (G), p-hydroxyl phenol (H), and syringyl (S) groups (**Figure 2**), respectively (Horn et al., 2012; Terashima & Fukushima, 1989). The abundance and composition of these monomers vary significantly between different lignin types. For example, lignin from softwood (e.g., Spruce) consists of primarily G units. In contrast, lignin from hardwood (e.g., Birch) consists of mainly G and S units, while grass lignin usually comprises all three units (Horn et al., 2012; Muraleedharan et al., 2018). Lignin contributes to plant cell wall recalcitrance and is considered a significant obstacle in the industrial processing of lignocellulosic biomass (Cesarino et al., 2012).

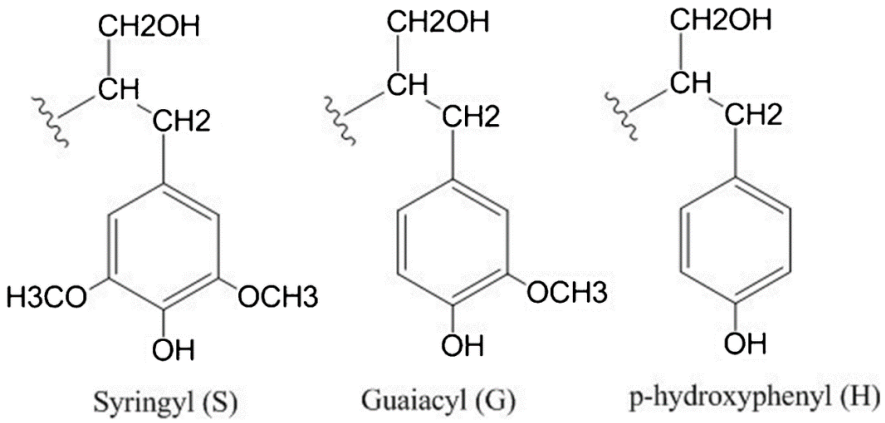

Figure 2. Structural model of the different lignin units. The figure shows the different lignin units, Syringyl (S), Guaiacyl (G), and p-hydroxyphenyl (H). The difference between the lignin units is their degree of methoxylation, with two, one or zero methoxyl-groups, for the S, G, and H units, respectively. The figure was taken from (Sameni et al., 2020).

1.2. Enzymatic degradation of lignocellulose

The main problems with the degradation of lignocellulosic biomass are the recalcitrance, heterogeneity, and inaccessibility of some of lignocellulosic biomass individual components (Horn et al., 2012). The breakdown of lignocellulosic biomass depends on a complex interplay among various proteins, i.e., endo- and exo-acting enzymes (**Figure 3**). Cellulose degrading enzymes include endo-1,4-β-glucanases, which act randomly and cleave internal bonds of cellulose, and cellobiohydrolases (also called exo-1,4-β-glucanase), which cleave of cellobiose from reducing or non-reducing chain ends. The use of endo- and exo-1,4-β-glucanases result in the production of cellobiose and cello-oligomers, which can be further hydrolyzed to glucose by β-glucosidases (Bissaro et al., 2018; Chylenski et al., 2019; Horn et al., 2012). Non-cellulose degrading enzymes are also important contributors to lignocellulose degradation, these include for example, hemicellulases and swollenins. Hemicellulases breaks down various hemicelluloses, while swollenins loosen the plant cell wall structure to increase the accessibility

for other enzymes. Non-enzymatic reactions can also play a role in biomass turnover by hydroxyl radicals generated by Fenton chemistry. In the Fenton reaction, hydroxyl radicals are produced from hydrogen peroxide that reacts with reduced transition metals (i.e., Cu(I), Fe(II), Mn(II)) generated by small phenolic compounds (**Figure 3**) (Bissaro et al., 2018). The presence of these biomass-degrading enzymes differs between various microorganisms. Regardless of the microorganism and the type of biomass, a complex interplay between multiple enzymes is needed for the breakdown of lignocellulose (Bissaro et al., 2018).

Our understanding of enzymatic hydrolysis of recalcitrant polysaccharides was revolutionized when the LPMOs were discovered. LPMOs act on the surface of polysaccharides and cut directly in the crystalline structure (**Figure 3**) (Horn et al., 2012). Thus, the use of LPMOs improves the accessibility of recalcitrant polysaccharides for the classical hydrolytic enzymes (Chylenski et al., 2019). To accomplish this activity, LPMOs employ redox chemistry, with O_2 or H_2O_2 as co-substrate (see Section 1.3.3). LPMO action depends on an external reductant and is thus dependent on an interplay with other molecules or enzymes to receive the required reducing power and co-substrate (Bissaro et al., 2018). The use of LPMOs has opened opportunities for more efficient enzymatic processes that are essential for sustainable use of biomass (Bissaro et al., 2017), for example, in the production of energy and biofuel.

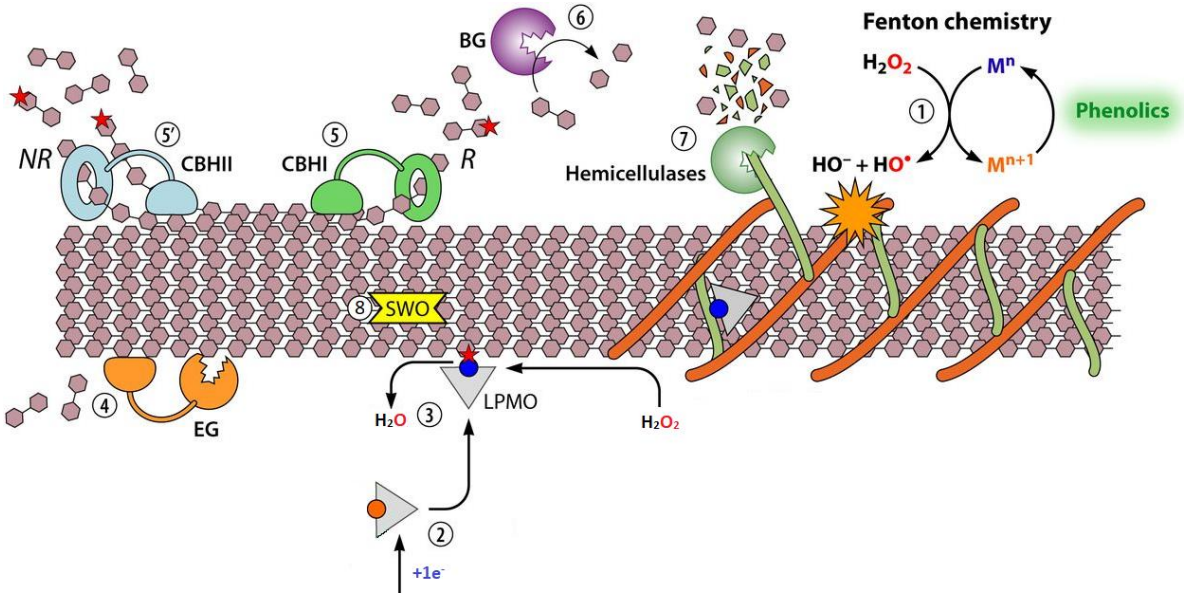

Figure 3. Different reactions that contribute to the breakdown of lignocellulosic biomass. The figure shows an overview of different reactions that may take place during the breakdown of lignocellulosic biomass. The number indicates the various processes: Nonenzymatic Fenton chemistry where H_2O_2 is converted into hydroxyl radicals **(1)**, reduction of the LPMO by various sources, like AscA **(2)**, LPMOs oxidizing cellulose or other polysaccharides with H_2O_2 as co-substrate **(3)**, endo-1,4-β-glucanases cleaving internal bonds of cellulose **(4)**, cellobiohydrolases cleaving off cellobiose, from the reducing (CBHI) **(5)** or reducing (CBHII) end **(5')**, conversion of cello-oligomers to glucose by β-glucosidases **(6)**, degradation of hemicellulose by hemicellulases **(7),** and loosening of the plant wall structure by swollenins **(8)**. This figure is an adapted version of a figure appearing in (Bissaro et al., 2018).

1.2.1. Classification of carbohydrate-active enzymes

The diversity of enzymes involved in the degradation, modification, or assembly of complex carbohydrates has been categorized in the Carbohydrate-Active Enzyme (CAZy) database since 1999, including enzymes from all domains of life. The classification creates families based on sequence, aiming to link the sequence to the 3D structure and specificity of the enzymes (Lombard et al., 2014). The original families in the CAZy database were polysaccharide lyases, glycosyltransferases, glycoside hydrolases (GHs), carbohydrate esterases, and carbohydrate-binding modules (CBMs) (Levasseur et al., 2013). CBMs are proteins without enzymatic activity and are often associated with carbohydrate-active enzymes such as GHs (Cantarel et al., 2009). After the discovery of LPMOs, the CAZy database was extended to include redox-active enzymes acting on lignocellulosic polysaccharides (some do also possess activity towards chitin), which are categorized as auxiliary activity (AA) families (Levasseur et al., 2013; Lombard et al., 2014). Today there are 16 AA families of which families AA9 - 11 and AA13 – 16 contains LPMOs (Bissaro et al., 2020; Henrissat et al., 2013).

Among the different carbohydrate-active enzymes, glycoside hydrolases are the most abundant (Berlemont & Martiny, 2016). GHs break down single polysaccharide and oligosaccharide chains, by hydrolytically cleaving glycosidic bonds, releasing metabolizable products (Berlemont & Martiny, 2016). Enzymes within GH families may have different substrate specificities. For example, Cel5A from *Thermobifida fusca* (*Tf*Cel5A) and Cel6A from *Thermobifida fusca* (*Tf*Cel6A) are cellulose specific glycoside hydrolases, belonging to family GH5 and GH6, respectively. These GHs break down cello oligosaccharides with chain lengths with a degree of polymerization of four or higher to cellobiose and/or cellotriose. Until the discovery of LPMOs, GHs were thought to be the main contributor to the enzymatic degradation of polysaccharides (Cragg et al., 2015; van den Brink & de Vries, 2011).

1.2.2. Redox enzymes involved in lignocellulose degradation

Redox enzymes catalyze reactions by electron transfer and play a crucial part in, for example, degradation of lignocellulose (Bissaro et al., 2018). Such enzymes are referred to as oxidoreductase (EC 1) and catalyze the exchange of electrons from a reductant (donor molecule) to an oxidant (acceptor molecule). Next to LPMOs (see below), oxidoreductases potentially involved in biomass turnover include laccase (EC 1.10.3.2), catalase (EC 1.11.1.6), and superoxide dismutase (SOD) (EC 1.15.1.1). Laccase is a multicopper oxidase using molecular oxygen as a co-substrate. The oxidative

power resulting from the conversion of O_2 to H_2O by laccase is used to oxidize phenolic compounds. These oxidized phenolic compounds can further function as an electron shuttle to oxidize other non-phenolic substrates (Bissaro et al., 2018; Eggert et al., 1996). Catalases catalyze the conversion of H_2O_2 into H_2O and O_2, and is often considered as a "housekeeping" enzyme that prevents accumulation of H_2O_2 (Peciulyte et al., 2018).

Superoxide dismutase scavenges superoxide, $O_2^{\bullet-}$, a reactive oxygen species (ROS), by converting $O_2^{\bullet-}$ into H_2O_2 ($2O_2^{\bullet-} + 2H^+ \rightarrow O_2 + H_2O_2$). There are three different families of SOD, Fe- and Mn-SOD, CuZn-SOD, and Ni-SOD. The difference between the SOD families is the type of transition metal in the active site (Perry et al., 2010; Ryan et al., 2010). Superoxide is a common intermediate in single-electron reduction of molecular oxygen, and has been shown to function both as a reductant and an oxidant (Fridovich, 1975). At physiological pH, the enzymatic conversion of $O_2^{\bullet-}$ to H_2O_2 by SOD happens 10^4-fold faster than the spontaneous dismutation reaction (Fridovich, 1975). In *Lactobacillus plantarum,* Mn(II) has been shown to function as a SOD analog by reaction with $O_2^{\bullet-}$ in a redox reaction to produce Mn(III) and H_2O_2 (Archibald, 1986). The oxidized Mn(III) can in turn react with H_2O_2, resulting in the production of O_2 and reduction of Mn(III) to Mn(II), which prevents accumulation of H_2O_2. Accumulation of ROS in cells can damage to cellular components, and possibly cell death. The presence of SOD (Nantapong et al., 2019) or Mn(II) (Archibald, 1986) are essential defense mechanisms against ROS for microorganisms.

1.3. Lytic polysaccharide monooxygenases

1.3.1. Discovery of LPMOs

Lytic polysaccharide monooxygenases (LPMOs) are copper-dependent redox enzymes found in all kingdoms of life (Voshol et al., 2017). LPMO's catalytic activity was first discovered by Vaaje-Kolstad and colleagues in 2010 (Vaaje-Kolstad et al., 2005; 2010), but their influence on chitin degradation was first described in 2005. Here, Vaaje-Kolstad et al. showed that a protein called chitin-binding protein (CBP21), at the time classified as a family 33 carbohydrate-binding module (CBM33), promoted the activity of classical chitinases during chitin degradation (Vaaje-Kolstad et al., 2005; 2010). In 2010, it was shown that CBP21, from the gram-negative bacterium *Serratia marcescens,* breaks down crystalline chitin by catalyzing oxidative cleavage of β-1,4-glycosidic bonds. The enzymatic activity of CBP21 was confirmed by isotope labeling of $^{18}O_2$ and $H_2{}^{18}O$. The groundbreaking 2010 study further showed that CBP21 requires molecular oxygen and electrons in form of a reductant to break down

crystalline chitin. Vaaje-Kolstad et al. noted that fungal proteins with structural similarities to CBM33, at the time classified as family 61 glycoside hydrolases (GH61), would be likely to oxidatively cleave cellulose (Vaaje-Kolstad et al., 2010). The demonstration of GH61's oxidative cleavage of cellulose came in 2011 and showed that it was dependent on the presence of a copper ion in the active site (Quinlan et al., 2011). In 2011, it was shown that CelS2, the AA10C from *Streptomyces coelicolor*, a CBM33 protein of bacterial origin, was able to catalyze oxidative cleavage of cellulose (Forsberg et al., 2011). The widespread occurrence of CBM33 proteins in various organisms shows the importance of these proteins for breaking down recalcitrant polysaccharides in Nature (Horn et al., 2012).

1.3.2. LPMO structure

There are significant sequence differences among the various LPMO families, but they are structurally similar, due to a pyramidal core structure and a surface-exposed active site. Typically, 8-10 β-sheets connected by multiple loops and helices make up the core structure, as a distorted β-sandwich fold (Vaaje-Kolstad et al., 2017). This structure is also found in the fibronectin type III-domains and immunoglobins (Aachmann et al., 2012; Beeson et al., 2015). The active site is a "histidine brace" consisting of two conserved histidine's coordinating a copper atom, in a T-shaped geometry (**Figure 4**) (Bissaro et al., 2018; Quinlan et al., 2011). The catalytic activity of LPMOs depends on reduction of the copper atom in the "histidine brace", i.e., from LPMO-Cu(II) to LPMO-Cu(I) (Bissaro et al., 2017; Horn et al., 2012). Some studies imply that a conserved glutamine or glutamate pointing towards the active site play an important role in LPMO catalysis (**Figure 4**) (Bissaro et al., 2020; Vaaje-Kolstad et al., 2017). The structural surface properties presumably control the substrate specificity of LPMOs. Some LPMOs possess additional modules that enhance their substrate affinity (Bissaro et al., 2018), as is the case for *Sc*AA10C. *Sc*AA10C is a strict cellulose oxidizing LPMO in the AA10 family, which has its catalytic (LPMO) domain connected to a cellulose-binding module (CBM2) by a flexible linker (Forsberg et al., 2011).

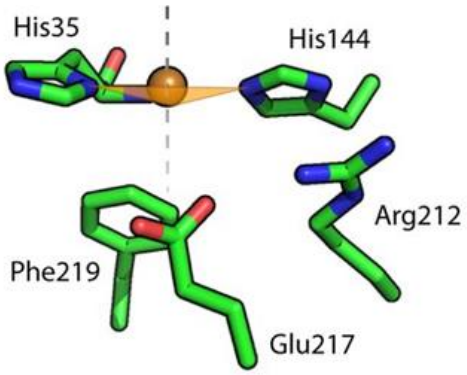

Figure 4. The catalytic site of *Sc*AA10C. The figure shows the "histidine brace" from *Sc*AA10C, which consists of two conserved histidines (His35 and His144), coordinating a copper atom (represented as an orange sphere). The gray dotted line shows the axial axis, and the orange triangle represents the equatorial plane. The figure also shows a surface-exposed glutamate (Glu217) pointing toward the catalytic copper, a more buried phenylalanine (Phe219), and an arginine (Arg212). The figure was taken from (Bissaro et al., 2018).

1.3.3. LPMO reaction mechanism

LPMOs perform oxidative cleavage of glycosidic bonds in polysaccharides, but whether they utilize molecular oxygen or hydrogen peroxide is still under debate. The original reaction mechanism proposed in the seminal study by Vaaje-Kolstad et al. (2010) was based on the monooxygenase paradigm ($R\text{-}H + O_2 + 2e^- + 2H^+ \rightarrow R\text{-}OH + H_2O$) (**Figure 5, top**). For every catalytic cycle, this mechanism requires one O_2 molecule and two externally delivered electrons (Bissaro et al., 2017). The origin of this paradigm was based in part on similarities between the first discovered LPMO and the copper-dependent particulate methane monooxygenase (Bissaro et al., 2018). Hydrogen peroxide, H_2O_2, as a possible co-substrate for the LPMO mechanism, was first described by Bissaro and colleagues in 2016, who presented the peroxygenase paradigm ($R\text{-}H + H_2O_2 \rightarrow R\text{-}OH + H_2O$) (**Figure 5, bottom**) (Bissaro et al., 2016a; 2016b). Hydrogen peroxide has the electrons, protons, and oxygen needed in the catalytic cycle. Thus, the reaction only requires a priming reduction of the copper, after which the LPMO can perform multiple turnovers until occasionally re-oxidation of the copper (Bissaro et al., 2017; 2018). The discovery that hydrogen peroxide can be used as co-substrate came in the wake of a study by Cannella and colleagues, who used a photoexcited pigment to drive LPMO reactions. Bissaro et al. hypothesized that the "light-effect" found by Cannella et al. was probably due to the formation of hydrogen peroxide, as was indeed confirmed by experiments very recently (Bissaro et al., 2020). In their 2016 & 2017 study, Bissaro and colleagues performed an isotope-labeling test, which showed that the oxygen atom that is introduced into the LPMO products came from isotope-labeled $H_2{}^{18}O_2$ and not from O_2, despite the presence of 10-fold more O_2 than H_2O_2 in the reaction (Bissaro et al., 2016b). Although there is still debate regarding the co-substrate of LPMOs, recent studies have shown that the

H_2O_2 driven LPMO reaction is much faster than the monooxygenase reaction with O_2 (Chylenski et al., 2019).

Regardless of the co-substrate being molecular oxygen or hydrogen peroxide, the LPMO reaction depends on the activated copper species in the active site. Both scenarios result in the hydroxylation of carbon in the scissile glycosidic bond in the polysaccharides. Upon hydroxylation, the glycosidic bonds become unstable and are spontaneously broken (Phillips et al., 2011), which may be at either C_1 or C_4, whereas some LPMOs produce a mix of C_1 and C_4 oxidized products (Bissaro et al., 2017; Horn et al., 2012). C_1 oxidation leads to the formation of a lactone, which spontaneously hydrolyzes to its aldonic acid form (**Figure 5, right**), while C_4 oxidation results in a ketoaldose that hydrolyzes to a gemdiol. In the past few years, several potential catalytic mechanisms responsible for the hydroxylation have been proposed. The hydroxylation is a result of a complex formation between hydrogen peroxide and reduced LPMO (LPMO-Cu(I)). Which complex is still uncertain, by recent studies suggest the LPMO-copper complex that is responsible for the hydrogen abstraction leading to subsequent hydroxylation of the polysaccharide is either Cu(II)-oxyl species, a Cu(III)=O, or a protonated oxyl (Bissaro et al., 2017; Chylenski et al., 2019).

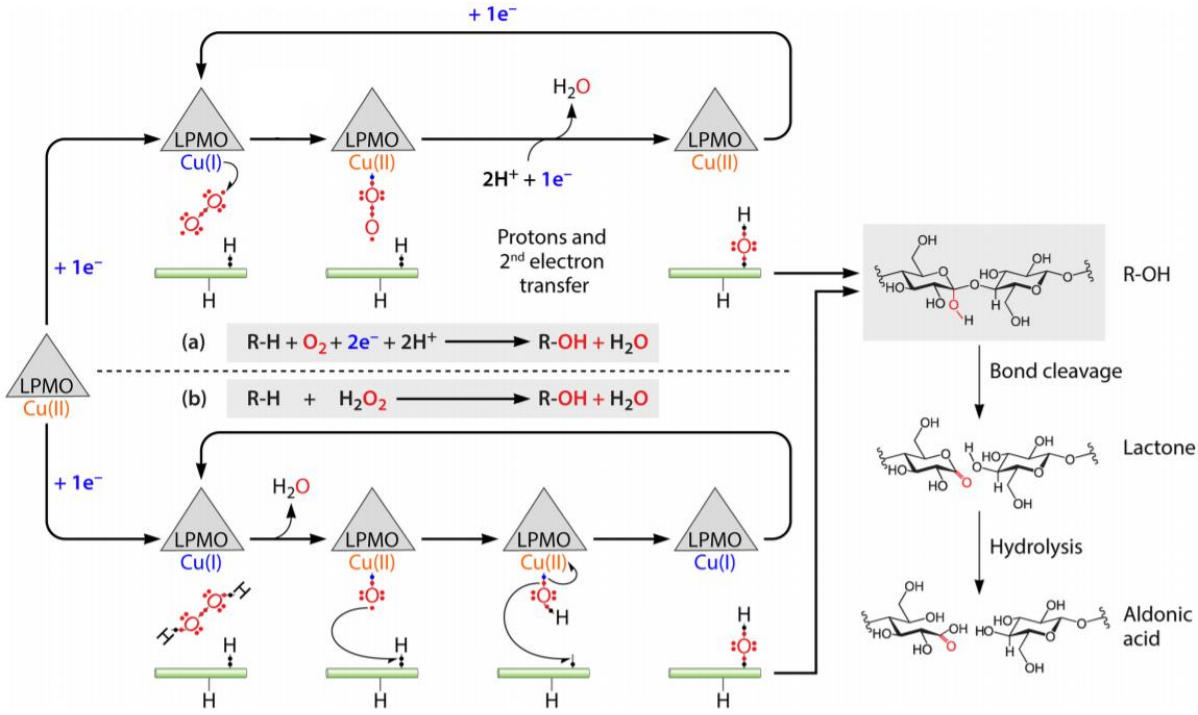

Figure 5. Cleavage of glycosidic bonds by an LPMO using a monooxygenase or peroxygenase mechanism. The figure shows the monooxygenase paradigm (R-H + O_2 + $2e^-$ + $2H^+$ → R-OH + H_2O) **(a, top)**, the peroxygenase paradigm (R-H + H_2O_2 → R-OH + H_2O) **(b, bottom)** and C_1 hydroxylation of cellulose **(right)**. Both mechanisms start with the reduction of LPMO-Cu(II) to LPMO-Cu(I). The monooxygenase mechanism uses O_2 as a co-substrate and requires two externally delivered electrons for every cycle. The peroxygenase mechanism uses H_2O_2 as co-substrate and can perform multiple catalytical cycles after a priming reduction. Both mechanism result in the hydroxylation of polysaccharides, in this example, at C_1, leading to the formation of lactone that hydrolyzes spontaneously to an aldonic acid. This figure is an adapted version of a figure appearing in (Bissaro et al., 2018).

Hydrogen peroxide appears to be the key to the successful depolymerization of polysaccharides by LPMOs. In contrast, studies have also shown that hydrogen peroxide can be detrimental to LPMOs, in particular in the absence of substrate or at too high concentrations (Bissaro et al., 2016b). LPMOs in the reduces state and in the absence of substrate can react with O_2 and produce H_2O_2 (Bissaro et al., 2016b) or other reactive oxygen species (Chylenski et al., 2019; Schmermund et al., 2019). The reduction of transition metals in the reaction solution can lead to Fenton chemistry producing hydroxyl radicals. These are very reactive and able to perform unspecific oxidization of various compounds (Bissaro et al., 2018). In addition to these side reactions producing ROS, which can lead to "general" oxidative damage, reactions of H_2O_2 itself with the reduced LPMO in the absence of substrate may lead to oxidative damage of the catalytic module, and inactivation of the LPMO (Bissaro et al., 2017). The addition or production of hydrogen peroxide must be strictly controlled to maintain effective hydrolysis of polysaccharides over time (Bissaro et al., 2020).

1.3.4. The interplay between LPMOs action and lignin

In a recent study, the ability of different lignin types to promote catalytic activity of three fungal LPMOs, namely *Mt*LPMO9 from *Termothelomyces thermophila* (previously called *Myceliophthora thermophila*), *Pc*LPMO9D from *Phanerochaete chrysosporium,* and *Nc*LPMO9C from *Neurospora crass*a, was tested (Muraleedharan et al., 2018). Based on the well-known fact that lignin alone is enough to drive LPMO reaction (Harris et al., 2010; Westereng et al., 2015), they investigated how the origin and pretreatment of the various lignin types influenced LPMO activity. The study revealed that a high amount of free aromatic hydroxy (-OH) side groups allows lignin to donate electrons more easily. The study also showed the importance of different pretreatments of lignin, as these cause structural and chemical modifications that influence lignin's possibility to donate electrons to LPMOs. Obviously, the amount of added lignin to the reaction is also an essential factor. Even if the same total amount of lignin is used, the potential for electron donation will still vary because various lignin types may contain different amounts of reactive groups. For example, softwood (e.g., Spruce) usually has more -OH groups than hardwood (e.g., Birch). There is still inadequate information on how the properties of lignin, including molecular weight, solubility, amount of hydroxyl groups, and the relative composition of different monolignols influence lignin reactivity towards LPMOs (Muraleedharan et al., 2018).

Importantly, lignin structures in various forms and oxidation states may not only engage in electron transfer to LPMOs, but may also react with O_2 to generate H_2O_2, or react with H_2O_2 to produce H_2O. This was illustrated in a recent study with laccases by Perna et al. (2019). Laccases are known to oxidize

lignin either directly or indirectly through a mediator (Mate & Alcalde, 2017), and it has been shown that the action of laccases on lignin induces production of H_2O_2 (Perna et al., 2019). The proposed mechanism for laccase induced H_2O_2 generation is shown in **Figure 6** and starts with the laccase oxidizing a phenolic hydroxyl in compound 1. The generated radical is stabilized by resonance (compound 2 and 3) and will, in the presence of molecular oxygen, react in the para position producing an unstable peroxyl intermediate (compound 4) that spontaneously produces an unstable quinone molecule (compound 5). The quinone molecule will tautomerize into a Cα-ketone (compound 6) and release a hydroperoxyl radical, $HOO^{\bullet}$ (**Figure 6, A**). The hydroperoxyl radical can either react with another hydroperoxyl radical to form hydrogen peroxide and oxygen, or abstract a hydrogen atom from another lignin molecule, producing H_2O_2 and a similar radical to the radical that was generated by the laccase (**Figure 6, B**). The proposed mechanism shows how G monolignol radicals may react with O_2 to produce H_2O_2 via $HOO^{\bullet}$, but it is still uncertain if other monolignols and types of lignin will react in the same way (Perna et al., 2019). In the presence of oxygen, lignin can produce hydrogen peroxide, as shown by Neumann & Machado (1989), who investigated the role of oxygen in photodegradation of lignin in solution. They found that hydroperoxides are formed in dark reactions as intermediates when low molecular weight soluble lignin is exposed to molecular oxygen. Thus, the generation of hydrogen peroxide from lignin is not dependent on the action of a laccase, although the presence of laccases will improve H_2O_2 generation, as shown by Perna et al. (2019).

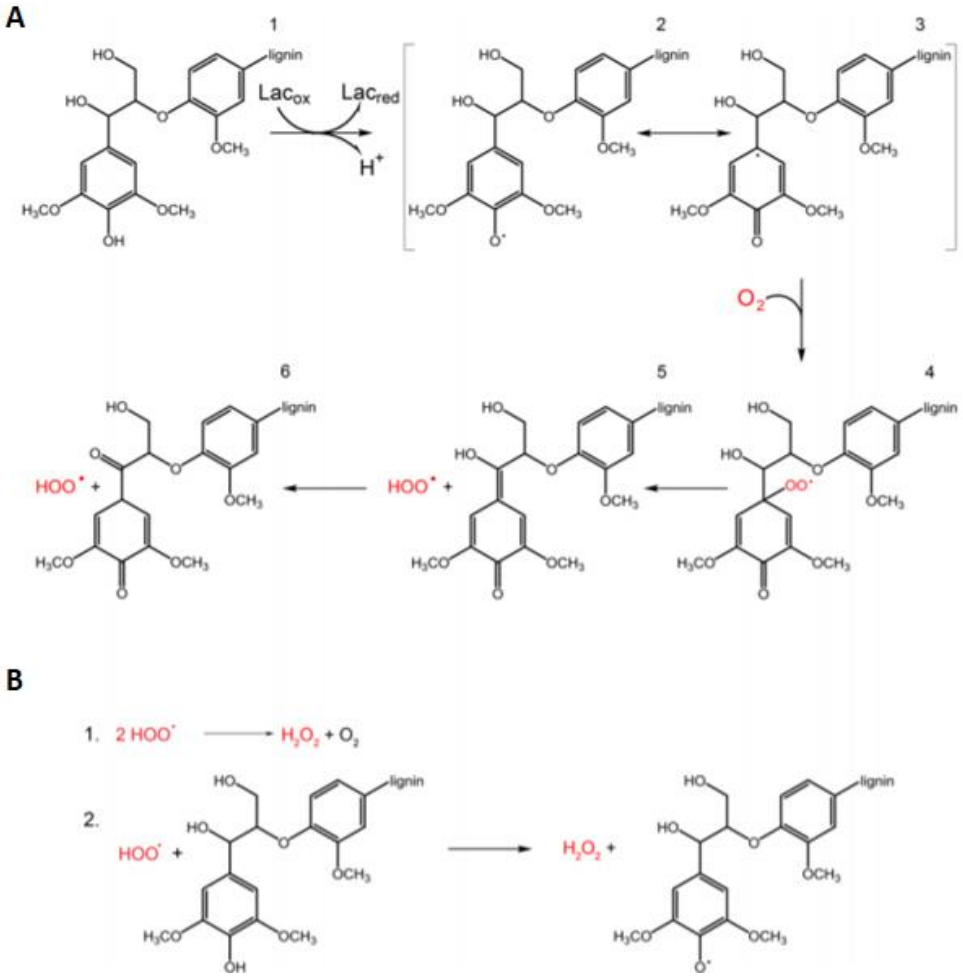

Figure 6. Possible mechanism for the production of H_2O_2 by lignin radicals via HOO•. Panel A shows the production of lignin radicals by laccase (1). The resonance structure of the resulting lignin radical (2, 3) and the subsequent reaction where the radical reacts with oxygen and produce an unstable peroxyl intermediate (4). This intermediate is further converted into a quinone molecule (5), which will tautomerize into a Cα-ketone and release a hydroperoxyl radical (HOO•) (6). Panel B shows that the hydroperoxyl radical will either react with another hydroperoxyl radical (1) or with another lignin molecule (2), and that both mechanisms result in the production of H_2O_2. The figure was taken from (Perna et al., 2019).

Kont and colleagues have demonstrated that a liquid fraction from hydrothermally pretreated wheat straw, sustains LPMO activity. They showed that the chitin-active *Sm*AA10A and the cellulose-active *Tr*AA9A could degrade chitin and cellulose, respectively, when mixed with a liquid fraction from hydrothermally pretreated wheat straw. This indicates that the liquid fraction contains enough reducing power to drive the LPMO reaction (Kont et al., 2019). Importantly, Kont et al. related this to the generation of H_2O_2, and they showed that H_2O_2 was generated independently of LPMOs. It was proposed that the presence of phenolic compounds in the liquid fraction is responsible for the production of H_2O_2. Also, that electron transfer from these compounds to the LPMO ensures priming reduction of the LPMO (**Figure 7**) (Kont et al., 2019). The study reported that hydrogen peroxide most likely is produced as an intermediate in the oxidation of the phenolic compounds, and also clearly

showed that H_2O_2 production was the liming factor for LPMO activity. Notably, Kont et al. pointed out that if H_2O_2 is an intermediate during oxidation of compounds in the liquid fraction, this would mean that H_2O_2 does not accumulate in the system, which may be favorable since too high concentrations can lead to inactivation of LPMOs. They proposed that in this system, the H_2O_2 concentration is maintained at a 'constant' level, which is determined by the production rates and LPMOs consumption rates. They also noted an initial boost in the LPMO reactions, which was due to the accumulation of H_2O_2 as a result of the pre-incubation of the liquid fraction. It should be noted that there, as in all LPMO reactions, also a possibility for re-oxidation of the LPMO by O_2, which will contribute to the production of H_2O_2 in the system (**Figure 7**). This study by Kont et al. provides another indication that biomass-derived components, most likely lignin-derived phenolic compounds, can drive LPMO reactions, by providing electrons, H_2O_2, or both.

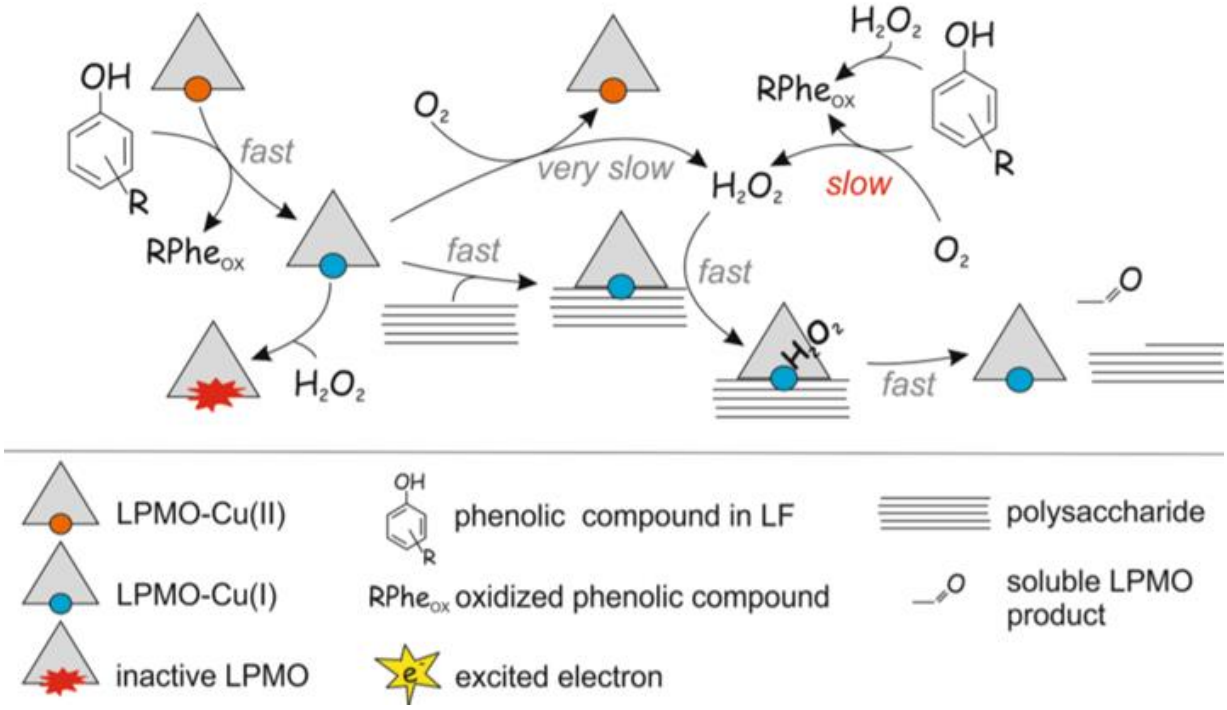

Figure 7. Possible mechanism for driving LPMO reactions by phenolic compounds. The figure display how LPMO activity on polysaccharides may be driven by the liquid fraction of hydrothermally pretreated wheat straw, most likely by the phenolic groups present in the fraction, as shown. The presence of phenolic compounds is responsible for the production of H_2O_2, but also the priming reduction of the LPMO. LPMOs can be re-oxidized by O_2, thus also produce H_2O_2. Other possible processes include the futile reaction of the reduced LPMO with H_2O_2, possibly leading to enzyme inactivation and reactions of phenols with H_2O_2; see text for details. The figure was taken from (Kont et al., 2019).

1.3.5. Photobiocatalysis

Photobiocatalysis is a recent field of research inspired by the conversion of light exposure to chemical energy in plant photosynthesis using chlorophyllin as a photosensitizer. The aim is to photochemically produce energy to perform chemical synthesis (Lee et al., 2018). In most photobiocatalytic reactions, the photosensitizer or photocatalyst is used to generated redox equivalents to promote the activity of redox-active enzymes (Maciá-Agulló et al., 2015). In response to light, a photosensitizer molecule will change its chemical configuration in a photochemical process (Lee et al., 2018), transferring excitation energy without being consumed in the reaction. While a photocatalyst usually is involved in the chemically conversion of the redox partner (Michelin & Hoffmann, 2018). The photosensitizer absorbs light to excite an electron from its highest occupied molecular orbital to the lowest unoccupied molecular orbital. Electron excitation leads to either direct electron transfer from the photosensitizer to the redox-enzyme or indirect electron transfer from the photosensitizer via a mediator or cofactor to the redox-enzyme (**Figure 8**). This activation provides the chemical energy necessary for enzymatic reaction to take place (Schmermund et al., 2019).

The use of photosensitizers depends on the presence of a sacrificial electron donor or acceptor to facilitate electron transfer. The sacrificial electron donor or acceptor enables the photosensitizer to return to its ground state in order to perform multiple rounds of electron transfer (**Figure 8**). Commonly used sacrificial electron donors include ethylenediaminetetraacetate (EDTA), ascorbic acid (AscA), or water (Schmermund et al., 2019). Molecular oxygen is an abundant and efficient electron acceptor in aerobic conditions where it can be reduced to superoxide by single electron transfer ($O_2 + e^- \rightarrow O_2^{\bullet -}$), or to hydrogen peroxide, by transfer of two electrons and two protons ($O_2 + 2e^- + 2H^+ \rightarrow H_2O_2$) (Maciá-Agulló et al., 2015). Proper interactions between a photosensitizer, a sacrificial electron donor and an electron acceptor are needed to provide and shuttle reducing power to the redox enzyme in photobiocatalytic reactions.

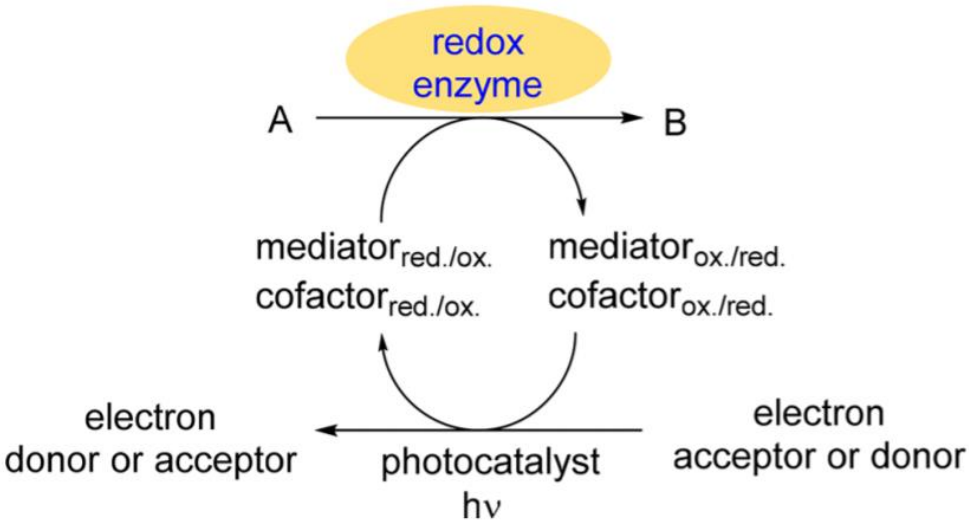

Figure 8. Photobiocatalytic generation of redox equivalents for a redox-enzyme by the use of a photocatalyst/ photosensitizer. The figure shows an illustration of a photobiocatalytic system, where irradiation of a photocatalyst results in the activation of a redox enzyme. The photocatalyst (or photosensitizer) absorbs light to excite an electron from its highest occupied molecular orbital to the lowest unoccupied molecular orbital. This excitation results in either direct electron transfer of the excited electron from the photocatalyst to the redox enzyme, or indirectly, via a mediator or a cofactor, using an electron transport mechanism. Both the direct and indirect mechanisms will provide the chemical energy needed for the enzymatic reaction to occur. The figure was taken from (Schmermund et al., 2019).

The first demonstration of using water as a sacrificial electron donor in photobiocatalytic reactions came in 2014 in a study by Mifsud and coworkers. Here the authors showed that by illuminating vanadium doped (V-TiO_2) or gold doped (Au-TiO_2) titanium dioxide with visible or UV-light, respectively, they could sustain the activity of Old Yellow Enzyme from *Thermus scotoductus* SA-01 using the cofactor flavin mononucleotide as a redox mediator. TiO_2 doped with vanadium showed a 2-fold increase in reaction rate compared to gold-doped TiO_2. Thus the activity depended on the type of photosensitizer (Mifsud et al., 2014). In 2016, it was demonstrated that light-driven water oxidation by V-TiO_2 could be used to sustain oxidative hydroxylation of polysaccharides by LPMOs (family AA9 and AA10) (Bissaro et al., 2016a). The catalytic activity of the LPMO towards Avicel was shown to be dependent on the light intensity, for example, reactions with V-TiO_2 in the dark no activity was observed (Bissaro et al., 2016a). The light-driven LPMO activity was lower compared to non-photobiocatalytic (standard) reactions using AscA as a source of reducing power, possibly because of the presence of free Cu(II) in solution which can react with AscA and then O_2 to produce H_2O_2 (Bissaro et al., 2020). Still, these studies confirmed that water could be used as a sacrificial electron donor for different photobiocatalytic reactions.

In 2020, Bissaro and colleagues revisited the V-TiO_2 photobiocatalytic system to investigate the possible role of reactive oxygen species, in light of the discovery from 2016, that LPMOs prefer

hydrogen peroxide over molecular oxygen. To determine the role of hydrogen peroxide, they performed experiments in the presence of horseradish peroxidase (HRP), which will compete for H_2O_2. They showed that increasing HRP concentrations resulted in growing inhibition for light-driven LPMO activity. In their study from 2016, they concluded that the LPMOs were reduced directly on the surface of the V-TiO_2 particles. Since then, it has been shown that superoxide can reduce LPMOs (Bissaro et al., 2017). Therefore, experiments with SOD were performed to investigate the role of superoxide, but the results did not reveal an effect of SOD on LPMO activity in these conditions.

In a breakthrough study published in 2016, Cannella et al. exposed a combination of plant pigments and AscA to visible light and reported a 100-fold increase in LPMO activity relative to commonly reported LPMO catalytic rates. The authors showed that pigments (thylakoids or chlorophyllin (Chl)), in combination with AscA, would when exposed to visible light, dramatically improved the catalytic activity of an AA9 LPMO on both Avicel and phosphoric acid swollen cellulose. They hypothesized that the increase in activity was due to the involvement of high energy electron transfer from photoexcited pigments. Möllers et al. investigated the same Chl/light system, aiming to uncover the role of ROS by using coupled enzymatic assays with catalase or superoxide dismutase to remove H_2O_2 or $O_2^{\bullet-}$, respectively. Their study, based on single time-point measurements of product levels, did not show any effect of these enzymes, leading Möllers et al. to conclude that ROS do not play a role in light-driven LPMO reactions. However, the recent study by Bissaro and coworkers, based on studying progress curves rather than single time-points, showed that $O_2^{\bullet-}$ and H_2O_2 are keys to controlling LPMO activity in the Chl/light system. The study also showed that there is no need for an external reductant such as AscA to promote LPMO activity. Further, they showed that certain combinations of Chl/light and AscA yielded high initial rates, but rapidly inactivated the enzyme because of hydrogen peroxide accumulated in the system (Bissaro et al., 2020).

Lignin has been shown to function as a multiple electron donor in the Chl/light system (Cannella et al., 2016), as would be expected based on the lignin-LPMO interaction studies described above. Interestingly, recent studies showed that lignin not only functions as a reductant (Möllers et al., 2017; Müller et al., 2018; Peciulyte et al., 2018) but also as a photocatalyst that can reduce O_2 and produce H_2O_2 (Miglbauer et al., 2020). Lignin has been shown to produce H_2O_2 upon irradiation, either coupled with autooxidation of lignin or oxidation of sacrificial electron donors in the solution. Miglbauer et al. (2020) showed that the addition of electron donors increases the hydrogen peroxide yield, indicating that oxidation of electron donors by irradiation, competes with autooxidation of lignin and resulting in bleaching of the lignin. The light-sensitivity of lignin is well known and has been described as a photo-yellowing process that involves the oxidation of free phenolic groups and hydroquinones (Paulsson & Parkås, 2012). The visible observation of lignin bleaching over time indicates that lignin undergoes

chemical modifications when exposed to light. The recent study by Miglbauer et al. (2020), showing that lignosulfonate exposed to visible blue light produces H_2O_2, most likely via single-electron reduction of oxygen to superoxide indicates that light-exposed lignin can provide LPMOs with reducing equivalents and co-substrate similar to what has been shown for the Chl/light system.

1.4. Aim of the study

The study aimed to investigate how exposure to visible light influences the capability of lignin to support the activity of an AA10 from *Streptomyces coelicolor*, *Sc*AA10C, by providing both reducing equivalents and hydrogen peroxide, or one of them.

The first step towards understanding the influence of visible light-exposed lignin on LPMO activity was to perform assays with varying amounts of lignin in the presence and absence of light. The same experiments were carried out in the presence of priming amounts of a reductant, AscA, to check if starting the reactions with the LPMO in its active state would lead to either different kinetics and/or product levels. The influence of different AscA concentrations on light-driven LPMO activity was also investigated to assess potential limitations due to lacking reducing power. To further characterize this photobiocatalytic system, reactions aimed at evaluating the effects of LPMO concentration, light intensity, and lignin origin were performed.

The second part of this work concerned the role of reactive oxygen species. Previous work on the same model LPMO in another photobiocatalytic system has shown that superoxide, $O_2^{\bullet-}$, is an important intermediate. Superoxide can act as a reducing agent for LPMOs, and it can generate the preferred co-substrate of LPMOs, hydrogen peroxide, by a disproportionation reaction. The hydrogen peroxide generation must be strictly controlled in order to avoid the inactivation of the LPMO (Bissaro et al., 2020). To probe the role of superoxide in this system, the effect of adding superoxide dismutase, a superoxide scavenging enzyme, was investigated.

2. Materials

2.1. Laboratory equipment

Table 1. Overview of equipment used in this thesis, including specifications and suppliers

Equipment	Specification	Supplier
Automatic pipettes		Thermo scientific
Balance	Quintix® Lab Balance	VWR
	Entis	VWR
Centrifuge	Heraeus™ Pico™ 21 Microcentrifuge	Thermo scientific
	Heraeus™ Multifuge™ X1 Centrifuge	Thermo scientific
	Avanti™ J-25 High-Performance Centrifuge	Beckman Coulter
Centrifuge rotors	JA-10	Beckman Coulter
	JA-25.50	Beckman Coulter
Columns	PD MidiTrap™, with Sephadex G-25 resin (3.5 mL)	GE Healthcare
	HiLoad™ 16/600 Superdex™ 75 prep grade (120 mL)	GE Healthcare
	HiTrap® DEAE Sepharose FF (5 mL)	GE Healthcare
	HiTrap® IMAC Fast Flow (5 mL)	Thermo scientific
	Dionex™ CarboPac™ PA200	
Eppendorf tubes	1.5 & 2 mL	Sigma-Aldrich
Falcon tubes	15 & 50 mL	Greiner bio one
Filter plate	96-well, 0.45 µm filter	Millipore
Filters bottle tops	0.2 & 0.45 µm	VWR
Fraction collector	Fraction collector F9-R	GE Healthcare
	Frac-920	GE Healthcare
Fume hood	Telstar AV-100	Telstar
Gel electrophoresis equipment	Mini-Protean® Tetra Cell	BioRad
	Mini-Protean® Tetra Electrode Assembly	BioRad
	PowerPac 3000 power supply	BioRad
	Gel Doc™ EZ Imager	BioRad
	Stain-Free Sample Tray	BioRad
	Mini-Protean® TGX Stain-Free™ Precast Gels	BioRad
Gold electrode	Dionex™ gold disposable electrode	Thermo Scientific
Heating block		Thermo Scientific
HPLC	Dionex™ ICS-5000 system with PAD detection	Thermo Scientific
ICS snap ring cap	11 mm	VWR
ICS snap ring micro vial	0.3 mL	VWR
Incubator	37°C	Termaks
LightningCure Spotlight source LC8	Model L9588, equipped with a L9588-03 filter, λ = 400 - 700 nm	Hamamatsu

Magnetic stirrer	IKA RCT classic	Sigma Aldrich
Microfluidizer	LM20 Digital Microfluidizer®	Microfluidics
Microtiter plate	96-well	VWR
Mini star spinner		VWR
Pasteurpipettes	1 mL	VWR
pH benchtop meter	913 Metrohm	Metrohm
Pipette tips		VWR
Reacti-Vial™	1 mL	Thermo Scientific
Serological pipette	10 mL	Sarstedt
Sonicator bath	Branson 3510DTH	Sigma-Aldrich
Spectrophotometer	BioPhotometer® D30	Eppendorf
Syringe filters	0.2 & 0.45 µm	Sarstedt
Syringes	2 & 5 mL	BD Emerald
	20 & 50 mL	BD Plastipak
Thermomixer		Eppendorf
Ultrafiltration tube	Amicon® Ultra-15 Centrifugal Filters, molecular mass cut-off of 10 kDa	Sigma-Aldrich
Uvettes	1x1 cm	Eppendorf
Vacuum Manifold	MultiScreen^{HTS}	Millipore
Vacuum Pump		Millipore
Vortex		Sigma-Aldrich
Water bath		VWR

2.2. Chemicals

Table 2. Overview of chemicals used in this thesis, including formulas and suppliers

Chemical	Formula	Supplier
Bacto™ Tryptone		Thermo Scientific
Bacto™ Yeast Extract		Thermo Scientific
Bis-Tris	$C_8H_{19}NO_5$	VWR
Copper sulfate	$Cu(II)SO_4$	VWR
Disodium phosphate	Na_2HPO_4	Sigma-Aldrich
Ethanol	EtOH	VWR
Ethylenediaminetetraacetic acid (EDTA)	$C_{10}H_{16}N_2O_8$	Merck
Hydrochloric acid, 37 %	HCl	VWR
Hydrogen peroxide	H_2O_2	Merck
Imidazole	$C_3H_4N_2$	PanReac AppliChem
L-Ascorbic acid	$C_6H_8O_6$	Sigma-Aldrich
Magnesium chloride	$MgCl_2$	Sigma-Aldrich
Manganese sulfate	$Mn(II)SO_4$	Sigma-Aldrich

Milli-Q® Sterile Water	dH_2O	MilliQ
NuPAGE™ LDS Sample Buffer (4X)		Thermo Scientific
NuPAGE™ Sample Reducing Agent (10X)		Thermo Scientific
Sodium acetate (NaOAc)	CH_3COONa	Sigma-Aldrich
Sodium chloride	NaCl	VWR
Sodium hydroxide, 1 M	NaOH	Merck
Sodium hydroxide, 50 % (w/v)	NaOH	Sigma-Aldrich
Sodium phosphate	NaH_2PO_4	Sigma-Aldrich
Sucrose	$C_{12}H_{22}O_{11}$	VWR
TraceSELECT™ H_2O	tsH_2O	Honeywell
Tris	$NH_2C(CH_2OH)_3$	Sigma-Aldrich
Tris-Glycine-SDS (TGS) buffer (10X)		Sigma-Aldrich
Tris-hydrochloride (Tris-HCl)	$NH_2C(CH_2OH)_3 \cdot HCl$	Sigma-Aldrich

2.3. Proteins and enzymes

Table 3. Overview of proteins and enzymes, including specifications and suppliers

Proteins and enzymes	Specification	Supplier
Benchmark ladder	BenchMark™ Protein Ladder	Thermo scientific
*Sc*AA10C		Self-made (see Sections 3.1 & 3.2)
SOD	From *Escherichia coli,* contains manganese (Mn-SOD)	Sigma-Aldrich
*Tf*Cel5A		Self-made (a kind gift of Dr. Zarah Forsberg)
*Tf*Cel6A		Self-made (see Section 3.3.)

2.4. Substrates and standards

Table 4. Overview of substrates and standards, including specifications and suppliers

Substrates and standards	Specification	Supplier
Avicel		Sigma-Aldrich
Cellobionic acid (GlcGlc1A)	$C_{12}H_{22}O_{12}$	Self-made (see Section 3.7.1)
Cellotrionic acid (Glc_2Glc1A)	$C_{18}H_{32}O_{17}$	Self-made (see Section 3.7.1)
Cellotriose, cellotetraose, cellopentaose (Glc_3 - Glc_5)	$C_{18}H_{32}O_{16}$, $C_{24}H_{42}O_{21}$, $C_{30}H_{52}O_{26}$	Megazyme
Glucose and cellobiose (Glc_1 & Glc_2)	$C_6H_{12}O_6$, $C_{12}H_{22}O_{11}$	Sigma-Aldrich

Lignin	Kraft, alkali	Sigma-Aldrich
Lignin, Birch-wood	Steam-exploded at 210°C	Self-Made (the Bioprocess Technology and Biorefining group at NMBU, described by Mulat et al. (2018))
Lignin, Spruce-wood	Steam-exploded at 210°C	Self-Made (the Bioprocess Technology and Biorefining group at NMBU)
Lignin, Spruce-wood	Impregnated with 2-naphthol & steam-exploded at 210°C	Self-Made (the Bioprocess Technology and Biorefining group at NMBU)
Lignin, Spruce-wood	Steam-exploded at 220°C	Self-Made (the Bioprocess Technology and Biorefining group at NMBU)
Lignin, Spruce-wood	Impregnated with 2-naphthol & steam-exploded at 220°C	Self-Made (the Bioprocess Technology and Biorefining group at NMBU)

2.5. Bacterial strains and antibiotics

Table 5. Overview of bacterial strains and antibiotics, including specifications and suppliers

Bacterial strains and antibiotics	Supplier
Ampicillin stock solution, 100 mg/mL	Sigma-Aldrich
E. coli One Shot® BL21 Star™ (DE3), containing the expression plasmid pRSET-B_CelS2, coding for *Sc*AA10C.	Self-made (Forsberg et al., 2014)

2.6. Cultivation medium

Lysogeny broth medium

- 10 g Bacto™ Tryptone
- 5 g Bacto™ Yeast Extract
- 10 g NaCl
- dH_2O

10 g Bacto™ Tryptone, 5 g Bacto™ Yeast Extract, and 10 g NaCl were dissolved in 800 mL dH_2O. The pH was modified to 7.0 with 1 M NaOH, and the total volume was adjusted to approximately 1 L in a blue cap bottle, before autoclaving at 121°C for 20 min. The sterilized medium was stored at room temperature.

2.7. Buffers and other solutions

2.7.1. Buffers for Ion-Exchange Chromatography

Binding buffer: 50 mM Tris-HCl, pH 7.5

- 6.06 g Tris-HCl
- dH_2O

Elution buffer: 50 mM Tris-HCl with 1 M NaCl, pH 7.5

- 6.06 g Tris-HCl
- 58.55 g NaCl
- dH_2O

6.06 g Tris-HCl was dissolved in approximately 800 mL dH_2O to make the binding buffer. 37 % HCl was used to adjust the pH to 7.5, and the final volume was adjusted with dH_2O in a 1 L volumetric flask. To prepare the elution buffer an equal amount of Tris-HCl and 58.55 g NaCl were dissolved in approximately 800 mL dH_2O, and the pH and total volume were adjusted in the same way as above. Both solutions were filtered through a 0.2 µm PES membrane using a vacuum filtration system and stored at room temperature.

2.7.2. Buffer for Size-Exclusion Chromatography

Running buffer: 50 mM Tris-HCl with 150 mM NaCl, pH 7.5

- 6.06 g Tris-HCl
- 8.77 g NaCl
- dH_2O

6.06 g Tris-HCl and 8.77 g NaCl were dissolved in approximately 800 mL dH_2O. The pH was adjusted to 7.5 by adding 37 % HCl, and the final volume was adjusted with dH_2O to 1 L in a volumetric flask. The solution was filtered through a 0.45 µm PES membrane using a vacuum filtration system and stored at room temperature.

2.7.3. Buffers for Immobilized Metal Ion Affinity Chromatography

Binding buffer: 50 mM Tris-HCl with 500 mM NaCl and 5 mM imidazole, pH 8.0

- 6.06 g Tris-HCl
- 29.22 g NaCl
- 0.34 g imidazole
- dH_2O

Elution buffer: 50 mM Tris-HCl with 500 mM NaCl and 500 mM imidazole, pH 8.0

- 6.06 g Tris-HCl
- 29.22 g NaCl
- 34.04 g imidazole
- dH_2O

To make binding buffer, 6.06 g Tris-HCl, 29.22 g NaCl, and 0.34 g imidazole were dissolved in approximately 800 mL dH_2O. An equal amount of Tris-HCl and NaCl, together with 34.04 g imidazole, was dissolved in approximately 800 mL dH_2O to make elution buffer. The pH was adjusted to 8.0 with 37 % HCl, for both buffers, and the volumes were adjusted to 1 L, before both solutions were filtered through a 0.45 µm PES membrane using a vacuum filtration system and stored at room temperature.

2.7.4. Eluents for High-Performance Anion-Exchange Chromatography with Pulsed Amperometric Detection

Eluent A: 0.1 M NaOH

- 10.4 mL 50 % (w/v) NaOH
- dH_2O

Eluent B: 0.1 M NaOH with 1 M NaOAc

- 82.03 g NaOAc (anhydrous)
- 5.2 mL 50 % (w/v) NaOH
- dH_2O

Eluent C: dH_2O

- dH_2O

To make eluents A and C, 2 L dH_2O measured with a volumetric flask was poured into two separate ICS eluent bottles. 82.03 g NaOAc was dissolved in dH_2O in a 1 L volumetric flask and filtered through a 0.2 µm PES membrane using a vacuum filtration system, to make eluent B. All eluents were degassed for 20 minutes. After degassing, 10.4 mL and 5.2 mL of 50 % (w/v) NaOH was added to flasks A and B, respectively, and mixed well, before all eluents were placed under N_2 gas.

2.7.5. Other buffers and solutions

Table 6. Overview of other buffers and solutions used in this study, including reagents, preparation, and total volume

Buffers and solutions	Reagents/preparation	Total volume
Ascorbic acid, pH 2.5, 100 mM	88.9 mg L-Ascorbic acid 5.045 mL tsH_2O pH 2.5 Filtered through a 0.2 µm PES syringe filter Stored in 50 µL portions at -20°C covered in aluminum foil	5.045 mL
Avicel solution, 50 g/L	2.5 g Avicel dH_2O Stored at 4°C	50 mL
Bis-Tris buffer, pH 6.2 (pH 6.0 at 37°C), 0.5 M	52.3 g Bis-Tris dH_2O pH was adjusted with 37 % HCl Filtered through a 0.45 µm PES membrane	500 mL
$Cu(II)SO_4$, 1 M, 10 M and 15 mM	16 g $Cu(II)SO_4$ tsH_2O pH 2.5 Diluted as appropriate in tsH_2O pH 2.5	10 mL
EDTA solution, pH 8.0, 0.5 M	9.3 g EDTA dH_2O pH was adjusted with 1 M NaOH Filtered through a 0.45 µm PES membrane	50 mL
$MgCl_2$, 0.5 M and 10 mM	5.1 g $MgCl_2$ dH_2O Diluted to 10 mM in dH_2O	50 mL

$Mn(II)SO_4$, 100 mM	151 mg $Mn(II)SO_4$ tsH_2O pH 2.5	10 mL
Na_2HPO_4 solution, 0.5 M	17.8 g Na_2HPO_4 dH_2O Filtered through a 0.45 µm PES membrane	250 mL
NaH_2PO_4 solution, 0.5 M	15 g NaH_2PO_4 dH_2O Filtered through a 0.45 µm PES membrane	250 mL
Sodium phosphate buffer, pH 7.0, 0.5 M and 50 mM	Na_2HPO_4 solution, 0.5 M NaH_2PO_4 solution, 0.5 M Solutions mixed until pH 7.0 Diluted to 50 mM in dH_2O	100 mL
Spheroplast buffer	17.1 g Sucrose 10 mL Tris-HCl buffer, pH 8.0, 20 mM 0.1 mL EDTA solution, pH 8.0, 0.5 M dH_2O Stored at 4°C	100 mL
Tris-HCl buffer, pH 8.0 and 7.5, 1 M, 0.5 M and 20 mM	121.14 g Tris-HCl dH_2O pH was adjusted with 37 % HCl Filtered through a 0.45 µm PES membrane Diluted as appropriate in dH_2O	1 L
tsH_2O, pH 2.5	100 mL tsH_2O pH was adjusted with one drop of 37 % HCl	100 mL

2.8. Software and online resources

Table 7. Overview of software and online resources

Software and online resources	Specifications
Chromeleon® 7 Chromatography Data system software	Thermo Scientific
ExPASy ProtParam	https://web.expasy.org/protparam/
Liverpool	https://www.liverpool.ac.uk/pfg/Research/Tools/BuffferCalc/Buffer.html
Protein data bank (PDB) database	https://www.rcsb.org/
Unicorn™ 6.4 Software	GE Healthcare

3. Methods

3.1. Expression of *Sc*AA10C

Materials:

- Lysogeny broth medium (see Section 2.6)
- Ampicillin stock solution (100 mg/mL)
- Glycerol stock with *E. coli* One Shot® BL21 Star™ (DE3) containing the pRSET-B_CelS2 plasmid, coding for *Sc*AA10C

Method:

0.5 L lysogeny broth medium was poured into a sterile 2 L baffled Erlenmeyer flask together with 500 µL ampicillin and inoculated with the bacterial glycerol stock. The culture was incubated for 24 h at 37°C and 200 rpm. Expression levels of the LPMO are such that the use of an inducer is not necessary.

3.2. Purification of *Sc*AA10C

3.2.1. Periplasmic extracts

Periplasmic extraction is a method used to obtain proteins in the periplasm of gram-negative bacteria. The periplasm is the space between the inner and outer membrane in a gram-negative bacterium, and the pRSET-B plasmid contains an N-terminal signal peptide that directs translocation of the LPMO to the periplasm where the signal peptide is cleaved off. Extracting proteins from the periplasm rely on a cold osmotic shock to rupture the outer membrane, allowing the content of the periplasm to leak into the solution. First, resuspending cells in a spheroplast buffer with high sugar content will cause water to diffuse from the cell to the solution to account for the difference in osmotic pressure, which causes the cells to shrink. By resuspending the cells in ice-cold dH_2O, H_2O will rapidly diffuse into the periplasm, leading to rupture the outer membrane.

Materials:

- Avanti™ J-25 High-Performance Centrifuge, with a JA-10 rotor
- Overnight culture (see Section 3.1)
- Spheroplast buffer, ice-cold (see Section 2.7.5)
- 10 mM $MgCl_2$ (see Section 2.7.5)
- 1 M Tris-HCl buffer, pH 7.5 (see Section 2.7.5)
- dH_2O, ice-cold

Method:

The overnight culture from Section 3.1 was distributed in two centrifuge tubes and centrifuged at 6500 rpm for 12 min at 4°C with Avanti™ J-25 High-Performance Centrifuge with rotor JA-10. The supernatant was poured off, and the pellets were resuspended in 100 mL ice-cold spheroplast buffer in total. The resuspended pellets were centrifuged at 8000 rpm for 12 min at 4°C, before discarding the supernatant. After incubating the pellets at room temperature for 30 min, the cells were resuspended in 25 mL ice-cold dH_2O each, and the two suspensions were pooled to 50 mL, to which 700 µL 10 mM $MgCl_2$ was added. The suspension was centrifuged at 8000 rpm for 12 min at 4°C, and the supernatant was filtered using a 0.45 µm syringe filter. Prior to storage at 4°C, the concentration of the periplasmic extract was measured by A_{280} and adjusted to 50 mM by adding 1 M Tris-HCl, pH 7.5.

3.2.2. Ion-Exchange Chromatography

Purification of proteins using chromatography is based on proteins having different affinity to a column material. The column resin consists of polymer beads, e.g., agarose- or acrylamide-beads, to which a functional group is attached. The functional group provides an affinity for specific proteins under specific conditions. Ion-Exchange Chromatography (IEX) enables the separation of proteins based on their net surface charge. The method is based on reversible adsorption of charged molecules to a resin of opposite charge and can separate proteins with small charge differences, thus providing high-resolution separation. Depending on the protein's charge, either anion-exchange chromatography or cation-exchange chromatography can be applied. Anion-exchange chromatography binds negatively-charged molecules, whereas cation-exchange chromatography binds positively charged molecules. Proteins are amphoteric molecules meaning that they can display a net zero charge, at a pH value that

is called the isoelectric point, pI. Protein binding affinity to a column material is a function of the pI and the pH of the solution. When a protein sample is applied to an IEX column, the conditions must favor the binding of the protein of interest to the column. At pH values below the isoelectric point, the protein will display a positive charge. This would be suitable for purification by a cation-exchange resin, while if the pH is above the pI, the protein will carry a net negative charge and bind to an anion-exchange resin. Separating the proteins bound to the column material is done by increasing the salt concentration in the elution buffer, either linearly or stepwise. Proteins with weak ionic interactions to the column material will be released first, while proteins with strong interactions will be released later.

Materials:

- ÄKTA™ Pure chromatography system
- HiTrap® DEAE Sepharose FF, 5 mL column
- Periplasmic extracts (see Section 3.2.1)
- IEX binding buffer (see Section 2.7.1)
- IEX elution buffer (see Section 2.7.1)

Method:

An ÄKTA™ Pure protein purification system was equipped with a HiTrap® DEAE Sepharose FF, 5 mL column, and was used to purify *Sc*AA10C from the periplasmic extract. The ÄKTA™ Pure system has a built-in UV module that detects proteins eluted from the column by measuring A_{280}. Prior to connecting the column, the system was washed with elution buffer and water. The column was connected and washed with water and equilibrated with binding buffer. The sample was applied to the column using a sample pump with a flow rate of 1 mL/min. Non-bound proteins were eluted from the column using the binding buffer and a flow rate of 3 mL/min. Once the UV signal stabilized, *Sc*AA10C was eluted from the column by applying a linear gradient of NaCl (0 - 0.5 M NaCl over 100 min) with a 3 mL/min flow rate and collected as 3 mL fractions using a fraction collector. Eluted fractions were analyzed by LDS-PAGE, and those containing *Sc*AA10C were pooled and concentrated to approximately 1 mL, using Amicon® Ultra-15 Centrifugal Filters with a molecular mass cut-off of 10 kDa, followed by Size-Exclusion Chromatography as described in Section 3.2.3.

3.2.3. Size-Exclusion Chromatography

Gel filtration, or Size-Exclusion Chromatography (SEC), is a commonly used technique to separate proteins based on their size. In SEC, the column material does not bind proteins, but it provides a porous matrix through which proteins can flow. Tightly packed spherical beads make up the column material, and these beads contain pores with different sizes. Smaller protein can access smaller pores while larger proteins cannot, this allows larger proteins to pass through the gel faster than smaller proteins. As such, larger proteins will elute first in SEC while smaller proteins will elute last.

Materials:

- ÄKTA™ Pure chromatography system
- HiLoad™ 16/600 Superdex™ 75 prep grade column, 120 mL
- Concentrated protein solution after IEX (see Section 3.2.2)
- SEC running buffer (see Section 2.7.2)

Method:

A HiLoad™ 16/600 Superdex™ 75 prep grade column was connected to the ÄKTA™ Pure chromatography system and equilibrated with running buffer. The concentrated protein solution (sample volume less than 1 mL) obtained after IEX was loaded onto the column through a 2 mL sample loop, and the running buffer was applied with a flow rate of 1 mL/min. Protein elution was monitored by $A_{280,}$ and 2 mL fractions were collected using a fraction collector. Eluted fractions were analyzed by LDS-PAGE, and those containing *Sc*AA10C were pooled and concentrated to approximately 1 mL, using Amicon® Ultra-15 Centrifugal Filters with a molecular mass cut-off of 10 kDa and the resulting protein solution was stored at 4°C.

3.2.4. Copper saturation

LPMOs are copper-dependent redox enzymes in which a conserved histidine brace forms the active site. Therefore, purified LPMOs are usually copper saturated with $Cu(II)SO_4$ in a 3:1 molar ratio to ensure that each active site contains copper. The unbound, excess copper is removed from the copper saturated LPMO by a desalting step, using desalting columns.

Materials:

- PD MidiTrap™ column with Sephadex G-25 resin
- Purified *Sc*AA10C (see Section 3.2.3)
- Equilibration buffer: 50 mM sodium phosphate buffer, pH 7.0 (see Section 2.7.5)
- 15 mM Cu(II)SO_4, pH 2.5 (see Section 2.7.5)
- 20 % EtOH
- dH_2O

Method:

100 µL of *Sc*AA10C solution was mixed with a 3-fold molar excess of Cu(II)SO_4 and incubated for 30 min at room temperature, followed by desalting on a PD MidiTrap™ G-25 column to remove excess copper. The column was first washed with three column volumes (CVs) of dH_2O (15 mL), followed by an equilibration step of three CVs of equilibration buffer. After the equilibration buffer had completely entered the packed beads, the solution containing copper saturated LPMO and excess Cu(II)SO_4 (approximately 110 µL) was applied to the column. The PD MidiTrap™ G-25 columns require a sample volume of 1 mL, thus, after the sample solution had entered the bed completely, equilibration buffer (890 µL) was loaded to the column to achieve 1 mL total sample volume. The sample was eluted by adding 1 mL equilibration buffer, and the eluted protein was collected in an Eppendorf tube, and the protein concentration was determined by measuring A_{280}. After elution, the column was washed with three CVs dH_2O followed by three CVs 20 % EtOH. The column was stored in 20 % EtOH at room temperature.

3.3. Purification of *Tf*Cel6A

Dr. Zarah Forsberg kindly provided a bacterial cell pellet containing intracellular his-tagged *Tf*Cel6A corresponding a 250 mL *Escherichia coli* culture. The *E. coli* cells grown to express *Tf*Cel6A had been harvested by centrifugation and resuspended in Immobilized Metal Ion Affinity Chromatography (IMAC) binding buffer (50 mM Tris-HCl pH 8.0 supplemented with 500 mM NaCl and 5 mM imidazole; Section 2.7.3), before storage at -20°C.

3.3.1. Cell lysis and protein extraction

Cell lysis is a method used to obtain proteins in a cell, including proteins located in the cytoplasm. A microfluidizer relies on shear forces experienced by a cell in a solution and can disrupt bacterial cell walls and membranes. The sample is fed into an intensifier pump, which in turn forces the cells to an interaction chamber at very high pressure. In the interaction chamber, the sample is distributed into microchannels, which accelerate the cells. The cells collide with each other and the chamber, and the resulting large forces of impact and shear lead to total cell disruption. Here, the cells were lysed by a microfluidizer to release intercellular proteins, including *Tf*Cel6A into solution. The resulting cell-free protein extracted was then used for purification of the cellulase by Immobilized Metal Ion Affinity Chromatography.

Material:

- LM20 Digital Microfluidizer®
- Avanti™ J-25 High-Performance Centrifuge, with a JA-25.20 rotor
- Bacterial pellet containing his-tagged *Tf*Cel6A
- IMAC binding buffer (see Section 2.7.3)
- dH_2O

Method:

The bacterial cells were thawed on ice, and IMAC binding buffer was added to achieve a total sample volume of 25 mL prior to microfluidization. After washing the microfluidizer with dH_2O, the sample was added to the reservoir, the pressure set to 15 000 psi, and the cells were lysed. The cell lysate was collected in a 100 mL blue cap bottle. The cell lysate was further distributed into four centrifuge tubes and centrifuged at 15 000 g for 15 min at 4°C in an Avanti™ J-25 High-Performance Centrifuge using a JA-25.20 rotor. The supernatant was filtrated with a 0.45 µm PES membrane syringe filter into a 50 mL Falcon tube and stored at 4°C.

3.3.2. Immobilized Metal Ion Affinity Chromatography

Immobilized Metal Ion Affinity Chromatography is a method for purifying proteins with terminal his-tags. IMAC is an affinity-based technique in which the resin has a specific affinity for the protein of interest. His-tagged proteins are separated from non-his-tagged protein by their affinity for a nickel ion. The nickel ion is chelated by the resin and reversibly binds the his-tagged protein, while proteins with no affinity for the Ni-ion are washed out. To elute the protein, an elution buffer with imidazole is applied to outcompete the His-tagged protein for Ni-binding.

Materials:

- ÄKTA™ Pure chromatography system
- HiTrap® IMAC Fast Flow, 5 mL column
- *Tf*Cel6A containing cell-free protein extract obtained by microfluidizer (see Section 3.3.1)
- IMAC binding buffer (see Section 2.7.3)
- IMAC elution buffer (see Section 2.7.3)
- 20 mM Tris-HCl buffer, pH 8.0 (see Section 2.7.5)
- dH_2O

Method:

A HiTrap® IMAC Fast Flow column was connected to the ÄKTA™ Pure chromatography system. Prior to connecting the column, the system was washed with elution buffer and water. The column was washed with five column volumes (25 mL) with dH_2O, followed by five CVs elution buffer and equilibration with ten CVs binding buffer. The sample was applied to the column using a sample pump with a flow rate of 1 mL/min. Non-bound proteins were eluted from the column using the binding buffer and a flow rate of 3 mL/min. Once the UV signal stabilized, *Tf*Cel6A was eluted from the column by applying a linear gradient of elution buffer (0 – 100 % over 50 min) with 3 mL/min flow rate, while 3 mL fractions were collected using a fraction collector. The eluted fractions showing the highest protein concentration were analyzed using LDS-PAGE, and those containing pure *Tf*Cel6A were pooled and buffer exchanged by centrifugation using Amicon® Ultra-15 Centrifugal Filters with a molecular mass cut-off of 10 kDa, from the elution buffer to 20 mM Tris-HCl pH 8.0. The buffer exchange step was done to remove imidazole, which was diluted at least 1000 times by this procedure. The resulting protein solution (approximately 1 mL) was filtered using a 0.45 µm syringe filter and stored at 4°C.

3.4. Protein concentration determination by A_{280}

The protein concentration can be determined spectrophotometrically by measuring absorbance at 280 nm (A_{280}). The absorbance of UV-light at 280 nm is due to tyrosine and tryptophan residues. Tryptophan has the highest extinction coefficient and is the principal amino acid responsible for absorbing UV-light at 280 nm. The absorption at 280 nm is proportional to the amount of tyrosine and tryptophan residues in a sample and can, therefore, be used to determine the protein concentration by Beer-Lambert's law:

$$A = C \cdot \varepsilon \cdot l$$

Beer-Lambert's law states that the absorbance (A) is proportional to the molar concentration (C) of a solution that can absorb light. In the equation above, l represents the light's pathlength in the absorption cell (cm), and in this thesis, all measurements were carried out with l = 1 cm. ε is the molar extinction coefficient ($M^{-1}cm^{-1}$) and is dependent on the wavelength and the amount of tyrosine and tryptophan in the protein. Theoretical extinction coefficients can be determined using ExPASy ProtParam, which determines the extinction coefficient based on the amino acid sequence. The extinction coefficient used is listed in Table 8, and the values reported are those 'assuming all pairs of Cys residues form cysteines'.

Table 8. Calculated molar extinction coefficients for *Sc*AA10C and *Tf*Cel6A

Enzyme	Extinction coefficient ($M^{-1}cm^{-1}$)
*Sc*AA10C	75 775
*Tf*Cel6A	81 275

Materials:

- BioPhotometer® D30
- Uvettes, disposable cuvettes
- Protein solution of interest
- Sample buffer corresponding to the buffer in the protein solution

Method:

The A_{280} of the protein solution was measured with BioPhotometer® D30 using sample buffer as blank. Protein samples were diluted with sample buffer to obtain A_{280} values below 2. The measurements were carried out using disposable cuvettes, and the protein concentration in the samples was calculated using Beer-Lambert's law and the extinction coefficients, shown in Table 8.

3.5. Lithium Dodecyl Sulfate Polyacrylamide Gel Electrophoresis

Lithium Dodecyl Sulfate Polyacrylamide Gel Electrophoresis (LDS-PAGE) is a commonly used technique to separate proteins based on their molecular mass and to assess protein purity. The separation of protein through the polyacrylamide matrix requires negatively charged proteins. Prior to separation, the protein samples are denatured. Denaturing conditions are achieved by boiling the protein solution in the presence of a reducing agent, dithiothreitol (DTT), and an anionic detergent, lithium dodecyl sulfate (LDS). DTT reduces disulfide bonds, whereas the combination of boiling and LDS molecules will denature the proteins, which will stay denatured upon cooling due to LDS binding. Binding of LDS will provide each protein with a uniform negative charge that is proportional to the protein's chain length, which implies that proteins will be separated by size only. Separation is achieved as the negatively charged proteins migrate through the gel towards the anode. The pore structure of the polyacrylamide matrix allows smaller proteins to migrate faster than large proteins. Protein size is estimated from a molecular marker (BenchMark™ Protein Ladder) containing proteins of known mass. The predicted sizes of the proteins of interest in this thesis were obtained from ExPASy ProtParam, which are listed in Table 9. It must be noted that the gels used in this study contained trihalo components. These components will react with tryptophan residues present in the proteins once the gel is imaged with UV-light. The reaction between tryptophan and the trihalo components will emit fluorescence as it is irradiated with UV-light. Thus, proteins without tryptophan residues cannot be analyzed using this method.

Table 9. Molecular weight (signal peptides not included) of *Sc*AA10C and *Tf*Cel6A

Enzyme	Molecular weight (kDa)
*Sc*AA10C	34.6
*Tf*Cel6A	42.9

Materials:

- Protein containing samples
- LDS buffer (2X)
    - 5 mL NuPAGE™ LDS Sample Buffer (4X)
    - 2 mL NuPAGE™ Sample Reducing Agent (10X)
    - 3 mL dH_2O
- BenchMark™ Protein Ladder
- Tris-Glycine-SDS (TGS) buffer (10X)
- Mini-Protean® TGX Stain-Free™ Precast Gels
- Mini-Protean® Tetra Electrode Assembly
- Mini-Protean® Tetra Cell
- PowerPac 3000 power supply
- Stain-Free Sample Tray
- Gel Doc™ EZ Imager

Method:

Protein samples were mixed 1:1 with LDS buffer and boiled at 95°C for 5 min. A Mini-Protean® TGX Stain-Free™ Precast Gels cassette was assembled in a Mini-Protean® Tetra Electrode Assembly. The electrode assembly was placed in a buffer chamber, and the internal chamber with the precast gel was filled with TGS buffer, diluted to 1X in dH_2O, before filling the buffer chamber with TGS buffer (1X). 10 µL protein ladder solution was applied first in the well in the middle. 20 µL protein samples were loaded into the remaining wells before connecting the buffer chamber to a PowerPac 3000 power supply. The gels were run for 19 min at 270 V before the gels were removed from the chamber and transferred to a Stain-Free Sample Tray and imaged using the Gel Doc™ EZ Imager.

3.6. Photobiocatalytic activity of *Sc*AA10C on cellulose

*Sc*AA10C had previously been used as a model cellulolytic LPMO in photobiocatalytic reactions using chlorophyllin and V-TiO_2. This study aimed at elucidating the effect of light-exposed lignin on the catalytic activity of *Sc*AA10C on Avicel. Throughout this study, *Sc*AA10C has been tested in a variety of reaction conditions to elucidate effects on LPMO catalysis. The various experimental setups were aimed at investigating the effect of lignin concentration in the presence and absence of light, with and without a small amount of AscA, the effect of light intensity, and the effect of different *Sc*AA10C and

AscA concentrations. Previous research had found that LPMOs prefer H_2O_2 over O_2 and that photochemically produced superoxide can be an important intermediate for LPMOs in photobiocatalytic reactions. Thus, another important aspect of this study was to assay the effect of superoxide dismutase on LPMO activity. The superoxide dismutase used was manganese dependent, Mn-SOD, therefore a control reaction with free Mn(II) was also conducted. Furthermore, to elucidate the effect of the lignin source, experiments with three different lignin source materials were also carried out. ICP-MS analysis of commercial Kraft lignin (Sigma-Aldrich) and in-house produced lignin form Birch-Wood showed that Birch-Wood lignin contained 5-fold more copper than Kraft lignin. Reactions were supplemented with various amounts of copper(II) to investigate if copper(II) influenced LPMO activity. In addition, a number of control reactions were performed (Section 3.6.9).

3.6.1. Standard reaction conditions

The standard conditions used in this study were chosen arbitrarily at the start, except for the lignin concentration, which was varied in the first set of reactions (Section 3.6.2), after which preferred levels were selected. The standard conditions for each reaction, unless otherwise specified, were 0.5 µM *Sc*AA10C, 50 mM sodium phosphate buffer pH 7.0, 0.9 g/L Kraft lignin (Sigma-Aldrich), 10 g/L Avicel and a light intensity, I, corresponding to 10 % of I_{max} (approximately 16.8 $W.cm^{-2}$). The light source used in this study was a LightningCure Spot light source LC8 model L9588, equipped with an L9588-03 filter. This filter only allows wavelengths between 400 and 700 nm to pass. All reactions were done in 1 mL glass vials (Reacti-Vial™) and incubated at 40°C, with magnetic stirring and were, when applicable, illuminated by visible light from an optic fiber cable positioned at approximately 1 cm above the liquid surface in the reaction vial. The total reaction volumes were typically 500 or 600 µL, depending on the number of samples that were to be taken during the reaction. All solutions were mixed directly in the glass vials and incubated for 15 min, at 40°C, with magnetic stirring, in the dark, before starting the reactions by either turning on the external visible light source or covering the samples in aluminum foil. The reactions were stopped by filtration to separate insoluble and soluble materials. 55 µL samples were taken from the reaction vessels at regular intervals and transferred to a 96-well filter plate operated with a vacuum manifold. Filtered samples (35 µL) were stored at -20°C. All samples were thawed on ice and hydrolyzed with *Tf*Cel5A or *Tf*Cel6A (Section 3.7.1) to produce a mixture of only oxidized dimers and trimers, prior to analysis using High-Performance Anion-Exchange Chromatography with Pulsed Amperometric Detection (HPAEC-PAD) analysis (Section 3.7.2).

3.6.2. The effect of lignin, in the presence or absence of light and a reductant

To determine the effect of lignin on LPMO efficiency, reactions with various amounts of lignin (0, 0.009, 0.09, 0.9, 9 g/L) were performed. The reactions were either kept in the dark or exposed to visible light (I = 0 % or 10 % of I_{max}, corresponding to approximately 0 or 16.8 $W.cm^{-2}$, respectively), with or without a priming amount of AscA. For the reactions with AscA priming, the reactions were supposed to be initiated by the addition of 20 µM AscA, to ensure complete reduction to the catalytically efficient Cu(I)-state, but AscA was added 15 min prior to reaction start, incubating together with the other reaction components. The reactions were performed in duplicates, and samples for analysis were taken out after 5, 10, 15 min, and 1, 3, 6, and 24 h, aiming to capture putative differences in initial rates, reaction progress, or 24 h end-point product levels. Prior to HPAEC-PAD analysis of soluble LPMO products, these products were treated with *Tf*Cel5A to convert oxidized oligomers to a mixture of only oxidized dimers and trimers [GlcGlc1A and Glc_2Glc1A], see Section 3.7.1 for further details.

3.6.3. The effect of light intensity

To determine the effect of the light intensity on LPMO efficiency, reactions exposed to different light intensities (I = 0, 1, 3, 10, 30 % of I_{max}, corresponding to approximately 0, 1.7, 5.0, 16.8, 50.4 $W.cm^{-2}$, respectively), were performed with 0.9 or 9 g/L lignin. The reactions were performed in duplicates, and samples for analysis were taken out after 5, 10, 15 min, and 1, 3, 6, and 24 h for reactions exposed to light intensities I = 0, 10, 30 % of I_{max}. For reactions exposed to light intensities I = 1, 3 % of I_{max} samples for analysis were taken out after 0.5, 1, 1.5, 3, 6, and 24 h, aiming to capture putative differences in initial rates, reaction progress, or 24 h end-point product levels. Prior to HPAEC-PAD analysis of soluble LPMO products samples exposed to I = 0, 10 % of I_{max} were treated with *Tf*Cel5A, and samples exposed to I = 1, 3 and 30 % of I_{max} were treated with *Tf*Cel6A, to convert oxidized oligomers to a mixture of only oxidized dimers and trimers [GlcGlc1A and Glc_2Glc1A], see Section 3.7.1 for further details. After depleting *Tf*Cel5A, *Tf*Cel6A was used, both endoglucanases provide the same activity.

3.6.4. The effect of LPMO concentration

To determine the effect of different *Sc*AA10C concentration on LPMO efficiency, reactions with various concentrations of *Sc*AA10C (0.1, 0.5, 1, 5, 10 µM) were performed. The reactions were performed in duplicates, and samples for analysis were taken out after 0.5, 1, 1.5, 3, and 6 h aiming to capture putative differences in initial rates, reaction progress, or 6 h end-point product levels. Prior to HPAEC-PAD analysis of soluble LPMO products, these products were treated with *Tf*Cel5A to convert oxidized oligomers to a mixture of only oxidized dimers and trimers [GlcGlc1A and Glc_2Glc1A], see Section 3.7.1 for further details.

3.6.5. The effect of a reductant

To determine the effect of AscA at the initial priming on LPMO efficiency, reactions with various concentrations of AscA (0, 20, 200, 2000 µM) were performed. Unlike the reactions in Section 3.6.2, where AscA was added before the 15 min incubation step allowing the LPMO to bind its substrate, here AscA was the last component to be added to the reactions. This addition ensured complete reduction of the LPMO to its catalytically active Cu(I)-state at reaction start. The reactions were performed in duplicates, and samples for analysis were taken out after 5, 10, 15 min, and 1, 3, 6, and 24 h, aiming to capture putative differences in initial rates, reaction progress, or 24 h end-point product levels. Prior to HPAEC-PAD analysis of soluble LPMO products, these products were treated with *Tf*Cel6A to convert oxidized oligomers to a mixture of only oxidized dimers and trimers [GlcGlc1A and Glc_2Glc1A], see Section 3.7.1 for further details.

3.6.6. The effect of lignin from various sources and subjected to different pretreatments

Lignin's structure varies depending on its origin and how it has been pre-treated, here the goal was to determine how this influences photobiocatalytic LPMO reactions. Reactions were carried out with either commercial Kraft lignin (Sigma-Aldrich), lignin-rich fraction from Birch-wood obtained after steam-explosion (Costa et al., 2019), or steam-exploded Spruce-wood. The Spruce-wood was steam exploded at 210°C or 220°C with or without prior 2-naphthol treatment at each temperature. The reactions conducted with the various Spruce-wood lignin samples were done in duplicate, while the comparison between the reactions with either Kraft lignin or lignin from Birch-wood was only tested

with one replicate. Samples for analysis were taken out after 5, 10, 15 min, and 1, 3, and 6 h, aiming to capture putative differences in initial rates, reaction progress, or 6 h end-point product levels. Prior to HPAEC-PAD analysis of soluble LPMO products, these products were treated with *Tf*Cel5A to convert oxidized oligomers to a mixture of only oxidized dimers and trimers [GlcGlc1A and Glc_2Glc1A], see Section 3.7.1 for further details.

3.6.7. The effect of superoxide dismutase

To determine the role of superoxide in this photobiocatalytic system, reactions with different concentrations of Mn-SOD (0, 10, 100, 300, 1000, 3000 nM) were performed. The reactions were performed in duplicates, and samples for analysis were taken out after 0.5, 1, 1.5, 3, and 6 h, aiming to capture putative differences in initial rates, reaction progress, or 6 h end-point product levels. The activity of the Mn-SOD enzyme had been verified prior to this study by Eirik Kommedal, as described in (Bissaro et al., 2020). Prior to HPAEC-PAD analysis, the samples from reactions with 0, 10, 100 and 1000 nM SOD were treated with *Tf*Cel5A while the samples from reactions with 300 and 3000 nM SOD were treated with *Tf*Cel6A, to convert oxidized oligomers to a mixture of only oxidized dimers and trimers [GlcGlc1A and Glc_2Glc1A], see Section 3.7.1 for further details. After depleting *Tf*Cel5A, *Tf*Cel6A was used, both endoglucanases provide the same activity

3.6.8. The effect of transition metals, Mn(II) and Cu(II)

To determine if there was any free manganese in the Mn-SOD solution, that possibly could influence the LPMO reaction, reactions with different concentrations of $Mn(II)SO_4$ (0, 0.1, 1, 10 mM) were done. To check if the amount of free copper in solution influenced the LPMO reaction, reactions with different concentrations of $Cu(II)SO_4$ (0, 2, 20, 200 µM) were also carried out. The reactions were performed as single experiments, and samples for analysis were taken out after 0.5, 1, 1.5, 3, and 6 h for the reactions with $Mn(II)SO_4$, and after 3 and 6 h for the reactions with $Cu(II)SO_4$, aiming to capture putative differences in reaction progress, or 6 h end-point product levels. Prior to HPAEC-PAD analysis, all samples from reactions with added $Mn(II)SO_4$ were treated with *Tf*Cel6A while the samples from reactions with $Cu(II)SO_4$ were treated with *Tf*Cel5A, to convert oxidized oligomers to a mixture of only oxidized dimers and trimers [GlcGlc1A and Glc_2Glc1A], see Section 3.7.1 for further details. After depleting *Tf*Cel5A, *Tf*Cel6A was used, both endoglucanases provide the same activity

3.6.9. Control reactions

Control reactions without *Sc*AA10C, with Avicel in the presence or absence of 0.9 g/L lignin and with or without light exposure, were performed to check that there wouldn't be any depolymerization of cellulose without LPMO present. The reactions were performed in duplicates, and samples for analysis were taken out after 1, 3, 6, and 24 h. Reactions, where LPMO was replaced with various amounts of $Cu(II)SO_4$ (1, 10, 100, 1000 µM), were performed to check if any nonspecific reaction between lignin and copper occurred when exposed to visible light. The reactions were performed in duplicates, and samples for analysis were taken out after 5, 10, 15 min, and 1, 3, 6, and 24 h, aiming to capture putative differences in initial rates, reaction progress, or 24 h end-point product levels. Prior to HPAEC-PAD analysis of soluble LPMO products, these products were treated with *Tf*Cel5A to convert oxidized oligomers to a mixture of only oxidized dimers and trimers [GlcGlc1A and Glc_2Glc1A], see Section 3.7.1 for further details.

3.7. High-Performance Anion-Exchange Chromatography with Pulsed Amperometric Detection

3.7.1. Preparation of samples and standards

All samples with soluble LPMO products obtained from the different photobiocatalytic reactions (Section 3.6) were subjected to HPAEC-PAD analysis in order to quantify oxidized sites. Only solubilized cello-oligosaccharides released during the reactions were analyzed as the reactions are stopped by separating the insoluble fraction from the soluble fraction. Prior to product quantification using HPAEC-PAD, the filtered samples were treated with purified endoglucanase from *T. fusca*, either Cel5A (kindly provided by Dr. Zarah Forsberg) or Cel6A (used after depleting the Cel5A solution, Section 3.3), *Tf*Cel5A and *Tf*Cel6A both performed the same function. The endoglucanases convert the solubilized cello-oligosaccharides with varying degrees of polymerization to a mixture of oxidized dimers and trimers [Cellobionic acid (GlcGlc1A) and Cellotrionic acid Glc_2Glc1A)]. Native sugars were not quantified but were also hydrolyzed by *Tf*Cel5A and *Tf*Cel6A to cellobiose and cellotriose. Peaks corresponding to GlcGlc1A and Glc_2Glc1A in the chromatograms were integrated, and the area for each peak was converted to the concentration of GlcGlc1A and Glc_2Glc1A, respectively, by using a standard curve. The obtained concentrations for GlcGlc1A and Glc_2Glc1A were summed up to yield the total concentration of soluble oxidized sites. A standard curve with known concentrations of GlcGlc1A (10, 20, 50, 100, 200 µM) was used to calculate the concentration of GlcGlc1A in samples from LPMO reactions, and the

standard curve was analyzed in duplicates or triplicates every time a new sample series was analyzed by HPAEC-PAD. The concentration of Glc_2Glc1A was quantified using a single point calibration at 50 µM, and Glc_1-Glc_5 standards were used to verify that the electrode was functioning adequately and that products were properly separated by the column.

Materials:

- Filtered samples from *Sc*AA10C reactions (see Section 3.6)
- Endoglucanase solution at 2 µM final concentration (*Tf*Cel5A or *Tf*Cel6A)
- 0.5 M Bis-Tris, pH 6.2 (pH 6.0 at 37°C) (see Section 2.7.5)
- Glc_1-Glc_5 standard solution (0.001 g/L)
- GlcGlc1A standard solutions (10, 20, 50, 100, 200 µM)
- Glc_2Glc1A standard solution (50 µM)

Method:

The endoglucanase was prepared as a 2 µM solution in 25 mM Bis-Tris pH 6.2. Filtered samples from the different photobiocatalytic reactions (Section 3.6) were mixed 1:1 with the endoglucanase solution to achieve a final concentration of 1 µM endoglucanase. The samples were incubated over-night in a heating cabinet at 37°C to achieve full conversion of the reaction products to a mixture of GlcGlc1A and Glc_2Glc1A. Samples were transferred to HPLC 'vials' prior to HPAEC-PAD analysis. Standard solutions for GlcGlc1A and Glc_2Glc1A were prepared from 1 mM stock solutions using dH_2O, while the standard solution for Glc_1-Glc_5 at 0.001 g/L was performed by diluting a 1 g/L stock solution with dH_2O. The stock solutions of GlcGlc1A and Glc_2Glc1A had been prepared prior to this study by oxidizing Glc_2 and Glc_3 in separate with cellobiose dehydrogenase from *Myriococcum thermophilum*, as described by Forsberg et al. (2014).

3.7.2. High-Performance Anion-Exchange Chromatography with Pulsed Amperometric Detection analysis

High-Performance Anion-Exchange Chromatography (HPAEC) is an analytical chromatography technique used to separate and quantify oligosaccharides of varying lengths and composition. Separation relies on the weakly acidic nature of carbohydrates. At high pH, the carbohydrates become negatively charged, and the negatively charged analytes bind to the positively charged groups on the

column material. Elution is achieved by introducing another negatively charged compound at a high concentration that will outcompete the analyte for binding to the column material, causing analytes to elute depending on the strength of the interaction with the column material. The method is well suited for the analysis of C_1-oxidized soluble cello-oligosaccharides as the alkaline environment favors the aldonic acid over the lactone configuration, meaning that the analytes are negatively charged.

Pulsed Amperometric Detection (PAD) can be applied to detect carbohydrates in a sample. PAD detection relies on a gold electrode to oxidize carbohydrates on its surface by changing the potential applied to the detector, resulting in the generation of a measurable current. The oxidation of the analytes generates a current that reflects the concentration of the analyte in the solution. The gold electrode is a disposable electrode that will lose sensitivity over time. During all analyses done in this study, a standard solution of glucose, cellobiose, cellotriose, cellotetraose, and cellopentaose (Glc_1-Glc_5) was analyzed at regular intervals to verify that products were properly separated by the column and that the electrode was functioning adequately. Solutions with known concentrations of GlcGlc1A were also analyzed at regular intervals to generate standard curves in order to quantify the amount of oxidized products generated (GlcGlc1A and Glc_2Glc1A) from each photobiocatalytic reaction. The Glc_2Glc1A solution, with known concentration, was only used for single-point calibration.

Materials:

- Dionex™ CarboPac™ PA200 column
- Dionex™ ICS-5000 system with PAD detection
- HPAEC eluent A (see Section 2.7.4)
- HPAEC eluent B (see Section 2.7.4)
- HPAEC eluent C (see Section 2.7.4)

Method

The chromatographic analyses were performed using Chromeleon® 7 Chromatography Data system software and a Dionex™ ICS-5000 system coupled to a PAD detection system. At the start of each analysis, a program designed to wash (eluent C) and equilibrate (eluent A) the Dionex™ CarboPac™ PA200 column was run. Samples (5 µL) were injected into the column by an automatic sampler, and the flow rate used for analysis was 0.5 mL/min. The oxidized carbohydrates were separated by applying a multi-step linear gradient with the following steps: first, 100 % A to 90 % A and 10 % B over 5 min; increase from 10 % B to 18 % B over next 5 min; increase to 30 % B over 0.5 min; increase to 100 % B

over 0.5 min. After applying the gradient, the column was returned to 100 % A in 0.05 min and equilibrated with 100 % A for 6.95 min before the next injection. The total run time per injection was 18 min.

4. Results

4.1. Production and purification of *Sc*AA10C

Protein expression of *Sc*AA10C was performed by inoculating lysogeny broth medium supplemented with 100 µg/mL ampicillin with the expression strain, and the culture was incubated in a baffled Erlenmeyer flask for 24 hours, at 37°C. After 24 hours, the bacterial culture was harvested by centrifugation, and a starting point for purification of *Sc*AA10C was obtained by periplasmic extraction. After the periplasmic extraction procedure, the supernatant (i.e., the periplasmic extract) and the cell pellet were analyzed by LDS-PAGE to verify that *Sc*AA10C primarily appeared in the supernatant, as was indeed the case (**Figure 9**). The presence of a thick band at 35 kDa in the extract and absence of the same band in the pellet fraction indicates that the periplasmic extraction was successful (**Figure 9**).

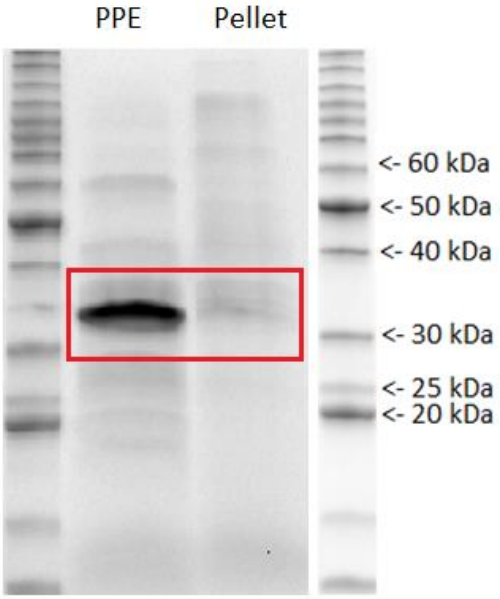

Figure 9. LDS-PAGE analysis of periplasmic extract. The left lane and the right lane contain a BenchMark™ Protein Ladder used to estimate the sizes of protein in the gel. The lane marked as PPE contains the supernatant obtained after periplasmic extraction and displays a band at 35 kDa, which is highlighted by the red square. This mass corresponds to *Sc*AA10C. The lane marked pellet contains the pellet obtained after periplasmic extraction and does not exhibit a band a 35 kDa, indicating that almost all *Sc*AA10C ends up in the periplasmic extract.

4.1.1. Ion-Exchange Chromatography

*Sc*AA10C was purified from the periplasmic extract by Ion-Exchange Chromatography. After the application of the periplasmic extract to the column, the bound proteins were eluted using a linear NaCl gradient, and fractions were collected continuously. A selection of fractions from the start, middle, and finish of the elution peak (marked as No. 2) in the chromatogram (**Figure 10**), were analyzed by LDS-PAGE to determine which fractions contained *Sc*AA10C, and the result is shown in **Figure 11**. The collected fractions contained *Sc*AA10C, but some fractions also had impurities that co-eluted with *Sc*AA10C (**Figure 11**). Based on the chromatogram (**Figure 10**) and the LDS-PAGE analysis (**Figure 11**), fractions 9 - 19 were pooled and concentrated by ultrafiltration to approximately 1 mL, after which Size-Exclusion Chromatography was carried out.

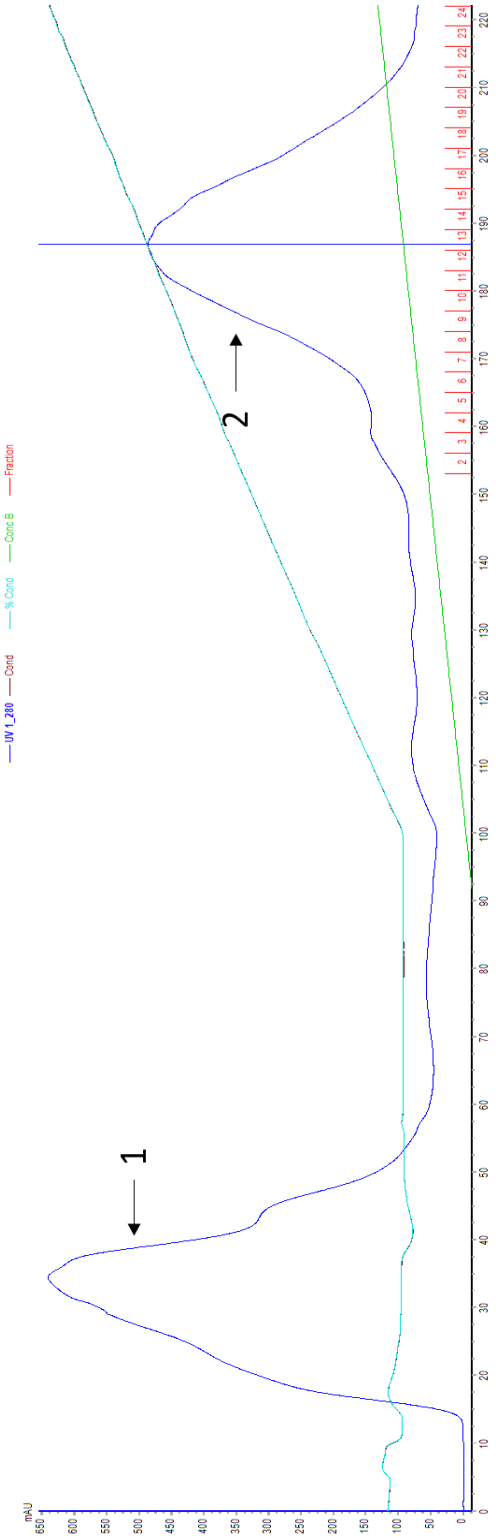

Figure 10. Chromatogram from purification of *Sc*AA10C by IEX. The figure shows 'elution profile' measured by A_{280}, from the purification of *Sc*AA10C by Ion-Exchange Chromatography. Protein elution from the column was detected by monitoring A_{280} of the column flow-through, represented by the dark blue curve. The light green curve shows the NaCl gradient (0 - 50 % IEX elution buffer, over 100 min) applied to elute proteins bound to the column. The conductivity of the solution within the column is represented by the light blue curve. The figure displays two major peaks in the chromatogram; the flow-through peak of non-bound proteins, marked with the number 1, while the peak representing the target protein is marked with the number 2. Fraction numbers (2-24) are shown along the x-axis in red. The chromatogram was generated by using the Unicorn™ 6.4 Software.

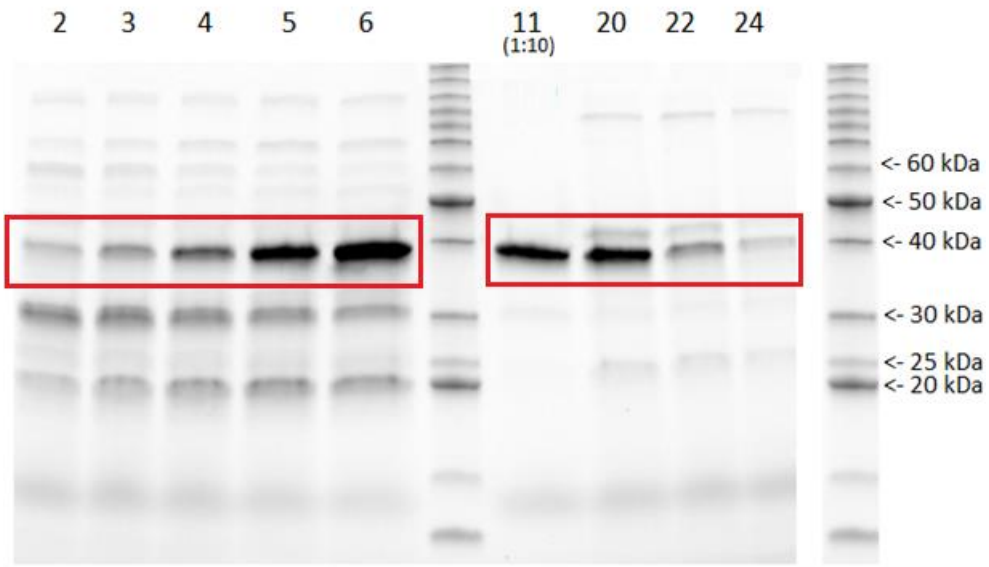

Figure 11. LDS-PAGE analysis of fractions obtained during IEX. The middle lane and the right lane contain a BenchMark™ Protein Ladder used to estimate protein size. The lanes are marked with the fraction number, which implies the order of the fractions obtained during Ion-Exchange Chromatography. All fractions display a band at 35 kDa, which corresponds to *Sc*AA10C and is highlighted by the red squares. Fraction 11 was diluted 10 times before application onto the gel.

4.1.2. Size-Exclusion Chromatography

The concentrated *Sc*AA10C solution obtained after Ion-Exchange Chromatography was used in a further purification step with Size-Exclusion Chromatography. After the application of the protein sample to the column, the bound proteins were eluted with one column volume running buffer, and fractions were collected continuously. A selection of fractions from the elution peak in the chromatogram (**Figure 12**) was analyzed by LDS-PAGE to determine which fractions contained *Sc*AA10C, and the result is shown in **Figure 13**. The analyzed fractions contained *Sc*AA10C, and some fractions showed impurities that co-eluted with *Sc*AA10C (**Figure 13**). Based on the chromatogram (**Figure 12**) and the LDS-PAGE analysis (**Figure 13**), fractions 6 - 9 were pooled and concentrated by ultrafiltration to approximately 1 mL, before storing at 4°C.

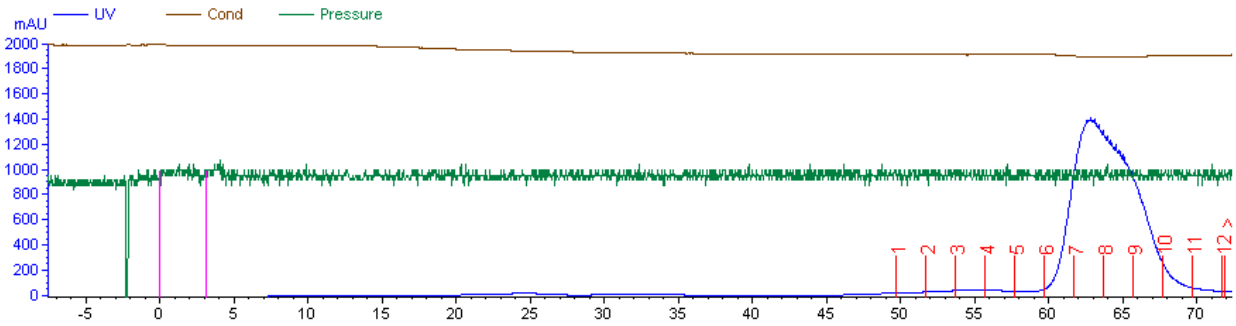

Figure 12. Chromatogram from purification of *Sc*AA10C by SEC. The figure shows 'elution profile' measured by $A_{280,}$ from the purification of *Sc*AA10C by Size-Exclusion Chromatography. Protein elution from the column was detected by monitoring A_{280} of the column flow-through, represented by the dark blue curve. The bound proteins were eluted from the column with one column volume running buffer. The conductivity of the solution within the column is represented by the brown line, and the pressure within the column is represented by the brown line. The figure displays a major peak representing the elution of the target protein. Fraction numbers (1-12) are shown along the x-axis in red. The Chromatogram was generated by using the Unicorn™ 6.4 Software.

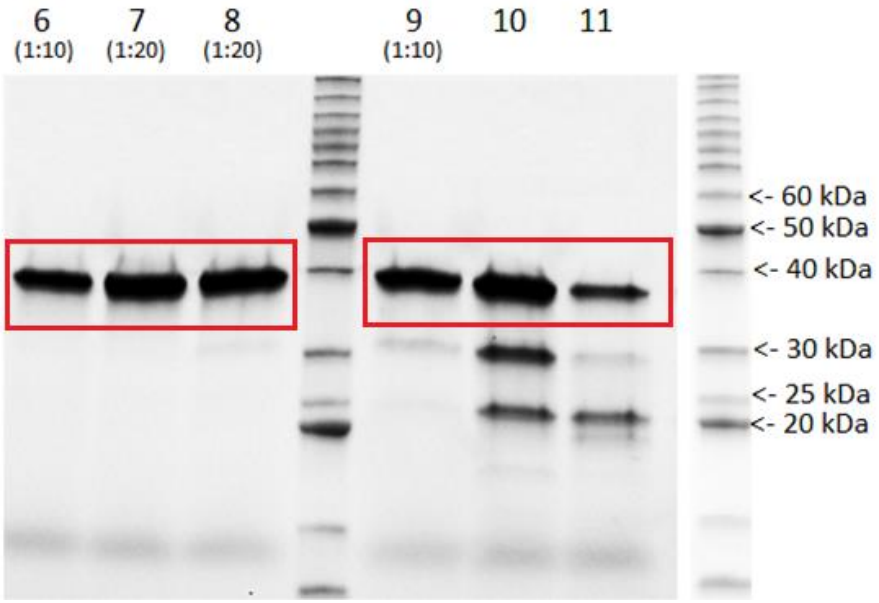

Figure 13. LDS-PAGE analysis of fractions obtained during SEC. The middle lane and the right lane contain a BenchMark™ Protein Ladder used to estimate the protein size. The lanes are marked with the fraction number, which implies the order of the fractions obtained during Size-Exclusion Chromatography. All fractions display a band at 35 kDa, which corresponds to *Sc*AA10C and is highlighted by the red squares. Fractions 6 and 9, and 7 and 8, were diluted 10 and 20 times, respectively, before application onto the gel.

4.1.3. Copper saturation

After Size-Exclusion Chromatography purification, copper saturation of *Sc*AA10C was carried out. To avoid carry-over of free copper from copper saturation, only 100 µL of concentrated *Sc*AA10C was copper saturated with a 3-fold molar excess of copper. If the copper saturation solution contains a high concentration of free copper in addition to the LPMO-bound copper, there is a risk of the LPMO co-eluting with free copper, which in turn may influence the LPMO reaction (Bissaro et al. 2020). Copper saturation was performed in one-tenth of the total sample volume applied to the column, and the final copper concentration during copper saturation never exceed 1 mM. After desalting, the concentration of copper saturated *Sc*AA10C was determined by measuring A_{280}. During the work described in this thesis, two batches of *Sc*AA10C were copper saturated, and their concentrations were determined to be 47.1 µM and 35.2 µM.

4.2. Production and purification of *Tf*Cel6A

A pellet of *E. coli* cells overexpressing *Tf*Cel6A cell was kindly provided by Dr. Zarah Forsberg. The cells were lysed by treatment with an LM20 Digital Microfluidizer®. *Tf*Cel6A was purified from the cell lysate by Immobilized Metal Ion Affinity Chromatography. After the application of the cell lysate to the column, the bound proteins were eluted using a linear imidazole gradient, and fractions were collected continuously. A selection of fractions from the elution peak (marked as No. 2) in the chromatogram (**Figure 14**) was analyzed by LDS-PAGE to determine which fractions contained *Tf*Cel6A, and the result is shown in **Figure 15**. The analyzed fractions contained *Tf*Cel6A, and some fractions showed impurities that co-eluted with *Tf*Cel6A (**Figure 15**). Based on the chromatogram (**Figure 14**) and the LDS-PAGE analysis (**Figure 15**), fractions 6 - 12 were pooled and concentrated by ultrafiltration, while at the same time, the buffer was exchanged from elution buffer to 20 mM Tris-HCl buffer pH 8.0 to remove imidazole, which was diluted at least a 1000 times by this procedure. Fractions 8 and 9 were pooled and concentrated to approximately 1 mL separately from the rest, to obtain an as clean as possible endoglucanase preparation for further use. The concentration of *Tf*Cel6A in the preparation derived from fractions 8 and 9 was 0.60 mM, and this solution was diluted in buffer (20 mM Tris-HCl buffer pH 8.0) to 60 µM, before storage at 4°C.

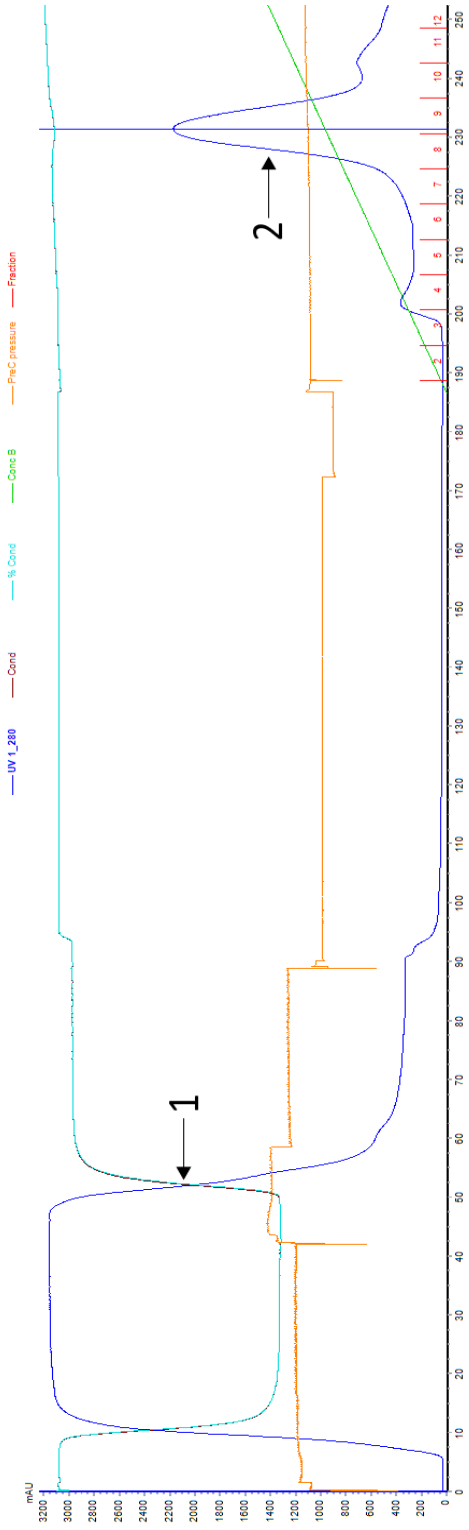

Figure 14. Chromatogram from purification of *Tf*Cel6A by IMAC. The figure shows 'elution profile' measured by A_{280}, from the purification of *Tf*Cel6A by Immobilized Metal Ion Affinity Chromatography. Protein elution from the column was detected by monitoring A_{280} of the column flow-through, represented by the dark blue curve. The light green curve shows the imidazole gradient (0 - 100 % IMAC elution buffer, over 50 min) applied to elute proteins bound to the column. The conductivity of the solution within the column is represented by the light blue curve, and the pressure within the column is represented by the orange line. The figure displays two major peaks in the chromatogram; the flow-through peak of non-bound proteins, marked with the number 1, while the peak representing the target protein is marked with the number 2. Fraction numbers (2-12) are shown along the x-axis in red. The chromatogram was generated by using the Unicorn™ 6.4 Software.

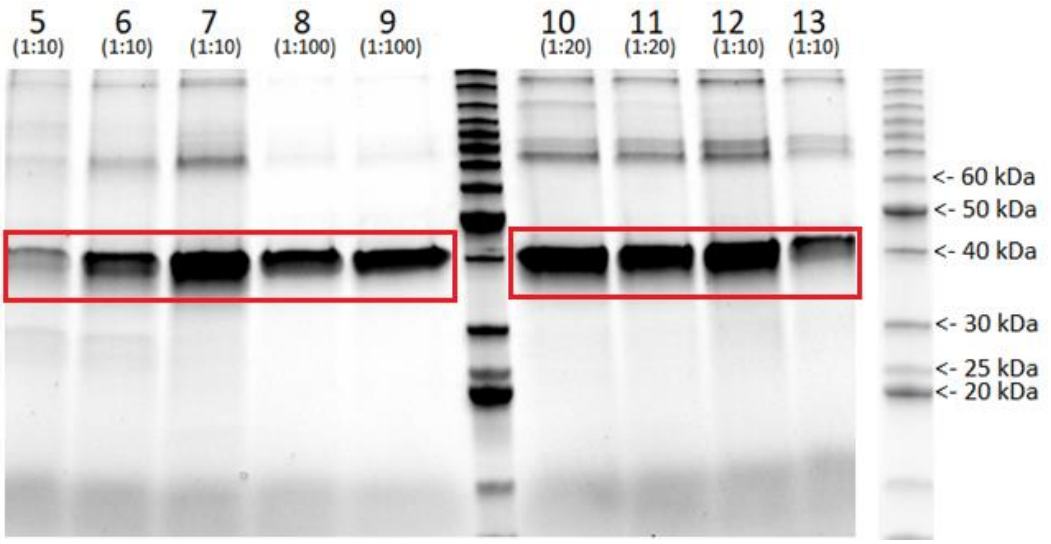

Figure 15. LDS-PAGE analysis of fractions obtained during IMAC. The middle lane and the right lane contain a BenchMark™ Protein Ladder used to estimate protein size. The lanes are marked with the fraction number, which implies the order of the fractions obtained during Immobilized Metal Ion Affinity Chromatography. All fractions display a band at 43 kDa, which corresponds to *Tf*Cel6A and is highlighted in the red squares. Fractions 5, 6, 7, 12 and 13, were diluted 10 times, while fractions 10 and 11 were diluted 20 times and fractions 8 and 9 were diluted 100 times, before application onto the gel.

4.3. Photobiocatalytic reactions

4.3.1. The effect of lignin, in the presence or absence of light and a reductant

The effect of lignin on the catalytic activity of *Sc*AA10C towards a model substrate, Avicel, was investigated in reactions exposed or not to visible light, and in the presence or absence of a reductant, AscA. The results, in **Figure 16**, generally show a clear effect of the lignin concentration on LPMO performance. Panels A and B show that in reactions exposed to light, at higher lignin concentrations, both the shape of the progress curve and the final amounts of oxidized products are not affected by the presence of AscA (**Figure 16**). Importantly, product formation was linear over time, except for the reaction with the highest lignin concentration, which showed a marked change (slow down) in reaction progress at approximately three hours. It is also worth noting that a positive effect of AscA on product formation is visible for the reactions with the lower lignin concentrations. Similar trends regarding the effect of AscA were observed for reactions carried out in the dark (**Figure 16, C & D**), which otherwise showed major differences from the reactions with light. The dark reactions showed slower product formation, and progress curves were linear, also at the highest lignin concentration.

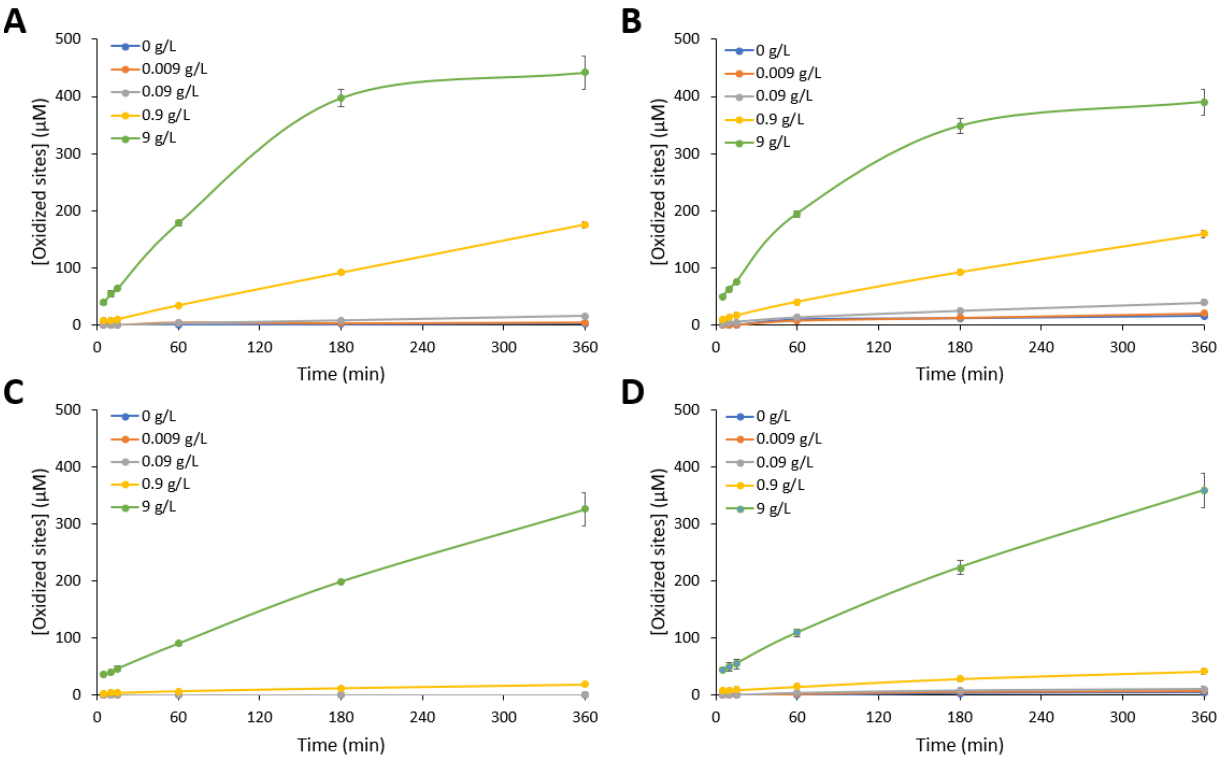

Figure 16. The impact of lignin on photobiocatalytic activity of *Sc*AA10C, in the presence or absence of AscA. The figure shows product formation for up to 6 h in reactions with *Sc*AA10C and Avicel that were exposed **(A, B)** or not exposed **(C, D)** to visible light (I = 10 % of I_{max}, approximately 16.8 W.cm^{-2}) and did **(B, D)** or did not **(A, C)** contain AscA (20 µM). **Figure A1** in **Appendix A** shows the full time-courses up to 24 h, and an overview of product levels at different time-points is provided in **Figure 17**. The concentration of *Sc*AA10C was 0.5 µM in all reactions. Reactions were performed in 50 mM sodium phosphate buffer pH 7.0 with 10 g/L Avicel and various concentrations of Kraft lignin (0, 0.009, 0.09, 0.9, 9 g/L), at 40°C, for 24 h, with magnetic stirring. Soluble products, of varying degrees of polymerization, were treated with endoglucanase, *Tf*Cel5A, to yield oxidized products with a degree of polymerization of 2 (GlcGlc1A) or 3 (Glc_2Glc1A), which were analyzed by HPAEC-PAD and quantified, to yield the total amount of solubilized oxidized sites. Reactions were performed in duplicates, and the standard deviations are shown as error bars.

The effect of light becomes perhaps even clearer when looking at product formation after 24 h (**Figure 17**). In the reactions with 0.9 g/L lignin, there is nearly an order of magnitude difference in product formation after 24 h between the light-exposed and non-light-exposed reactions (**Figure 17**). For the reactions containing 0.9 g/L lignin and exposed (**Figure 16, A**) or not (**Figure 16, C**) to visible light in the absence of AscA, this approximately 10-fold difference in oxidized products is already detectable after 1 h of reaction time and is subsequently observed at the last time-points (**Figure 17**). On the other hand, for the reaction containing 9 g/L lignin the difference between the light and dark reaction are smaller, indicating that the presence of a lot of lignin can partly compensate for the absence of light. Interestingly, in this case, the reaction without light-exposure yielded the highest level of oxidized products after 24 h, i.e., approximately 2-fold more than the reaction exposed to light (**Figure 17**). This difference related to the very different shapes of the progress curves: a massive boost followed by flattening in the reaction with light, versus an almost linear curve in the reaction without light.

These results show that, next to ascorbic acid, which is well known for its ability to drive LPMO reactions (Vaaje-Kolstad et al., 2010), lignin and light both affect the efficiency of LPMO reactions. The data also show that at higher lignin concentrations, the effect of a minor amount (20 µM) of AscA on LPMO activity becomes negligible.

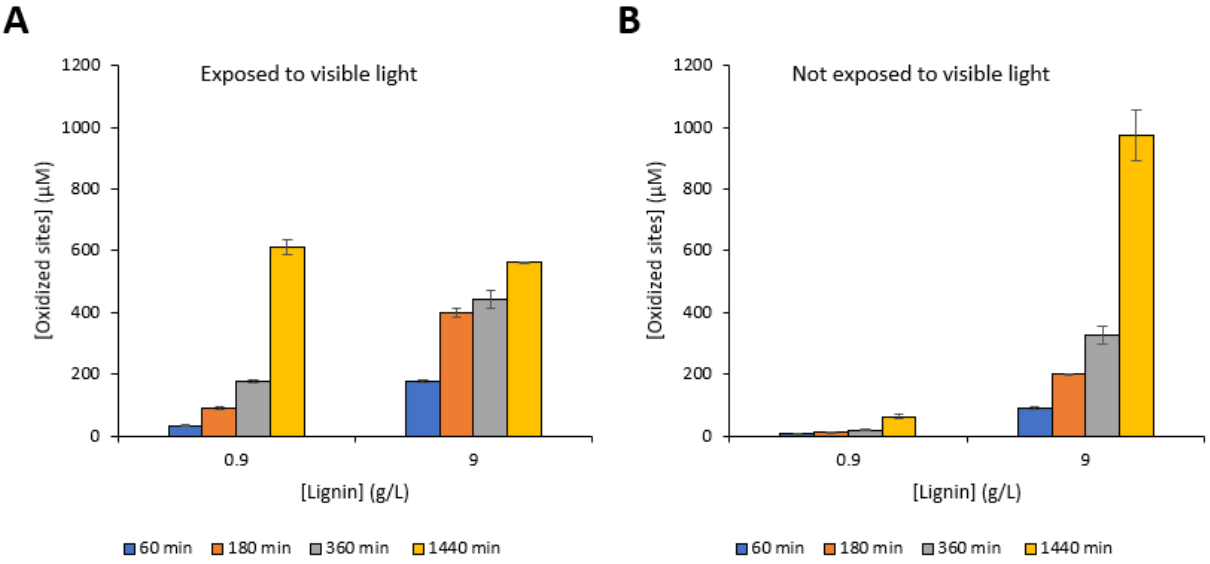

Figure 17. Product formation by *Sc*AA10C at given time points in reaction with lignin, in the presence or absence of visible light. The figure shows an overview of product levels at different time-points used to compare the reactions with *Sc*AA10C, Avicel and 0.9 or 9 g/L Kraft lignin from **Figure 16** up to 24 h, that were exposed **(A)** or not exposed **(B)** to visible light (I = 10 % of I_{max}, approximately 16.8 W.cm^{-2}). The concentration of *Sc*AA10C was 0.5 µM in all reactions. Reactions were performed in 50 mM sodium phosphate buffer pH 7.0 with 10 g/L Avicel and various concentrations of Kraft lignin (0.9, 9 g/L), at 40°C, for 24 h, with magnetic stirring. Soluble products, of varying degrees of polymerization, were treated with endoglucanase, *Tf*Cel5A, to yield oxidized products with a degree of polymerization of 2 (GlcGlc1A) or 3 (Glc_2Glc1A), which were analyzed by HPAEC-PAD and quantified, to yield the total amount of solubilized oxidized sites. Reactions were performed in duplicates, and the standard deviations are shown as error bars.

4.3.2. The effect of light intensity

The influence of light intensity on the ability of lignin to drive LPMO reactions was further characterized by applying different light intensities (0, 1, 3, 10, and 30 % of I_{max}) to reactions containing 0.9 or 9 g/L lignin, for up to 24 h. The results from these reactions are shown in **Figure 18**. Panel A shows that for reactions with 0.9 g/L lignin, the amount of product increased as the light intensity was increased, and that all progress curves were close to linear. Initially, there is a dose-response for light intensity at both lignin concentrations. But, as already observed above, the combination of high lignin concentration and high light intensity gives non-linear progress curves, as shown in panel B. The reaction in the dark progress linearly, while all reactions exposed to light show high rates at the beginning, followed by a decrease in reaction progress after approximately 1 hour (10 and 30 % light intensity) or 3 hours (1 and

3 % light intensity) reaction time. As a consequence, after 24 hours, the amount of product is less with 9 g/L lignin exposed to light (all light intensities), compared to the reactions in the dark (**Figure 18**). Interestingly, the figure shows that in the early phase of the reaction, the differences between the reactions with 0.9 or 9 g/L lignin is less at the highest light intensities. For example, at 60 min, the ratios between the amounts of products generated in the reactions with 9 and 0.9 g/L lignin are 13.7, 10.8, 10.6, 5.1, 5.5, for I = 0, 1, 3, 10, 30 %, respectively.

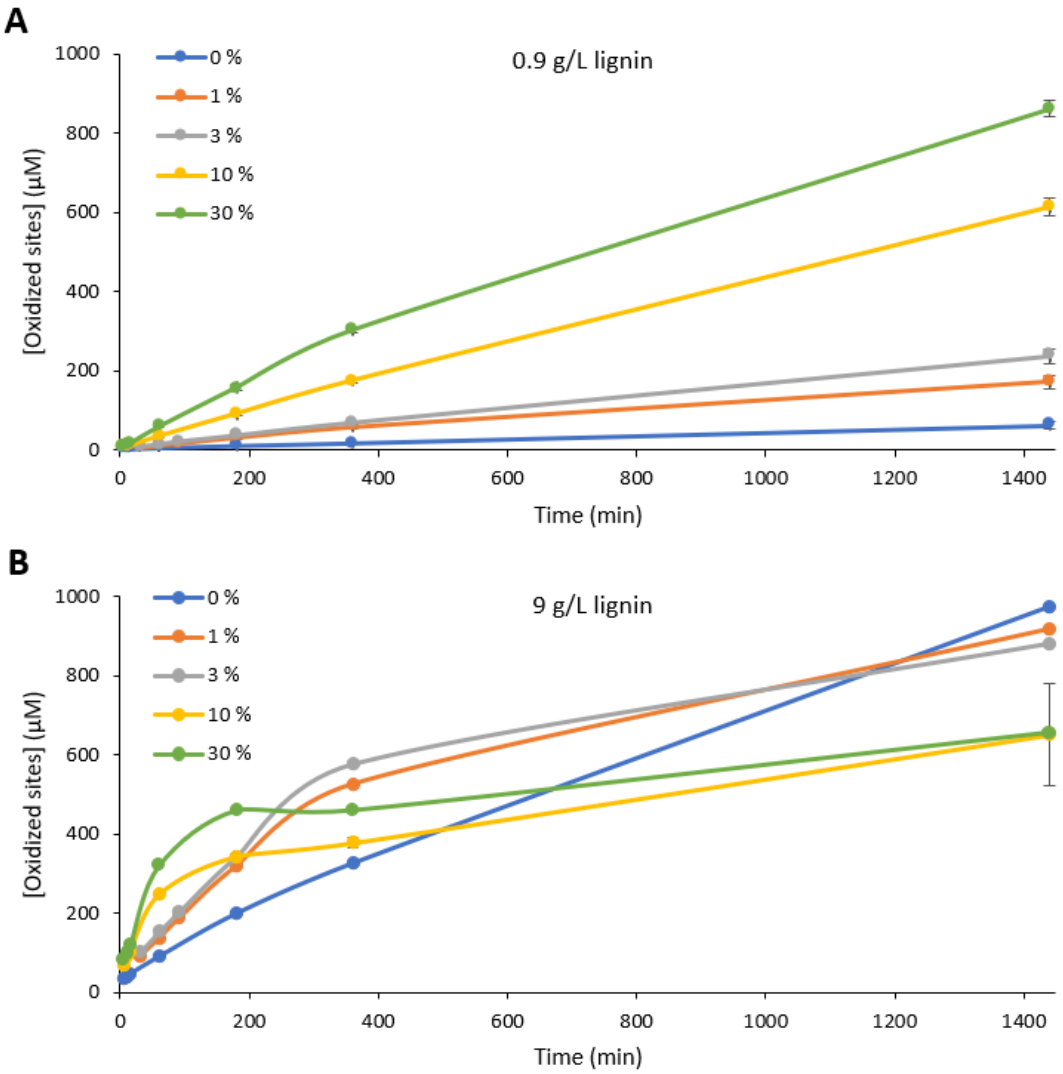

Figure 18. Effect of light intensity on LPMO product formation over time. The figure shows the influence of light intensity on the catalytic activity of *Sc*AA10C on Avicel in reactions with 0.9 g/L **(A)** or 9 g/L **(B)** Kraft lignin. The concentration of *Sc*AA10C was 0.5 µM in all reactions. Reactions were performed in 50 mM sodium phosphate buffer pH 7.0 with 10 g/L Avicel and various intensities of visible light (I = 0, 1, 3, 10, 30 % of I_{max}, corresponding to approximately 0, 1.7, 5.0, 16.8, 50.4 W.cm^{-2}, respectively), at 40°C, for 24 h, with magnetic stirring. Soluble products, of varying degrees of polymerization, were treated with endoglucanase. The reactions exposed to I = 0, 10 % of I_{max} were treated with *Tf*Cel5A, while the reactions exposed to I = 1, 3, 30 % of I_{max} were treated with *Tf*Cel6A, to yield oxidized products with a degree of polymerization of 2 (GlcGlc1A) or 3 (Glc_2Glc1A), which were analyzed by HPAEC-PAD and quantified, to yield the total amount of solubilized oxidized sites. Reactions were performed in duplicates, and the standard deviations are shown as error bars.

To illustrate the effect of light intensity, and the variation in the progress curves, the amount of oxidized products obtained after 24 h were plotted against the light intensity, as shown in **Figure 19**. For the reaction with 9 g/L lignin, the number of oxidized products obtained after 24 h was reduced by approximately one third when comparing the reaction in the dark (I = 0 % of I_{max}) with the reaction exposed to the highest light intensity (I = 30 % of I_{max}). It is worth noting that when looking at end-product levels only, and at this lignin concentration, the reaction in the dark is as productive (or better) as the reactions exposed to light. For the reactions with 0.9 g/L lignin, the amount of oxidized products obtained after 24 h was increased 13-fold, when comparing the reaction in the dark (I = 0 % of I_{max}) with the reaction exposed to the highest light intensity (I = 30 % of I_{max}). Without light exposure (I = 0 % of I_{max}) product accumulation in the reaction with 9 g/L lignin was approximately 16-fold higher compared to the reaction with 0.9 g/L lignin, and, as noted above, this difference becomes smaller with increasing light intensity (**Figure 19**).

These results show that increasing light intensity led to higher production rates at the beginning of the reactions, but also that the combination of high light intensity and high lignin concentration gave non-linear progress curves, thus lower end-product levels compared to reactions exposed to lower light intensities.

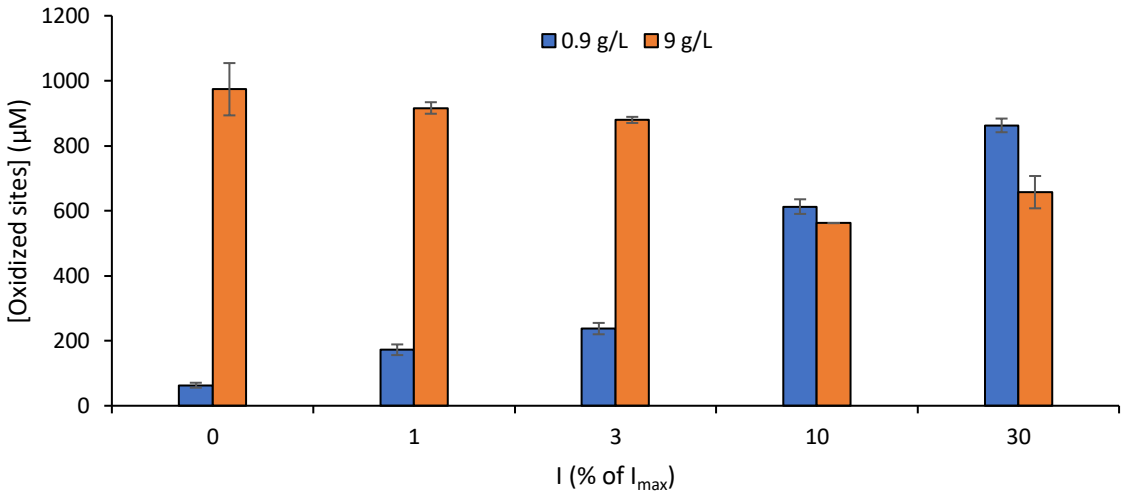

Figure 19. The effect of light intensity on product accumulation after 24 h. The figure shows the influence of light intensity on product formation after 24 h of the reactions in **Figure 18** with *Sc*AA10C and Avicel in the presence of 0.9 g/L **(blue)** or 9 g/L **(orange)** Kraft lignin. The concentration of *Sc*AA10C was 0.5 µM in all reactions. Reactions were performed in 50 mM sodium phosphate buffer pH 7.0 with 10 g/L Avicel and various intensities of visible light (I = 0, 1, 3, 10, 30 % of I_{max}, corresponding to approximately 0, 1.7, 5.0, 16.8, 50.4 $W.cm^{-2}$, respectively), at 40°C, for 24 h, with magnetic stirring. Soluble products, of varying degrees of polymerization, were treated with endoglucanase. The reactions exposed to I = 0, 10 % of I_{max} were treated with *Tf*Cel5A, while the reactions exposed to I = 1, 3, 30 % of I_{max} were treated with *Tf*Cel6A, to yield oxidized products with a degree of polymerization of 2 (GlcGlc1A) or 3 (Glc_2Glc1A), which were analyzed by HPAEC-PAD and quantified, to yield the total amount of solubilized oxidized sites. Reactions were performed in duplicates, and the standard deviations are shown as error bars.

4.3.3. The effect of LPMO concentration

To further characterize this photobiocatalytic system, reactions to investigate the effect of the LPMO-concentration were performed. This was achieved by varying the concentration of *Sc*AA10C from 0.1 to 10 µM in reactions with 0.9 g/L lignin exposed to visible light (I = 10 % of I_{max}), that were incubated for up to 6 h. The results show that there is no difference in terms of the amount of oxidized products obtained after 6 h nor in the production rate, between reactions with 0.1 or 10 µM *Sc*AA10C (**Figure 20**). Thus, under these conditions, the reaction was limited by other factors than the amount of enzyme, even at the lowest tested enzyme concentration.

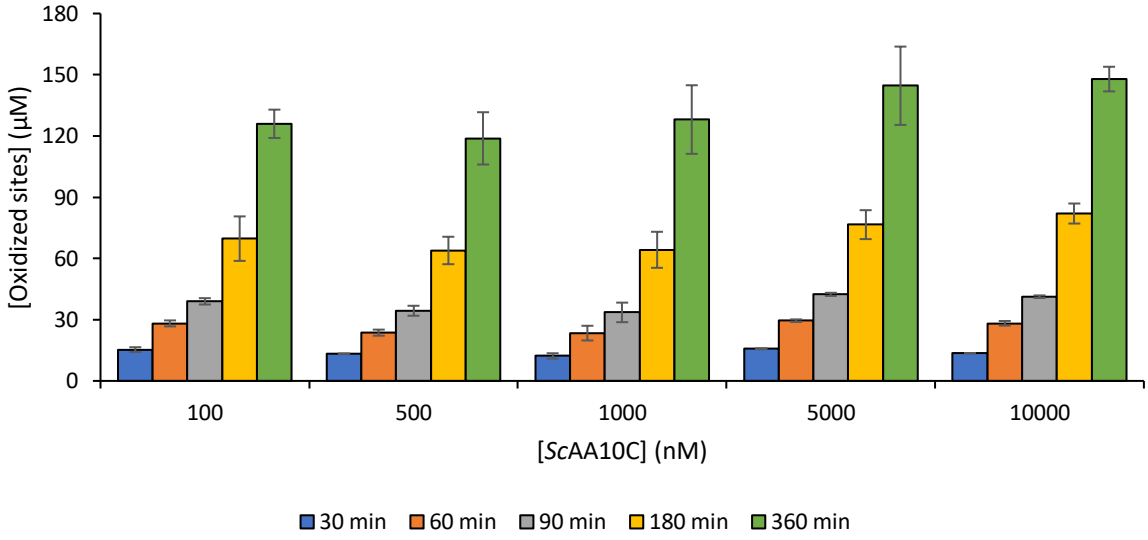

Figure 20. Influence of the LPMO concentration on *Sc*AA10C photobiocatalytic activity. The figure shows the influence of the LPMO concentration on the formation of oxidized products in reactions with Avicel, containing 0.9 g/L Kraft lignin, and exposed to visible light (I = 10 % of I_{max}, approximately 16.8 W.cm^{-2}). Reactions were performed in 50 mM sodium phosphate buffer pH 7.0 with 10 g/L Avicel, and various concentrations of *Sc*AA10C (0.1, 0.5, 1, 5, 10 µM), at 40°C, for 6 h, with magnetic stirring. Soluble products, of varying degrees of polymerization, were treated with endoglucanase, *Tf*Cel5A, to yield oxidized products with a degree of polymerization of 2 (GlcGlc1A) or 3 (Glc_2Glc1A), which were analyzed by HPAEC-PAD and quantified, to yield the total amount of solubilized oxidized sites. Reactions were performed in duplicates, and the standard deviations are shown as error bars.

4.3.4. The effect of a reductant

In Section 4.3.1, the effect of lignin on LPMO activity was investigated in reactions that did or did not contain 20 µM AscA. It was found that the minor amount of AscA, added 15 minutes prior to reaction start, did not influence the reaction that contained higher amounts of lignin. To properly characterize the putative role of AscA in these reactions, experiments were conducted in which AscA was added at

reaction start, as opposed to the reaction in 4.3.1, to final concentrations from 0 to 2000 µM, in reactions that contained 0.9 g/L lignin and were exposed to visible light (I = 10 % of I_{max}), for up to 24 h. The results, in **Figure 21**, shows that the reaction with the highest AscA concentration generated approximately 530 µM oxidized products within the first 60 min of the reaction, which corresponds to a rate of approximately 9 µM/min, after which the product accumulation curve flattened out and stabilized around 600 µM. The reaction with 200 µM AscA was slower, but in this case, the product formation continued over the full 24 hours incubation period, to reach approximately 1 mM product after 24 h. In this case, the rate estimated from the amount of product obtained after 60 min corresponds to 3 µM/min. The reactions with 0 and 20 µM AscA showed highly similar linear progress curves over 24 h, with rates in the order of 0.4 and 0.5 µM/min, respectively.

As presented above, the addition of AscA led to increased production rates and the total amount of accumulated end product levels for all reactions, except the reactions with the highest AscA concentration. The reactions with the highest AscA concentration showed high rates at the beginning, followed by flattening of the progression curve, thus yielded approximately equal accumulated end-product levels as the reactions without AscA.

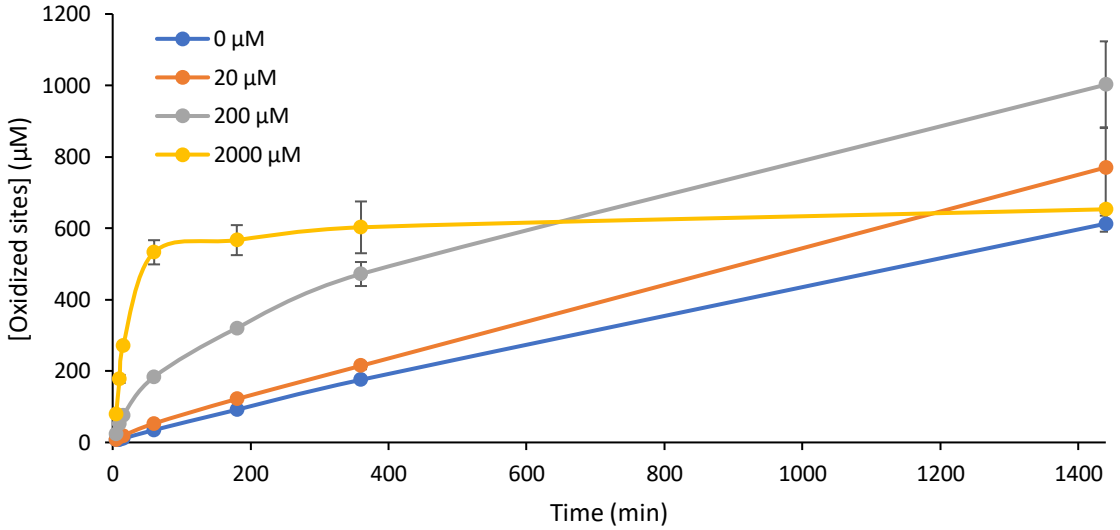

Figure 21. Influence of AscA on *Sc*AA10C photobiocatalytic activity. The figure shows the influence of AscA added at reaction start, on the catalytic activity of *Sc*AA10C on Avicel in reactions containing 0.9 g/L Kraft lignin, and exposed to visible light (I = 10 % of I_{max}, approximately 16.8 $W.cm^{-2}$). The concentration of *Sc*AA10C was 0.5 µM in all reactions. Reactions were performed in 50 mM sodium phosphate buffer pH 7.0 with 10 g/L Avicel, and various concentrations of AscA (0, 20, 200, 2000 µM), at 40°C, for 24 h, with magnetic stirring. Soluble products, of varying degrees of polymerization, were treated with endoglucanase, *Tf*Cel6A, to yield oxidized products with a degree of polymerization of 2 (GlcGlc1A) or 3 (Glc_2Glc1A), which were analyzed by HPAEC-PAD and quantified, to yield the total amount of solubilized oxidized sites. Reactions were performed in duplicates, and the standard deviations are shown as error bars.

4.3.5. The effect of superoxide dismutase

To probe the potential role of superoxide, $O_2^{\bullet-}$, in this photobiocatalytic system, reactions with increasing amounts of SOD were performed. This was achieved by varying the concentration of SOD from 0 to 3000 nM in reactions with 0.9 g/L lignin exposed to visible light (I = 10 % of I_{max}) and incubated for up to 6 h. Of note, SOD will convert superoxide to H_2O_2, which may be used as a co-substrate by the LPMO. The activity of the SOD enzyme had been verified prior to this study by Eirik Kommedal, as described by Bissaro et al. (2020). **Figure 22** shows that increasing SOD concentration led to an increase in the amount of oxidized products obtained after 6 h, and that the reactions go faster, but with similarly shaped progress curves for all SOD concentrations. The figure also shows that at lower SOD concentrations, the impact on the reactions was limited. For example, the reactions with 0, 10, and 100 nM SOD yielded 119, 148, and 179 µM of oxidized products after 6 h, and the rates derived from the first three time-points corresponded to 0.4, 0.5, and 0.6 µM/min, respectively. By increasing the SOD concentration to 300 nM, the end-product levels after 6 h increased to 287 µM, and the rate derived from the first three time-points increased to 0.9 µM/min. By further increasing the amount of SOD to 1000 and 3000 nM, yields of 375 µM and 478 µM oxidized products after 6 h, and rates of 1.1 and 1.3 µM/min were achieved, respectively. In summary, the use of 3000 nM SOD led to a 4-fold increase in the amount of oxidized products accumulated after 6 h compared to the reaction without SOD.

The clear effect of SOD on product formation by *Sc*AA10C indicates that superoxide formation indeed takes place in the photobiocatalytic reactions studied here.

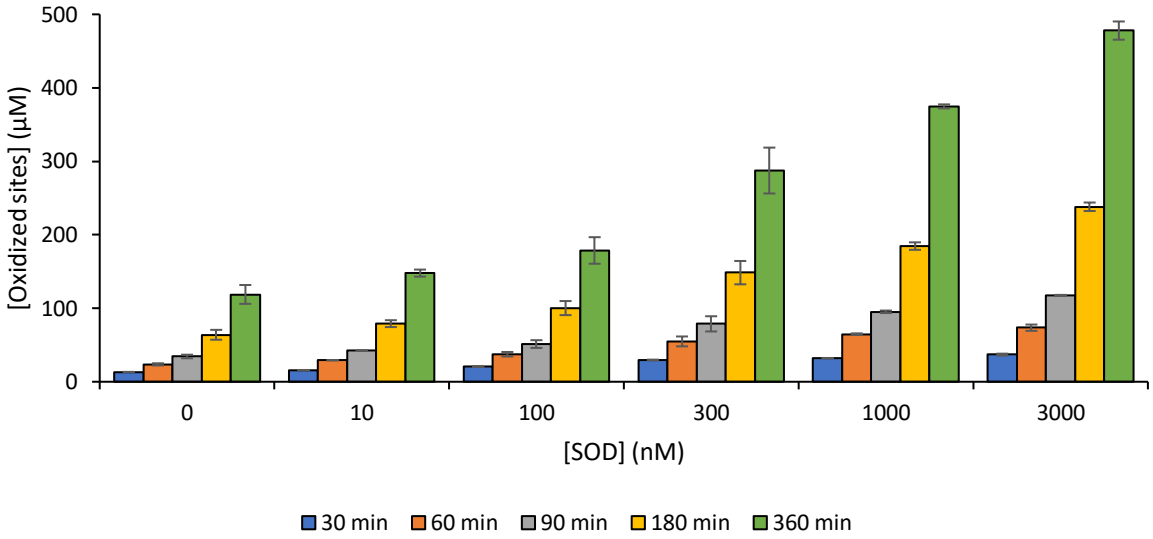

Figure 22. Influence of Superoxide Dismutase on *Sc*AA10C photobiocatalytic activity. The figure shows the influence of the SOD concentration on the catalytic activity of *Sc*AA10C on Avicel in reactions containing 0.9 g/L Kraft lignin and exposed to visible light (I = 10 % of I_{max}, approximately 16.8 W.cm^{-2}). The concentration of *Sc*AA10C was 0.5 µM in all reactions. Reactions were performed in 50 mM sodium phosphate buffer pH 7.0 with 10 g/L Avicel and various concentrations of SOD (0, 10, 100, 300, 1000, 3000 nM), at 40°C, for 6 h, with magnetic stirring. Soluble products, of varying degrees of the polymerization, were treated with endoglucanase. The reactions with 0 – 100 and 1000 nM SOD were treated with *Tf*Cel5A, while the reactions with 300 and 3000 nM SOD were treated with *Tf*Cel6A, to yield oxidized products with a degree of polymerization of 2 (GlcGlc1A) or 3 (Glc_2Glc1A), which were analyzed by HPAEC-PAD and quantified, to yield the total amount of solubilized oxidized sites. Reactions were performed in duplicates, and the standard deviations are shown as error bars.

4.3.6. The effect of transition metals, Mn(II) and Cu(II)

The LPMO activity depends on the coordination of a copper atom in the catalytic site, which can bind multiple bivalent metals (Aachmann et al., 2012). The superoxide dismutase used in these studies is manganese dependent (Mn-SOD), which means that by adding this enzyme, one also adds a transition metal. To look at the effect of free transition metals on the catalytic activity of *Sc*AA10C, reactions with various concentrations of Mn(II)SO_4 (0.1 to 10 mM) or Cu(II)SO_4 (2 to 200 µM), in reactions with 0.9 g/L lignin and exposed to visible light (I = 10 % of I_{max}), were conducted, and these were incubated for up to 6 h. The results are shown in **Figure 23.** Panel A shows that the addition of manganese indeed did influence the LPMO activity. The figure shows that the reaction with 0.1 mM Mn(II)SO_4 corresponds to the highest end-product level after 6 h reaction, 617 µM, an approximately 3.5-fold increase in the total amount of accumulated products after 6 h, when comparing to the reaction without added manganese. The rates derived from the first three time-points corresponded to 0.6, 2.0, 2.0, and 1.7 µM/min, for the reactions with 0, 0.1, 1 and 10 mM Mn(II)SO_4, respectively. The accumulated end product levels after 6 h are lower with the highest Mn(II)SO_4 concentrations, compared to the lowest

$Mn(II)SO_4$ concentration. Panel B shows that the presence of $Cu(II)SO_4$ up to 200 µM did not influence the amount of accumulated oxidized products obtained after 6 h, nor the apparent production rate of the reactions.

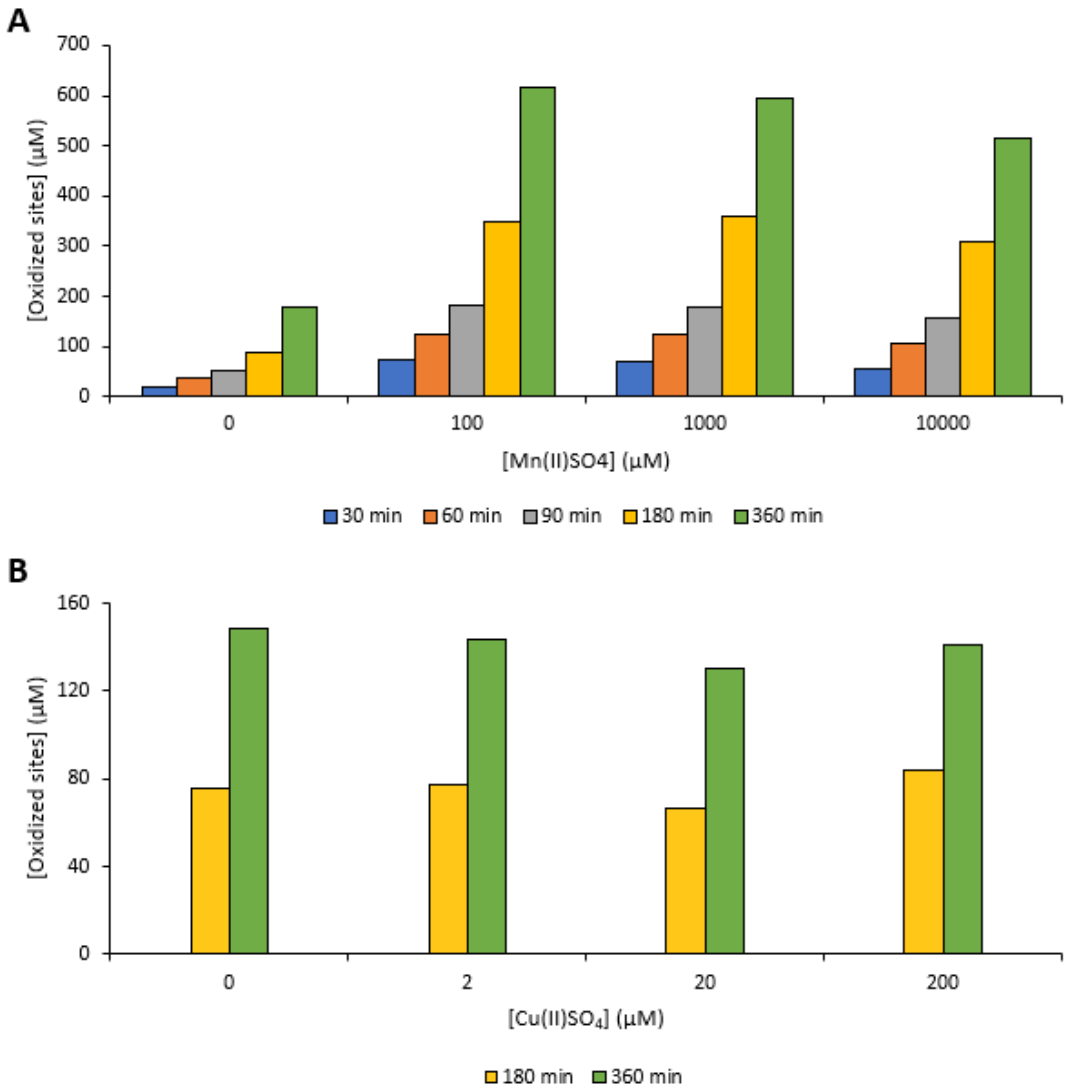

Figure 23. Influence of transition metals Cu(II) and Mn(II) on *Sc*AA10C photobiocatalytic activity. The figure shows the influence of $Mn(II)SO_4$ **(A)** or $Cu(II)SO_4$ **(B)** on the activity of *Sc*AA10C on Avicel in reactions containing 0.9 g/L Kraft lignin and exposed to visible light (I = 10 % of I_{max}, approximately 16.8 $W.cm^{-2}$). The concentration of *Sc*AA10C was 0.5 µM in all reactions. Reactions were performed in 50 mM sodium phosphate buffer pH 7.0 with 10 g/L Avicel, and various concentrations of $Mn(II)SO_4$ (0, 0.1, 1, 10 mM) or $Cu(II)SO_4$ (0, 2, 20, 200 µM), at 40°C, for 6 h, with magnetic stirring. Soluble products, of varying degrees of the polymerization, were treated with endoglucanase. The reactions with $Cu(II)SO_4$ were treated with *Tf*Cel5A, while the reactions with $Mn(II)SO_4$ were treated with *Tf*Cel6A, to yield oxidized products with a degree of polymerization of 2 (GlcGlc1A) or 3 (Glc_2Glc1A), which were analyzed by HPAEC-PAD and quantified, to yield the total amount of solubilized oxidized sites. Reactions were performed as single experiments.

4.3.7. The effect of lignin from various sources and subjected to different pretreatments

The effects of lignin samples of different origin and subjected to different pretreatments on the LPMO activity in light-fueled reactions are displayed in **Figure 24**. The lignins used were commercial Kraft lignin from Sigma-Aldrich and multiple wood samples treated by steam-explosion (SE). The steam-exploded wood samples originated from Birch-wood and Spruce-wood. The lignin sample from Birch-wood had been treated by SE at 210°C as described by Costa et al. (2019), and Spruce-wood lignin had been treated by SE at 210°C or 220°C with or without prior 2-naphthol (2-NAP) treatment at each temperature. Reactions containing 0.9 g/L lignin from either Sigma-Aldrich, lignin sample from Birch-wood, or lignin samples from Spruce-wood subjected to various pretreatments, exposed to visible light (I = 10 % of I_{max}) were conducted, and these were incubated for up to 6 h.

Figure 24 compares the LPMO activity between the reactions with lignin from the different sources. The initial production rates depended on the type of lignin used, but all reactions progressed linearly during the 6 h incubation period. The figure shows that the reaction with lignin from Spruce-wood yielded 2- and 4- fold higher total product accumulation after 6 h compared to the reaction with lignin from Birch-wood or Kraft lignin, respectively (**Figure 24**). The lignin samples from Spruce-wood impregnated included in **Figure 24** had been treated by impregnation with 2-NAP prior to SE at 220°C, the lignin samples showing the highest accumulated end product level in **Appendix B**. The comparison between the Spruce-wood lignin samples show increasing activity with the increasing SE temperature, and display a 2-fold increase between the samples with or without impregnation with 2-NAP, at the given temperatures (**Appendix B**).

The results show that different origin and pretreatment of lignin impacts lignin's ability to fuel LPMO reactions when exposed to visible light. However, it cannot be excluded that the observed differences in LPMO activity can be attributed to the different amount of lignin in the various samples. It has already been shown that a possible difference in lignin content between the lignin samples also strongly affected the progress curves (Muraleedharan et al., 2018).

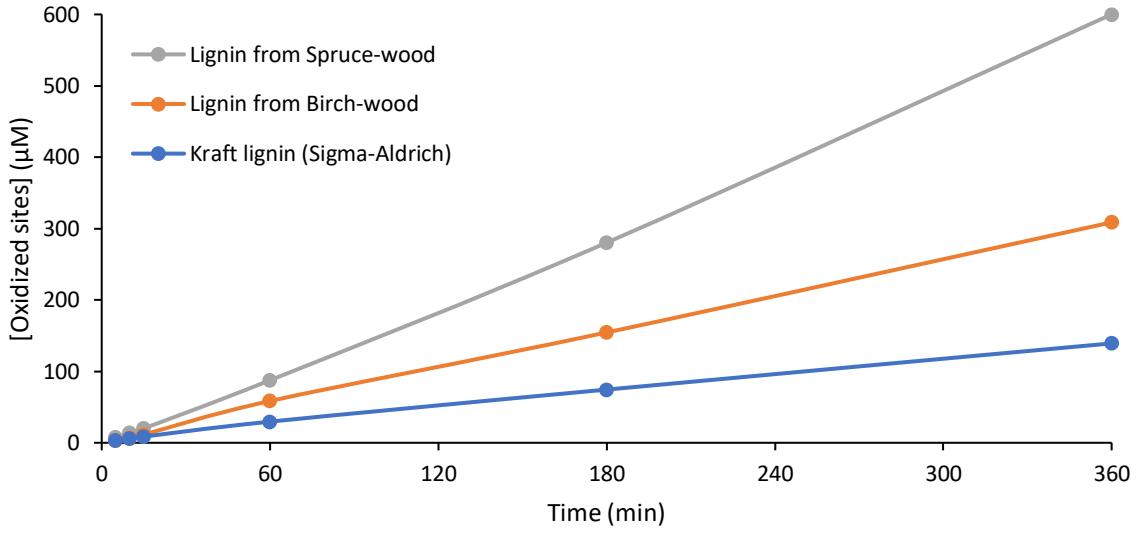

Figure 24. Influence of various types of lignin on *Sc*AA10C photobiocatalytic activity. The figure shows how lignin samples of different origin and subjected to different pretreatments influence the activity of *Sc*AA10C on Avicel in reactions containing 0.9 g/L lignin from the various lignin sources and exposed to visible light (I = 10 % of I_{max}, approximately 16.8 W.cm^{-2}). The concentration of *Sc*AA10C was 0.5 µM in all reactions. The various lignin sources were Kraft lignin from Sigma-Aldrich, lignin from Birch-wood, and lignin from Spruce-wood. The Spruce-wood lignin sample had been pretreated by impregnation with 2-NAP and SE at 220°C, and was the sample with the highest yield from **Figure B1** in **Appendix B,** which compares Spruce-wood lignin samples subjected to various pretreatments. Reactions were performed in 50 mM sodium phosphate buffer pH 7.0 with 10 g/L Avicel, at 40°C, for 6 h, with magnetic stirring. Soluble products, of varying degrees of polymerization, were treated with endoglucanase, *Tf*Cel5A, to yield oxidized products with a degree of polymerization of 2 (GlcGlc1A) or 3 (Glc_2Glc1A), which were analyzed by HPAEC-PAD and quantified, to yield the total amount of solubilized oxidized sites. Reactions were performed as single experiments.

4.3.8. Control reactions

To show that cellulose oxidation depended on the presence of the LPMO, various control reactions were performed. These controls included reactions without *Sc*AA10C, with Avicel, in the presence or absence of 0.9 g/L lignin and with or without exposure to visible light (I = 10 % of I_{max}, approximately 16.8 W.cm^{-2}), for up to 24 h. It was also conducted control reactions added 0.5 µM *Sc*AA10C, with Avicel, in the presence or absence of 20 µM AscA, and exposed to visible light (I = 10 % of I_{max}, approximately 16.8 W.cm^{-2}), for up to 24 h. The positive control reaction was a reaction with 0.5 µM *Sc*AA10C, 0.9 g/L lignin, Avicel, and exposed to visible light (I = 10 % of I_{max}, approximately 16.8 W.cm^{-2}), for up to 6 h. The chromatographic product profile for each control reaction and the positive control is shown in **Figure 25.**

Reactions in the absence of *Sc*AA10C do not show any oxidized products. Only the reaction containing *Sc*AA10C and a reductant, AscA or lignin, show oxidized products after a 24 h incubation period. The peaks in the chromatogram from the reaction with *Sc*AA10C exposed to visible light in the absence of

both lignin and AscA, is so small that they are not visible, but it is shown formation of approximately 15 µM oxidized sites in the reaction after 24 h in **Figure A1** in **Appendix A**. The peaks in the chromatogram from the positive control, from left to right, correspond to cellobiose, cellotriose, cellobionic acid (GlcGlc1A), and cellotrionic acid (Glc_2Glc1A) (**Figure 25**).

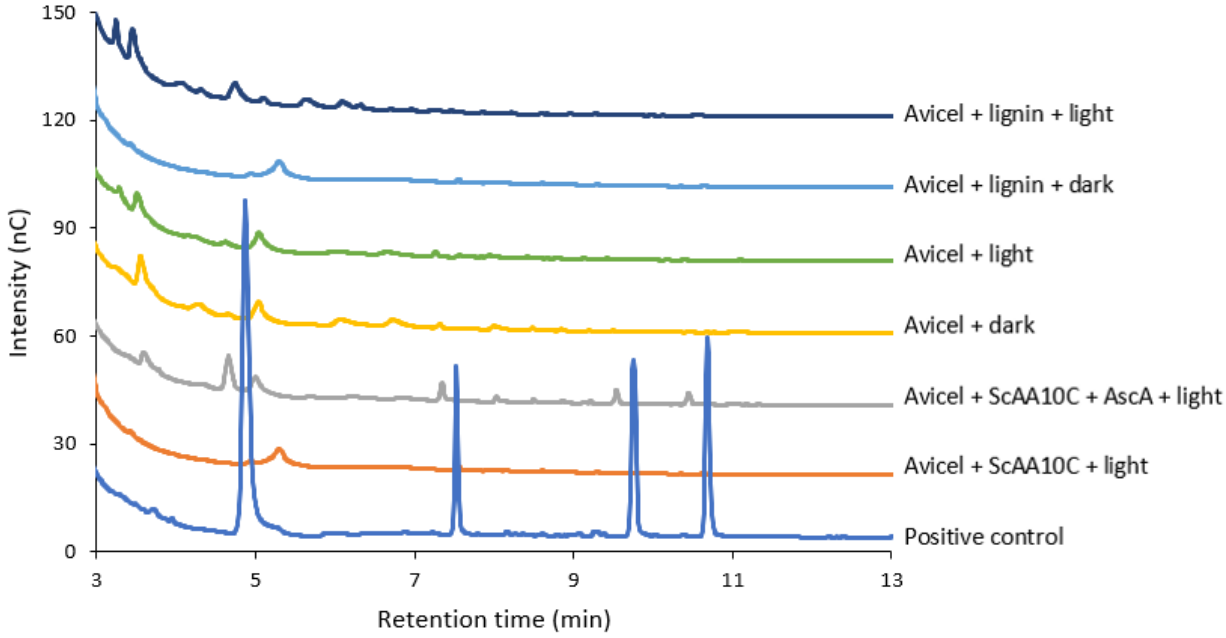

Figure 25. Control reactions to check for the occurrence of non-specific cellulose oxidation in the absence of *Sc*AA10C and/or reducing power. The figure shows chromatographic product profiles of various control reactions with or without the addition of 0.5 µM *Sc*AA10C, containing 10 g/L Avicel, and conducted in the dark or exposed to visible light (I = 10 % of I_{max}, approximately 16.8 $W.cm^{-2}$). Control reactions carried out without *Sc*AA10C, with 0.9 g/L lignin in the presence (**Avicel + lignin + light**) or absence (**Avicel + lignin + dark**) of visible light, for up to 24 h. Control reactions performed without both lignin and *Sc*AA10C in the presence (**Avicel + light**) or absence (**Avicel + dark**) of light, for up to 24 h. Control reactions carried out with 0.5 µM *Sc*AA10C, 0.9 g/L Kraft lignin, exposed to visible light and in the presence (**Avicel + *Sc*AA10C + AscA + light**) or absence (**Avicel + *Sc*AA10C + light**) of 20 µM AscA, for up to 24 h. The positive control includes 0.5 µM *Sc*AA10C, 0.9 g/L Kraft lignin, and exposed to visible light, and was incubated for up to 6 h (**Positive control**). The peaks in the chromatogram from the positive control, from left to right, correspond to cellobiose, cellotriose, cellobionic acid (GlcGlc1A), and cellotrionic acid (Glc_2Glc1A). All reactions were performed in 50 mM sodium phosphate buffer pH 7.0, at 40°C, with magnetic stirring. Soluble products, of varying degrees of polymerization, were treated with endoglucanase, *Tf*Cel5A, to yield oxidized products with a degree of polymerization of 2 (GlcGlc1A) or 3 (Glc_2Glc1A), which were analyzed by HPAEC-PAD and quantified, to yield the total amount of solubilized oxidized sites. Two independent replicates of the experiments were carried out.

To elucidate whether the presence of free copper in the solution can react in Fenton chemistry and contribute to the production of oxidized sites, reactions where *Sc*AA10C has been replaced with Cu(II)SO_4 up to 1 mM, with 0.9 g/ lignin and exposed for visible light (I = 10 % of I_{max}, approximately 16.8 W.cm^{-2}), were performed for up to 24 h. The chromatographic product profile for each control reaction is shown in **Figure 26,** including a positive control reaction conduced with 0.5 µM *Sc*AA10C, 0.9 g/L lignin, and exposed to visible light (I = 10 % of I_{max}, approximately 16.8 W.cm^{-2}), for up to 6 h.

There is not shown any oxidized products in the reactions with Cu(II)SO_4 up to 1 mM and without *Sc*AA10C (**Figure 26**). The peaks in the positive control chromatogram, from left to right, correspond to cellobiose, cellotriose, cellobionic acid (GlcGlc1A), and cellotrionic acid (Glc_2Glc1A) (**Figure 26**).

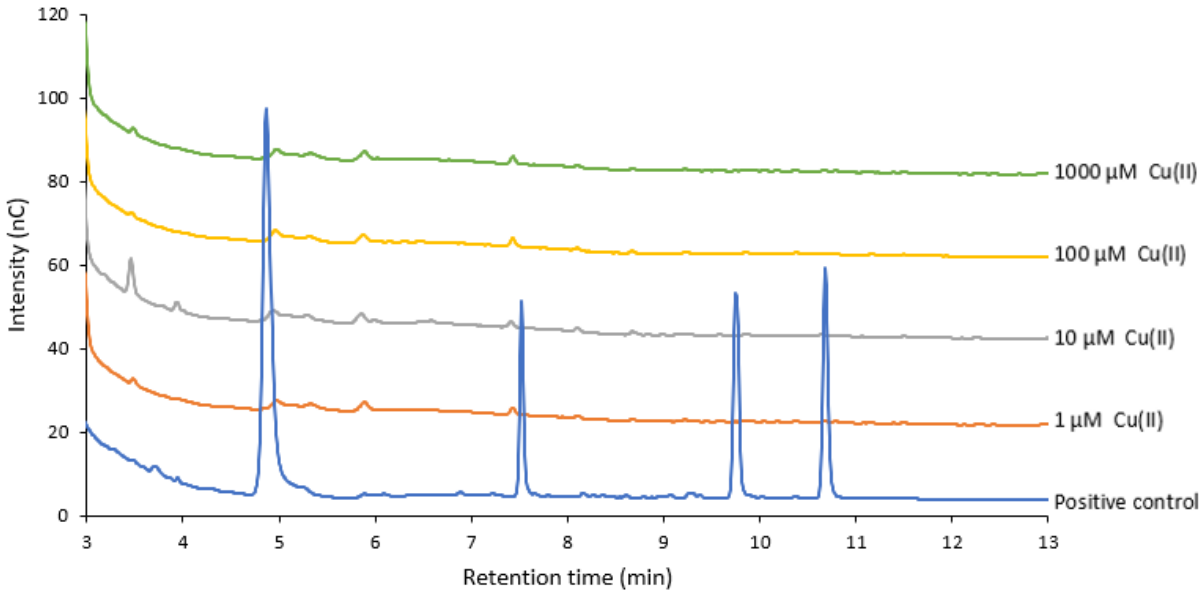

Figure 26. Control reactions to check for the occurrence of copper-catalyzed Fenton-type chemistry. The figure shows chromatographic product profiles for four control reactions where *Sc*AA10C was replaced by Cu(II)SO_4 (1 – 1000 µM). All reactions contained 10 g/L Avicel, 0.9 g/L Kraft lignin, and were exposed to visible light (I = 10 % of I_{max}, approximately 16.8 W.cm^{-2}), for up to 24 h. The control reactions were conducted without *Sc*AA10C with various concentrations of Cu(II)SO_4 (1, 10, 100, 1000 µM), for up to 24 h. The positive control was performed with 0.5 µM *Sc*AA10C, and incubating for up to 6 h, showing peaks representing Glc_2, Glc_3, GlcGlc1A, and Glc_2Glc1A, from left to right, respectively. All reactions were carried out in 50 mM sodium phosphate buffer pH 7.0, 40°C, with magnetic stirring. Soluble products, of varying degrees of polymerization, were treated with e, *Tf*Cel5A, to yield oxidized products with a degree of polymerization of 2 (GlcGlc1A) or 3 (Glc_2Glc1A), which were analyzed by HPAEC-PAD and quantified, to yield the total amount of solubilized oxidized sites. Two independent replicates of the experiments were carried out.

5. Discussion

The main objective of the work described in this thesis has been to study how light-exposed lignin influences the ability of cellulose-active LPMO, *Sc*AA10C, to depolymerize microcrystalline cellulose, Avicel. This thesis was based on previous studies in which light and a photosensitizer were combined to provide an LPMO with reducing equivalents and co-substrate, H_2O_2. These previous studies have looked at how combinations of chlorophyllin and AscA (Bissaro et al., 2020; Cannella et al., 2016; Möllers et al., 2017) or chlorophyllin alone (Bissaro et al., 2020) can drive an LPMO reaction. Other studies have investigated the potential of using vanadium-doped titanium dioxide (Bissaro et al., 2016a; 2020), an inorganic photocatalyst. The most recent study, by Bissaro et al. (2020), showed that fueling LPMO reactions via light-exposure of a photosensitizer does not require the addition of an external reductant and highlighted the importance of controlling the reactive oxygen species produced in the system. Reactive oxygen species have also been shown to contribute to photodegradation of lignin in solution (Neumann & Machado, 1989), and the formation of hydrogen peroxide by light-exposed lignin was recently demonstrated by Miglbauer et al. (2020). Thus, the goal of this work was to investigate light-driven LPMO reactions using lignin as a photosensitizer and study how different parameters such as lignin concentration, light intensity, enzyme concentration, the presence of a reductant such as AscA, and superoxide's role in the system, affect the catalytic action of *Sc*AA10C towards Avicel.

5.1. Lignin as a photosensitizer in LPMO reactions

Overall, the catalytic efficiency of *Sc*AA10C towards Avicel increased with increasing lignin concentration, both in terms of initial reaction rates and the total amount of oxidized products obtained after 24 hours of reaction. Comparing the light-exposed reactions to the reactions performed in the dark revealed substantial differences (**Figures 16 & 17**). Since the focus of this study was to investigate the interaction between visible light and lignin, the effect of lignin on *Sc*AA10C activity without light exposure is outside the scope of this thesis and will not be discussed further in other Sections. It is important to note, though, that the results described in Section 4.3.1 show that the effects of exposing a reaction with little lignin to light may also be obtained by increasing the lignin concentration in reactions performed in the dark. Overall, these results confirm that lignin in light-exposed reactions accelerates LPMO activity.

To ensure that the LPMO was in its catalytic state, i.e., the Cu(I)-state, a reductant, AscA, was added (**Figure 16**). The addition should have occurred immediately prior to turning on the light to start the LPMO reactions, but for these reactions, AscA was added prior to the 15 min pre-incubation step. This was rectified for the reactions studying the effect of a reductant (**Figure 21**). The difference in terms of both production rate and accumulated end product levels between the reactions exposed to light, in the presence or absence of AscA was negligible (**Figure 16**). The lack of effects by the addition of AscA confirms that lignin itself reduces *Sc*AA10C. Thus, the reduction of the LPMO in light-exposed reactions with lignin is not dependent on the addition of an external reductant. The same was shown in similar reactions performed in the dark. On the other hand, the addition of AscA had a higher impact on the reactions with low concentrations of lignin compared to the reactions with high concentrations of lignin. This probably reflects the absence of sufficient amounts of reducing equivalence produced by lignin, in the reactions with low lignin concentrations.

If hydrogen peroxide accumulates in LPMO reactions, enzymes that are not bound to the polysaccharide substrate may engage in futile H_2O_2 turnover which, may lead to damage to the catalytic center and LPMO inactivation (Bissaro et al., 2017; Loose et al., 2018). Miglbauer et al. (2020) showed that exposing lignosulfonate in solution to blue light (λ_{max} = 400 nm, 120 mW.cm^{-2}) with a continuous supply of O_2 yielded considerable amounts of H_2O_2. Thus, the most likely explanation for why product formation in the light-exposed reaction containing 9 g/L lignin levels off after a few hours was LPMO inactivation due to H_2O_2 accumulation. Increased production of H_2O_2 can also explain the massive boost in LPMO activity in the light-exposed reactions with 0.9 g/L lignin compared to those in the dark. These results are further substantiated by Kont et al. (2019). Kont et al. showed that the catalytic activity of LPMOs, in reactions supplemented with the liquid fraction obtained from hydrothermal pretreatment of wheat straw, was governed by LPMO-independent H_2O_2 formation in the liquid fraction. Although H_2O_2 levels were not measured in this work, based on previous work it seems likely that H_2O_2 is being produced in reactions with lignin (Cannella et al., 2016; Kont et al., 2019; Perna et al., 2019), and that light-exposure accelerates the generation of H_2O_2 (Miglbauer et al., 2020; Neumann & Machado, 1989).

The mechanism by which lignin in a photobiocatalytic reaction induces *Sc*AA10C activity is not known, but there are some hypotheses. Recent studies show that LPMOs are peroxygenases and that their catalytic activity depends on an initial priming reduction and supply of hydrogen peroxide (Bissaro et al., 2016a; Bissaro et al., 2017; Bissaro et al., 2020; Chylenski et al., 2019; Loose et al., 2018; Müller et al., 2018). Bissaro et al. (2020) showed that light-exposed chlorophyllin generated superoxide, thus providing *in situ* reducing power for LPMOs and removing the need for adding an external reductant. The work presented in this thesis also shows that light-exposed lignin does not depend on the external

addition of a reductant (**Figure 16**). Direct reduction of LPMOs by lignin-derived compounds is another possibility (Kracher et al., 2016; Westereng et al., 2015). Various studies have shown that reactions involving O_2 and lignin can produce H_2O_2 (Kont et al., 2019; Perna et al., 2019). In Miglbauer and colleagues' (2020) study of H_2O_2-production by light-exposed lignosulfonates, they speculate that the first step is a single-electron reduction of O_2 to $O_2^{\bullet-}$ which would further disproportionate into H_2O_2, similar to what Bissaro et al. (2020) showed using light-exposed chlorophyllin. Based on previous studies and the lack of need for externally delivered electrons in the light-exposed system with lignin (**Figure 16**), the production of $O_2^{\bullet-}$ in the system is believed to be responsible for the reduction of the LPMO, before it is spontaneously converted into H_2O_2. Further evidence for the formation and importance of superoxide comes from the experiments with SOD, Mn(II), higher amounts of AscA, and the exposure to various light intensities, which are discussed in the Sections below.

Combining previous studies showing that LPMOs can be fueled with H_2O_2 and reducing power in photobiocatalytic reactions (Bissaro et al., 2020; Cannella et al., 2016), together with lignin's ability to produce H_2O_2 in light-exposed reactions (Miglbauer et al., 2020), suggests that lignin functions as a photosensitizer. Lignin as a photosensitizer will be oxidized by light exposure, leading to the reduction of molecular oxygen to superoxide under aerobe conditions. The presence of superoxide will lead to the priming reduction of *Sc*AA10C, whereas most $O_2^{\bullet-}$ is spontaneously converted into H_2O_2. In addition, there has been shown that the presence of a reductant or other redox compounds, i.e., from lignin, enzymatically speeds up the conversion of $O_2^{\bullet-}$ to H_2O_2 (Bissaro et al., 2017).

Control reactions to verify that the oxidized products were formed due to the presence of lignin were performed. In the reactions without lignin, but in the presence of 20 µM AscA, only a low amount of oxidized products was detected, which was expected since the reactions contained a low amount of reducing agent (**Figure 25**). However, the reactions containing no lignin and no AscA also show minute amounts of oxidized products (**Figure A1, Appendix A**), while these reactions seemingly lack reducing power. The most plausible explanation for this result was that some residual lignin or AscA were left in the vials from previous experiments. Further, control reactions in the absence of *Sc*AA10C were performed to verify that the substrate, Avicel, did not contain any compounds possibly influencing the LPMO reaction. These control reactions did not show any product formation (**Figure 25**). No oxidized cello-oligosaccharides were observed when *Sc*AA10C was replaced by free Cu(II) in reactions with and without lignin, confirming that oxidized cello-oligosaccharides are the result of LPMO activity in these reactions (**Figure 26**).

To verify the hypothesis that the LPMO reactions in the present study were governed by H_2O_2 generation, assays measuring H_2O_2 production in this system should be performed. Such experiments

are not straightforward since lignin is a complex aromatic polymer that may absorb at the same wavelength as the reporter molecule used as a proxy for H_2O_2, and lignin may itself react with H_2O_2 resulting in a lower apparent H_2O_2 concentration. Another way to show that H_2O_2 production governs the LPMO activity would be a competition experiment with horseradish peroxidase, as described in Bissaro et al. (2017; 2020) and Kont et al. (2019). If H_2O_2 determines LPMO activity, then adding increasing amounts of HRP would inhibit LPMO activity, because HRP removes H_2O_2. The absence of LPMO activity by the addition of HRP would confirm that H_2O_2 is produced in the system.

Control experiments should be performed to determine if the flattening of the progress curves in specific reactions, such as the light-exposed reaction with 9 g/L lignin shown in **Figure 17,** was due to enzyme inactivation. To do so, reactions in similar conditions should be performed in which the reactions are supplemented with either substrate, reductant, lignin or LPMO, or combinations thereof after product formation had leveled off. Adding more substrate would determine if the reactions level off due to substrate depletion, but this seems unlikely given that other reactions proceeded to produce higher amounts of oxidized products. If there was a lack of reducing power in the system and all LPMOs are in a Cu(II)-state, then adding more AscA or lignin would result in more LPMO activity. Lastly, if only the addition of more *Sc*AA10C yields more oxidized products, then it was most likely such that the enzyme had been inactivated under these conditions. Bissaro et al. (2020) showed that in their reactions with Chl/light, only the addition of more LPMO resulted in more oxidized products under similar conditions as presented here.

To further investigate the mechanism for how the combination of lignin and light boosts the LPMO reactions, anaerobic reactions should be performed. Anaerobic reactions will show if this system depends on the presence of O_2 to reduce the LPMO and/or generate H_2O_2. It could be envisioned that lignin is able to reduce the LPMO in anaerobic settings, but not able to generate H_2O_2. This would confirm findings that lignin itself can directly reduce the LPMO. If lignin is able to both reduce the LPMO and generate H_2O_2 in anaerobic settings, then this would indicate that light-exposed lignin is able to oxidize water.

Even though multiples control reactions and other experiments should be performed to understand further the mechanism of this photobiocatalytic system, the results presented here clearly demonstrate that lignin acts as a photosensitizer. It further demonstrates that these reactions depend on the lignin concentration and that the combination of high lignin concentration exposed to visible light is detrimental to the LPMO, most likely due to oxidative damage of the catalytic site caused by H_2O_2 accumulation

5.2. Light intensity determines the efficiency of LPMO reactions

To study how the light intensity influences the LPMO activity, reactions with 0.9 or 9 g/L lignin exposed to various light intensities, up to 30 % of I_{max} (approximately 50.4 $W.cm^{-2}$), were performed. Overall the results show a clear correlation between increasing light intensity and increasing production rates. While combining high light intensity and high lignin concentrations revealed a negative effect on the accumulated end-product levels (**Figures 18 & 19**). These reactions experienced a massive boost in the production rate during the first few hours of reaction, followed by a rapid flattening of the progress curves. The flattening of the progress curve is most likely due to LPMO inactivation as a result of high levels of H_2O_2, as discussed in Section 5.1. The recently published study by Bissaro et al. showed a distinct correlation between the production of superoxide and the light intensity in a photobiocatalytic system with chlorophyllin and LPMO (Bissaro et al., 2020). Hence, it is reasonable to believe that the increased activity in the photobiocatalytic system described here also was due to the increasing generation of $O_2^{\bullet-}$ with higher light intensities and that $O_2^{\bullet-}$ disproportionates into H_2O_2, thus speeding up the *Sc*AA10C catalytic activity on Avicel.

The results show a significant difference between the amount of accumulated products in the first hour of reaction, when comparing reactions with 0.9 or 9 g/L lignin exposed to low light intensities. The difference in the total amount of accumulated products between the same reactions gets less significant with increasing light intensity (**Figure 19**). When comparing the reactions exposed to the highest light intensity against the reactions not exposed to light, the rate of total accumulated products between reactions with 9 or 0.9 g/L lignin is halved. The results indicate that the use of high light intensity can partly compensate for the amount of lignin present, by producing high amounts of $O_2^{\bullet-}$.

Product formation in the reactions with 9 g/L lignin exposed to high light intensities (I = 10 and 30 % of I_{max}) stagnated early but did not completely stop, and some products seemingly kept accumulating for up to 24 hours. Assuming that the enzyme became inactivated (see above), this is an unexpected observation. All reactions were performed at 40°C, which over time, probably led to some evaporation of the reaction solution. Indeed, for all reactions that were incubated for 24 hours, loss of reaction volume was observed, which probably increased with increasing light exposure. The apparent accumulation of oxidized products after *Sc*AA10C most likely had been inactivated (between 3 and 6 hours), probably is a result of increasing concentrations in the reaction solution over time due to evaporation, and not to further hydroxylating of Avicel by *Sc*AA10C.

The results show that the efficiency of the photobiocatalytic system increase with light intensity, but that the combination of high lignin concentration and high light intensity led to non-linear progress

curves due to harmful levels of H_2O_2, resulting in LPMO inactivation and less product accumulation over time.

5.3. The LPMO concentration is not limiting the reaction

The effect of the enzyme concentration on product formation from Avicel was studied by adding different concentrations of *Sc*AA10C to light-exposed reactions with lignin. There was no effect of varying LPMO concentration, on neither the product rate nor the amount of accumulated end product levels (**Figure 20**). The lack of effect indicates that the enzyme was not the rate-limiting factor in the system. Other possible limiting factors are the amount of H_2O_2 produced by lignin and, thus, the amount of lignin, the substrate concentration, or the amount of available reducing power. Further studies are needed to address these possibilities.

Studies of different substrate concentrations are complicated because varying the substrate concentration alters the optical properties of the solution and the light penetration in the reaction mixture (Brugger et al., 1998). As a consequence, reducing the substrate concentration will increase the number of photons that interact with lignin, which in turn can increase the H_2O_2 generation. On the other hand, if the substrate concentration is increased, this may limit the number of photons interacting with lignin and, in turn, decrease H_2O_2 generation. Substrate concentration was most likely not a rate-limiting factor in the present studies as linear progress curves leading toward the accumulation of up to 1 mM oxidized products were observed in other reactions. It was therefore unlikely that the substrate concentration was rate-limiting in reactions lasting for six hours, with a production of approximately 150 µM of oxidized products, as was the case in the experiment regarding the enzyme dosage.

To check if the substrate concentration was the limiting factor, a binding curve experiment could have been performed. A binding curve experiment would show the fractional saturation of enzymes bound to Avicel versus the added substrate concentration, thus, indicating if the substrate concentration is limiting in the reaction (or possibly even too high) (Pollard, 2010). Unbound LPMOs, can contribute to other reactions than oxidative cleavage of Avicel, i.e., produce H_2O_2 from O_2 (Bissaro et al., 2016b). As shown above, higher lignin concentrations and higher light intensity led to increasing LPMO activity, but also to non-linear progress curves, as a result of a high accumulation of H_2O_2 in the system. Considering that all reactions in the enzyme dosage experiment display linear progress curves, the H_2O_2 production from light-exposed lignin is believed to be slower than the consumption by *Sc*AA10C. Thus, H_2O_2 production is probably a rate-limiting factor in the reaction.

Another possibility is that *Sc*AA10C was provided with too little reducing power from lignin, i.e., the enzymes will not attain the Cu(I)-state. Both the addition of higher lignin concentration and the addition of priming amount of AscA have been elucidated in Section 5.1. Addition of priming amounts of AscA to the reactions did not lead to considerable differences in the production rate nor the total amount of accumulated products (**Figure 16**). The addition of higher lignin concentration (10 times higher) did lead to considerably higher production rates, but also inactivation after a few hours (**Figure 16**). Even though higher lignin concentration had a huge effect, is also led to inactivation because of such high H_2O_2 concentration, and since the addition of AscA has so little effect, reducing power is not believed to be a limiting factor in the reactions elucidating enzyme dosage, at least not with low LPMO concentrations. The addition of AscA or more lignin in reactions with higher concentrations of *Sc*AA10C would reveal if the reducing power were limiting at higher enzyme concentrations, but this seems unlikely.

Although further details need to be addressed, the enzyme-dosage experiment clearly shows that in the present set-up, at 0.9 g/L lignin, the reaction is completely limited by one of the reactants, which most likely is the generation of H_2O_2, that the LPMO uses as co-substrate.

5.4. The effect of ascorbic acid - faster formation of hydrogen peroxide?

AscA, typically at a concentration of 1 mM, has been used in many studies to reduce the LPMO and was initially thought to drive the LPMO reaction by supplying electrons to the copper ion in an O_2 driven (monooxygenase) reaction. Recent data indicate that the primary effect of AscA may lie in its ability to promote the generation of H_2O_2 (Bissaro et al., 2017) and it has recently been shown that the addition of a reductant (e.g., AscA) accelerates the conversion of $O_2^{\bullet-}$ to H_2O_2 (Bissaro et al., 2020). The reactions with low concentrations of AscA progress linearly, while the reactions with high concentrations of AscA (2000 µM) shows higher product rates, but less product formation over time (**Figure 21**). The reaction with the highest AscA concentration was supposedly inactivated already after one hour, probably as a result of oxidative damage to the catalytic site because of the presence of a high concentration of H_2O_2.

The near absent effect of priming amounts of AscA on the LPMO reactions (**Figure 16**) prompted an investigation into the effects of a reductant in these reactions. It is important to note that in Section 5.1, AscA was added to the reactions prior to the 15 min incubation step, while in this Section, AscA was added to start the reactions immediately before turning on the light (**Figure 21**). The reactions with AscA added prior to the incubation showed a slightly lower rate than the reactions with AscA

added at reaction start. The difference in accumulated end product levels between the reaction without or with 20 µM AscA was negligible when AscA was added prior to reaction start (**Figure 16**), but display a slightly bigger difference when AscA was added at reaction start (**Figure 21**). This is most likely as a result of that not all enzymes attained the reduced state (or that they had been reduced and re-oxidized) when AscA was added prior to the incubation because AscA can contribute to various reactions.

To elucidate the effect of AscA in these photobiocatalytic reactions with lignin is not straight forward since AscA can react in multiple reactions. As mentioned above, the addition of AscA is believed to reduce the LPMO and speed up the conversion of $O_2^{\bullet-}$ to H_2O_2. AscA can react with free copper in the solution in Fenton chemistry, producing hydroxyl radicals from hydrogen peroxide, which can lead to unspecific oxidization of various compounds, but AscA can also react with O_2 producing H_2O_2 (Bissaro et al., 2020). Lignin is believed to function as a photosensitizer that will be oxidized by light exposure and reduce O_2 to $O_2^{\bullet-}$. There is also a possibility that AscA function as a sacrificial electron donor that will reduce oxidized lignin, so that it can be reused and provide electrons multiple times. Even though the results clearly show that the addition of a considerable amount of AscA strongly influences the LPMO activity, further elucidating to decide how AscA influences the reaction is needed.

These results show that even though lignin itself can reduce and provide *Sc*AA10C with H_2O_2, the reaction is indeed accelerated by the presence of AscA, possibly because it speeds up the conversion of $O_2^{\bullet-}$ to H_2O_2. Further, the results show the amount of AscA needs to be carefully adapted as high concentrations lead to rapid enzyme inactivation.

5.5. Probing the role of superoxide with superoxide dismutase

Previous studies have investigated the effect of SOD and catalase on light-driven LPMO reactions to determine the role of various reactive oxygen species in photobiocatalytic reactions. The production of both $O_2^{\bullet-}$ and H_2O_2 was determined in the studies, but the authors couldn't conclude whether or not it was important for the mechanism (Bissaro et al., 2020; Cannella et al., 2016; Möllers et al., 2017). To determine the role of superoxide in reactions with light-exposed lignin, increasing amounts of superoxide dismutase were added to the reactions. Superoxide dismutase converts $O_2^{\bullet-}$ to H_2O_2, and if $O_2^{\bullet-}$ is generated in the system, then the addition of SOD would lead to more accumulated H_2O_2 and speed up the oxidation of Avicel. The results show that LPMO activity was boosted by the addition of SOD both in terms of initial production rates and accumulated end-product levels after six hours of incubation (**Figure 22**).

This finding indicates that $O_2^{\bullet-}$ is indeed generated and confirms the hypothesis by Miglbauer et al. (2020) that hydrogen peroxide formation by light-exposed lignosulfonate can proceed via single-electron reduction of oxygen to superoxide. The amount of accumulated products in reactions with up to 100 nM SOD did not show a significant increase in LPMO activity compared to the reaction without SOD, but by increasing the amount of SOD further, it was clearly demonstrated that an accelerated conversion of $O_2^{\bullet-}$ into H_2O_2 results in faster LPMO kinetics. These results suggest that as a result of lignin's ability to convert $O_2^{\bullet-}$ to H_2O_2, the SOD concentration must be sufficiently high to make a significant difference in the total amount of H_2O_2 that is generated in the system to accelerate the LPMO reaction.

The amount of $O_2^{\bullet-}$ generated in the system is believed to be rate-limiting. In their recent study, Bissaro et al. reported LPMO inactivation in reactions with lower SOD concentrations than those used in this study, but their reactions were carried out at higher light intensities. Increasing the light intensity leads to an increase in LPMO activity (**Figures 18 & 19**) (Bissaro et al., 2020) due to more superoxide being generated. In turn, this results in more $O_2^{\bullet-}$ available for conversion to H_2O_2 by SOD. The combination of higher light intensity, longer reaction time, and another type of photosensitizer can explain why LPMO inactivation was not observed in reactions with SOD in this study.

Further experiments should elucidate the effect of SOD in reactions with more $O_2^{\bullet-}$ present, produced by either more lignin, AscA, or higher light intensity. The impact of other types of SOD should also be elucidated because free Mn(II) in the solution has been shown to influence the LPMO activity (see below). Thus, the effect shown in the reactions with Mn-SOD was possibly influenced by the presence of any free Mn(II) from the Mn-SOD enzyme solution.

Overall, this study demonstrates that superoxide is an important intermediate for the production of H_2O_2 and point to H_2O_2 as the limiting factor for LPMO activity in this photobiocatalytic system.

5.6. Manganese and copper's effect on LPMO activity

The superoxide dismutase used in this study was manganese dependent (Mn-SOD), which means that by adding this enzyme, one also adds a transition metal. To look at the effect of Mn(II) on LPMO reactions, experiments with increasing concentrations of $Mn(II)SO_4$ were carried out. Surprisingly, the results show that addition of free manganese (all concentrations) resulted in increased production rates and a higher amount of accumulated end-product levels compared to the reaction without added Mn(II) (**Figure 23, A**). The highest LPMO activity was observed for the lowest concentration of Mn(II),

but since these experiments were carried out as single experiments, the emphasis is placed on the general observation that Mn(II) increases LPMO activity for all Mn(II) concentrations applied (**Figure 23, A**).

The presence of Mn(II) has previously been shown to have a significant effect in some Bacteria, i.e., *Lactobacillus plantarum. Lactobacillus plantarum* does not contain genes coding for SOD, but it is produced high levels of Mn(II), believably functioning as a SOD analog in complex with pyrophosphate, enzymatically converting $O_2^{\bullet-}$ to H_2O_2 (Archibald, 1986). Since the addition of Mn(II) to this photobiocatalytic system led to such high production rates and accumulated end product levels, Mn(II) seemingly did function as a SOD analog, converting $O_2^{\bullet-}$ into H_2O_2. Mn(II) has also been shown to have a high reactivity as a SOD analog in complex with K_2HPO_4 (Archibald, 1986). Since the present reactions were conducted in sodium phosphate buffer, it seems likely that Mn(II) formed complexes with phosphate, and that the increase in LPMO activity was a result of a so-called buffer effect. Given that Mn(II) did function as a SOD analog, it is believed that Mn(II) reacted with superoxide and produced hydrogen peroxide and oxidized itself to Mn(III). Further, it is also believed that Mn(III) possibly reduced itself back to Mn(II), at the same time as it converted some of the produced hydrogen peroxide to oxygen (Archibald, 1986). Thus, to some extent, the use of Mn(II) prevents high levels of H_2O_2 in the system and lower the probability of *Sc*AA10C inactivation. Another possibility is that lignin chelates manganese ions to form complexes, which has been shown to speed up the effectiveness of catalytical systems and redox reactions (Barbieri et al., 2019; Merdy et al., 2002). How the addition of manganese speeds up the LPMO activity is not known and needs further elucidating.

It was assumed that the presence of Mn(II) would not influence the reactions, and reactions supplemented with Mn(II) were performed in a single replicate with high Mn(II) concentrations relative to SOD. Another set of experiments should be carried out with lower Mn(II) levels, and they should at least include concentrations at the same concentration as the highest SOD values. Whether Mn(II) directly influenced the reaction or if the activity depended on the complex formation with phosphate or with lignin should be studied. This could be studied in light-exposed LPMO reactions in the presence and absence of lignin and by changing the buffer to decide whether it is a buffer effect or not. Even though these results are based on a single experiment, the results strongly indicate that the addition of free manganese to the reaction indeed does influence *Sc*AA10C catalytic activity on Avicel, possibly by function as a SOD analog, enzymatically converting $O_2^{\bullet-}$ into H_2O_2.

The catalytic activity of LPMOs depends on the coordination of a copper atom in the active site (Quinlan et al., 2011), and this is achieved by a copper saturation step prior to performing reactions. Adding AscA to a solution containing free copper leads to production of H_2O_2, and at micromolar

copper concentrations, the amount of H_2O_2 produced can inactivate the LPMO (Bissaro et al., 2020). Combined with knowledge from ICP-MS analysis that Birch-wood lignin contained 5-fold more copper than Kraft lignin from Sigma, reactions with addition of Cu(II)SO_4 were performed. The results show that the addition of Cu(II) up to 200 µM did not influence the LPMO activity (**Figure 23, B**). The absence of an effect of Cu(II) on LPMO activity indicates that the presence of Cu(II) does not increase H_2O_2-production, as is observed for Mn(II), and that the effect of transitions metals on H_2O_2-production depend on the type of transition metal.

5.7. The origin and pretreatment of lignin influences LPMO activity

The origin and pretreatment of lignin samples influence lignin's effect in light-exposed LPMO reactions. Lignin's composition affects how effectively they produce $O_2^{\bullet-}$ (Muraleedharan et al., 2018), but as have been discussed in Section 5.1, the amount of lignin present in the reaction do also strongly affect the LPMO activity. Light-exposed reactions with Kraft lignin from Sigma-Aldrich with sulfonate groups or wood samples from either Birch or Spruce treated by steam-explosion (**Figure 24**), were carried out. Also, the difference between lignin samples from Spruce-wood treated by SE at 210°C or 220°C with or without prior 2-naphthol treatment at each temperature was determined (**Figure B1, Appendix B**).

Comparing the ability of lignin of different origin to act as photosensitizers to promote LPMO activity shows that lignin from Spruce-wood led to the highest LPMO activity (**Figure 24**). The lignin from spruce wood that resulted in the highest LPMO activity had been pretreated by steam-explosion at 220°C with prior impregnation with 2-NAP. Lignin's ability to donate electrons to the LPMO is determined by the structure (Muraleedharan et al., 2018). Lignin from Spruce-wood does often contain more -OH groups than Birch-wood, which has been shown to have a positive effect on lignin's donation of electrons toward LPMOs (Muraleedharan et al., 2018). Besides structural variations, it can also be differences in molecular weight between the lignin samples, but also differences in lignin content as a result of pretreatment. In these reactions, 0.9 g/L lignin from the various sources was added. Since the structure and the lignin content of the wood samples have not been elucidated, it is not possible to decide if the LPMO activity depended on structural differences between the lignin samples, or purley on the amount of added lignin to the reactions due to variable lignin content in the samples .

Importantly, all Spruce lignin samples pretreatment with 2-NAP shows an increased LPMO activity (**Figure B1, Appendix B**). The effect of 2-NAP should have been tested to decide whether the presence of 2-NAP itself in the reaction solution, or the structural modifications of lignin as a result of the impregnation with 2-NAP contributed to the increased LPMO activity. Previous studies have shown

that 2-NAP is photodegraded in solution when exposed to light (Weng et al., 2013), and depending on the degradation products, this could influence LPMO activity. Experiments with different concentrations of 2-NAP should be performed to determine if 2-NAP exposed to visible can promote or inhibit LPMO activity.

Further, the structure of lignin should also be studied. The composition of the various lignin units, reactive groups, and the lignin content in the samples should be elucidated to get a better understanding of their reactivity toward *Sc*AA10C, but also to ensure the addition of an equal amount of lignin to all reactions. This can be done by, e.g., NMR or pyrolysis GC-MS, to quantify and structurally characterize lignin, as described by Van Erven et al. (2019). It has been conducted to little experiment to conclude whether the origin and the pretreatment of the lignin source affect the LPMO reactions, but the results strongly suggest that the pretreatment of lignin affect lignin's reactivity toward LPMOs.

6. Conclusions and future perspectives

The focus of this study was to investigate how light-exposed lignin influences the ability of *Sc*AA10C to depolymerize Avicel. This was based on previous studies which have shown that LPMOs can be provided with reducing equivalents and co-substrate, H_2O_2, by combining light and a photosensitizer (Bissaro et al., 2016a; Bissaro et al., 2020; Cannella et al., 2016; Möllers et al., 2017). This study aimed to investigate light-driven *Sc*AA10C reactions using lignin as a photosensitizer and study how different parameters such as lignin concentration, light intensity, enzyme concentration, and the presence of a reductant, affected the catalytic action of *Sc*AA10C towards Avicel. Another important aspect of the study was to probe the role of the superoxide anion in the reaction mechanism.

The results show that lignin can fuel *Sc*AA10C activity towards Avicel at concentrations in the 1-10 g/L range, both in the presence and absence of visible light. In these conditions, priming with AscA had little effect, while the addition of high concentrations of AscA and increasing lignin concentration led to increased activity. Confirming that lignin can provide *Sc*AA10C with reducing equivalence. Light exposure had a dramatic positive effect on the ability of lignin to drive the LPMO reactions, but at higher lignin concentrations, the application of light led to rapid cessation of product formation. The cessation of product formation is likely due to enzyme inactivation caused by excessive production of hydrogen peroxide. From these observations, it is clear that light- and lignin-driven LPMO catalysis can be highly effective, but that reaction conditions need to be carefully balanced to obtain optimal reactions.

Perhaps one of the most intriguing aspects of this study is the observation that varying the concentration of *Sc*AA10C between 0.1 to 10 µM did not have any effect on the catalytic rate, which indicates that the amount of enzyme was not limiting in this system. This shows that the reaction is totally controlled by one of the reactants and most likely by the generation of H_2O_2. The experiments with SOD and free manganese confirmed that the formation of superoxide and the resulting formation of hydrogen peroxide plays a major role in these systems. The addition of free Cu(II) did not affect the reactions, in contrast to the addition of Mn(II), showing that the effect of transitions metals on H_2O_2-production depends on the type of transition metal. Initial attempts to study the effects of various lignin types showed that the source and pretreatment of the lignin had a considerable impact on the outcome of the reaction. Still, since the lignin content in the samples is unknown, it can't be concluded whether or not the origin and pretreatments affect lignin role as a photosensitizer in a photobiocatalytic system with LPMOs.

As discussed above, future work is needed to determine the limiting factors in this photobiocatalytic system, and what factors eventually lead to termination of product formation. As mentioned previously, possible additional experiments include reactions with different substrate concentrations, with other (further reduced) enzyme concentrations, checking for *Sc*AA10C inactivation, and investigating if the reducing power provided by lignin is depleted under certain conditions. Furthermore, to determine if the observed boost in LPMO activity was due to the formation of a complex between Mn(II) and phosphate or lignin, reactions in the presence or absence of lignin should be done. The H_2O_2 concentration should be monitored, structural differences between lignin materials and structural modification of lignin due to light-exposure should be investigated. Also, perform anaerobic controls to determine if this is purely an aerobic phenomenon. An anaerobic control reaction would reveal if the direct reduction of LPMO from lignin was possible, or if it depended on the presence of oxygen in the solution. If lignin under anaerobic conditions could both reduce the LPMO and produce H_2O_2, this would suggest that light-exposed lignin could oxidize water.

All these results lead up to a possible mechanism where lignin functions as a photosensitizer that will be oxidized by light exposure and reduce O_2 to $O_2^{\bullet-}$ under aerobic conditions. The presence of superoxide will ensure priming reduction of *Sc*AA10C, while most $O_2^{\bullet-}$ is converted into H_2O_2 spontaneously, or chemically, by redox compounds in lignin, addition of AscA, Mn(II), or SOD. Hence, *Sc*AA10C will attain its reduced Cu(I)-state and be provided with H_2O_2, meaning that *Sc*AA10C can perform oxidative cleavage of Avicel in photobiocatalytic reactions with lignin. It is worth noting that the result of this study shows that it may be of relevance, whether saccharification of cellulose happens in the dark or when it is exposed to visible light. The biomass, e.g., lignocellulosic biomass, utilized in industrial biorefineries, often consist of both cellulose and lignin, and this study shows that light-exposed lignin strongly enhances LPMOs degradation of cellulose. This suggests that the saccharification of lignocellulose exposed to visible light and controlled levels of H_2O_2 would lead to a more efficient production of energy and biofuel.

7. References

Aachmann, F. L., Sørlie, M., Skjåk-Bræk, G., Eijsink, V. G. & Vaaje-Kolstad, G. (2012). NMR structure of a lytic polysaccharide monooxygenase provides insight into copper binding, protein dynamics, and substrate interactions. *Proceedings of the National Academy of Sciences*, 109 (46): 18779-18784.

Agger, J., Viksø-Nielsen, A. & Meyer, A. S. (2010). Enzymatic xylose release from pretreated corn bran arabinoxylan: differential effects of deacetylation and deferuloylation on insoluble and soluble substrate fractions. *Journal of Agricultural and food Chemistry*, 58 (10): 6141-6148.

Archibald, F. (1986). Manganese: its acquisition by and function in the lactic acid bacteria. *CRC Critical reviews in microbiology*, 13 (1): 63-109.

Bar-On, Y. M., Phillips, R. & Milo, R. (2018). The biomass distribution on Earth. *Proceedings of the National Academy of Sciences*, 115 (25): 6506-6511.

Barbieri, A., Kasper, J. B., Mecozzi, F., Lanzalunga, O. & Browne, W. R. (2019). Origins of Catalyst Inhibition in the Manganese-Catalysed Oxidation of Lignin Model Compounds with H_2O_2. *ChemSusChem*, 12 (13): 3126-3133.

Beeson, W. T., Vu, V. V., Span, E. A., Phillips, C. M. & Marletta, M. A. (2015). Cellulose degradation by polysaccharide monooxygenases. *Annual review of biochemistry*, 84: 923-946.

Berlemont, R. & Martiny, A. C. (2016). Glycoside hydrolases across environmental microbial communities. *PLoS computational biology*, 12 (12): e1005300.

Bissaro, B., Forsberg, Z., Ni, Y., Hollmann, F., Vaaje-Kolstad, G. & Eijsink, V. G. (2016a). Fueling biomass-degrading oxidative enzymes by light-driven water oxidation. *Green Chemistry*, 18 (19): 5357-5366.

Bissaro, B., Røhr, Å. K., Skaugen, M., Forsberg, Z., Horn, S. J., Vaaje-Kolstad, G. & Eijsink, V. G. H. (2016b). Fenton-type chemistry by a copper enzyme: molecular mechanism of polysaccharide oxidative cleavage. *BioRxiv*: 097022. doi: 10.1101/097022.

Bissaro, B., Røhr, Å. K., Müller, G., Chylenski, P., Skaugen, M., Forsberg, Z., Horn, S. J., Vaaje-Kolstad, G. & Eijsink, V. G. (2017). Oxidative cleavage of polysaccharides by monocopper enzymes depends on H_2O_2. *Nature chemical biology*, 13 (10): 1123.

Bissaro, B., Varnai, A., Røhr, Å. K. & Eijsink, V. G. (2018). Oxidoreductases and reactive oxygen species in conversion of lignocellulosic biomass. *Microbiol. Mol. Biol. Rev.*, 82 (4): e00029-18.

Bissaro, B., Kommedal, E., Røhr, Å. K. & Eijsink, V. G. (2020). Controlled depolymerization of cellulose by light-driven lytic polysaccharide oxygenases. *Nature Communications*, 11 (1): 1-12.

Brugger, A., Slezak, D., Obernosterer, I. & Herndl, G. J. (1998). Photolysis of dimethylsulfide in the northern Adriatic Sea: Dependence on substrate concentration, irradiance and DOC concentration. *Marine Chemistry*, 59 (3-4): 321-331.

Cannella, D., Möllers, K. B., Frigaard, N.-U., Jensen, P. E., Bjerrum, M. J., Johansen, K. S. & Felby, C. (2016). Light-driven oxidation of polysaccharides by photosynthetic pigments and a metalloenzyme. *Nature communications*, 7 (1): 1-8.

Cantarel, B. L., Coutinho, P. M., Rancurel, C., Bernard, T., Lombard, V. & Henrissat, B. (2009). The Carbohydrate-Active EnZymes database (CAZy): an expert resource for glycogenomics. *Nucleic acids research*, 37 (suppl_1): D233-D238.

Cesarino, I., Araújo, P., Domingues Júnior, A. P. & Mazzafera, P. (2012). An overview of lignin metabolism and its effect on biomass recalcitrance. *Brazilian Journal of Botany*, 35 (4): 303-311.

Chundawat, S. P., Beckham, G. T., Himmel, M. E. & Dale, B. E. (2011). Deconstruction of lignocellulosic biomass to fuels and chemicals. *Annual review of chemical and biomolecular engineering*, 2: 121-145.

Chylenski, P., Bissaro, B., Sørlie, M., Røhr, Å. K., Várnai, A., Horn, S. J. & Eijsink, V. G. H. (2019). Lytic Polysaccharide Monooxygenases in Enzymatic Processing of Lignocellulosic Biomass. *ACS Catalysis*, 9 (6): 4970-4991. doi: 10.1021/acscatal.9b00246.

Costa, T. H., Eijsink, V. G. & Horn, S. J. (2019). The use of lytic polysaccharide monooxygenases in anaerobic digestion of lignocellulosic materials. *Biotechnology for Biofuels*, 12 (1): 270.

Cragg, S. M., Beckham, G. T., Bruce, N. C., Bugg, T. D., Distel, D. L., Dupree, P., Etxabe, A. G., Goodell, B. S., Jellison, J. & McGeehan, J. E. (2015). Lignocellulose degradation mechanisms across the Tree of Life. *Current Opinion in Chemical Biology*, 29: 108-119.

Eggert, C., Temp, U. & Eriksson, K.-E. (1996). The ligninolytic system of the white rot fungus Pycnoporus cinnabarinus: purification and characterization of the laccase. *Appl. Environ. Microbiol.*, 62 (4): 1151-1158.

Fatma, S., Hameed, A., Noman, M., Ahmed, T., Shahid, M., Tariq, M., Sohail, I. & Tabassum, R. (2018). Lignocellulosic biomass: a sustainable bioenergy source for the future. *Protein and peptide letters*, 25 (2): 148-163.

Forsberg, Z., Vaaje-Kolstad, G., Westereng, B., Bunæs, A. C., Stenstrøm, Y., MacKenzie, A., Sørlie, M., Horn, S. J. & Eijsink, V. G. (2011). Cleavage of cellulose by a CBM33 protein. *Protein Science*, 20 (9): 1479-1483.

Forsberg, Z., Mackenzie, A. K., Sørlie, M., Røhr, Å. K., Helland, R., Arvai, A. S., Vaaje-Kolstad, G. & Eijsink, V. G. (2014). Structural and functional characterization of a conserved pair of bacterial cellulose-oxidizing lytic polysaccharide monooxygenases. *Proceedings of the National Academy of Sciences*, 111 (23): 8446-8451.

Fridovich, I. (1975). Superoxide dismutases. *Annual review of biochemistry*, 44 (1): 147-159.

Harris, P. V., Welner, D., McFarland, K., Re, E., Navarro Poulsen, J.-C., Brown, K., Salbo, R., Ding, H., Vlasenko, E. & Merino, S. (2010). Stimulation of lignocellulosic biomass hydrolysis by proteins of glycoside hydrolase family 61: structure and function of a large, enigmatic family. *Biochemistry*, 49 (15): 3305-3316.

Henrissat, B., Coutinho, P. M., Lombard, V., Drula, E., Garron, M.-L., Terrapon, N., Labourel, A. & Albani, A. (2013). Auxiliary Activities family classification. In *The Carbohydrate-active enzymes database (CAZy)*. Available at: http://www.cazy.org/ (accessed: 22.05.2020).

Horn, S. J., Vaaje-Kolstad, G., Westereng, B. & Eijsink, V. (2012). Novel enzymes for the degradation of cellulose. *Biotechnology for biofuels*, 5 (1): 45.

Imai, T. & Sugiyama, J. (1998). Nanodomains of Iα and Iβ cellulose in algal microfibrils. *Macromolecules*, 31 (18): 6275-6279.

Isikgor, F. H. & Becer, C. R. (2015). Lignocellulosic biomass: a sustainable platform for the production of bio-based chemicals and polymers. *Polymer Chemistry*, 6 (25): 4497-4559.

Kont, R., Pihlajaniemi, V., Borisova, A. S., Aro, N., Marjamaa, K., Loogen, J., Büchs, J., Eijsink, V. G., Kruus, K. & Väljamäe, P. (2019). The liquid fraction from hydrothermal pretreatment of wheat straw provides lytic polysaccharide monooxygenases with both electrons and H_2O_2 co-substrate. *Biotechnology for biofuels*, 12 (1): 235.

Kracher, D., Scheiblbrandner, S., Felice, A. K., Breslmayr, E., Preims, M., Ludwicka, K., Haltrich, D., Eijsink, V. G. & Ludwig, R. (2016). Extracellular electron transfer systems fuel cellulose oxidative degradation. *Science*, 352 (6289): 1098-1101.

Lee, H., Hamid, S. & Zain, S. (2014). Conversion of lignocellulosic biomass to nanocellulose: structure and chemical process. *The Scientific World Journal*, 2014.

Lee, S. H., Choi, D. S., Kuk, S. K. & Park, C. B. (2018). Photobiocatalysis: Activating redox enzymes by direct or indirect transfer of photoinduced electrons. *Angewandte Chemie International Edition*, 57 (27): 7958-7985.

Levasseur, A., Drula, E., Lombard, V., Coutinho, P. M. & Henrissat, B. (2013). Expansion of the enzymatic repertoire of the CAZy database to integrate auxiliary redox enzymes. *Biotechnology for biofuels*, 6 (1): 41.

Lombard, V., Golaconda Ramulu, H., Drula, E., Coutinho, P. M. & Henrissat, B. (2014). The carbohydrate-active enzymes database (CAZy) in 2013. *Nucleic acids research*, 42 (D1): D490-D495.

Loose, J. S., Arntzen, M. Ø., Bissaro, B., Ludwig, R., Eijsink, V. G. & Vaaje-Kolstad, G. (2018). Multipoint precision binding of substrate protects lytic polysaccharide monooxygenases from self-destructive off-pathway processes. *Biochemistry*, 57 (28): 4114-4124.

Lu, Y., Lu, Y.-C., Hu, H.-Q., Xie, F.-J., Wei, X.-Y. & Fan, X. (2017). Structural characterization of lignin and its degradation products with spectroscopic methods. *Journal of Spectroscopy*, 2017.

Maciá-Agulló, J. A., Corma, A. & Garcia, H. (2015). Photobiocatalysis: the power of combining photocatalysis and enzymes. *Chemistry–A European Journal*, 21 (31): 10940-10959.

Mate, D. M. & Alcalde, M. (2017). Laccase: a multi-purpose biocatalyst at the forefront of biotechnology. *Microbial biotechnology*, 10 (6): 1457-1467.

Merdy, P., Guillon, E. & Aplincourt, M. (2002). Iron and manganese surface complex formation with extracted lignin. Part 1: Adsorption isotherm experiments and EPR spectroscopy analysis. *New Journal of Chemistry*, 26 (11): 1638-1645.

Michelin, C. m. & Hoffmann, N. (2018). Photosensitization and Photocatalysis—Perspectives in Organic Synthesis. *ACS Catalysis*, 8 (12): 12046-12055.

Mifsud, M., Gargiulo, S., Iborra, S., Arends, I. W., Hollmann, F. & Corma, A. (2014). Photobiocatalytic chemistry of oxidoreductases using water as the electron donor. *Nature communications*, 5 (1): 1-6.

Miglbauer, E., Gryszel, M. & Głowacki, E. D. (2020). Photochemical evolution of hydrogen peroxide on lignins. *Green Chemistry*, 22 (3): 673-677.

Möllers, K., Mikkelsen, H., Simonsen, T., Cannella, D., Johansen, K., Bjerrum, M. J. & Felby, C. (2017). On the formation and role of reactive oxygen species in light-driven LPMO oxidation of phosphoric acid swollen cellulose. *Carbohydrate research*, 448: 182-186.

Mulat, D. G., Dibdiakova, J. & Horn, S. J. (2018). Microbial biogas production from hydrolysis lignin: insight into lignin structural changes. *Biotechnology for biofuels*, 11 (1): 61.

Müller, G., Chylenski, P., Bissaro, B., Eijsink, V. G. & Horn, S. J. (2018). The impact of hydrogen peroxide supply on LPMO activity and overall saccharification efficiency of a commercial cellulase cocktail. *Biotechnology for biofuels*, 11 (1): 209.

Muraleedharan, M. N., Zouraris, D., Karantonis, A., Topakas, E., Sandgren, M., Rova, U., Christakopoulos, P. & Karnaouri, A. (2018). Effect of lignin fractions isolated from different biomass sources on cellulose oxidation by fungal lytic polysaccharide monooxygenases. *Biotechnology for biofuels*, 11 (1): 1-15.

Nantapong, N., Murata, R., Trakulnaleamsai, S., Kataoka, N., Yakushi, T. & Matsushita, K. (2019). The effect of reactive oxygen species (ROS) and ROS-scavenging enzymes, superoxide dismutase and catalase, on the thermotolerant ability of Corynebacterium glutamicum. *Applied microbiology and biotechnology*, 103 (13): 5355-5366.

Neumann, M. G. & Machado, A. E. (1989). The role of oxygen in the photodegradation of lignin in solution. *Journal of Photochemistry and Photobiology B: Biology*, 3 (4): 473-481.

Paulsson, M. & Parkås, J. (2012). Light-induced yellowing of lignocellulosic pulps-mechanisms and preventive methods. *BioResources*, 7 (4): 5995-6040.

Pauly, M. & Keegstra, K. (2008). Cell-wall carbohydrates and their modification as a resource for biofuels. *The Plant Journal*, 54 (4): 559-568.

Peciulyte, A., Samuelsson, L., Olsson, L., McFarland, K., Frickmann, J., Østergård, L., Halvorsen, R., Scott, B. R. & Johansen, K. S. (2018). Redox processes acidify and decarboxylate steam-pretreated lignocellulosic biomass and are modulated by LPMO and catalase. *Biotechnology for biofuels*, 11 (1): 165.

Perna, V., Meyer, A. S., Holck, J., Eltis, L. D., Eijsink, V. G. & Wittrup Agger, J. (2019). Laccase-catalyzed oxidation of lignin induces production of H_2O_2. *ACS Sustainable Chemistry & Engineering*, 8 (2): 831-841.

Perry, J., Shin, D., Getzoff, E. & Tainer, J. (2010). The structural biochemistry of the superoxide dismutases. *Biochimica et Biophysica Acta (BBA)-Proteins and Proteomics*, 1804 (2): 245-262.

Phillips, C. M., Beeson IV, W. T., Cate, J. H. & Marletta, M. A. (2011). Cellobiose dehydrogenase and a copper-dependent polysaccharide monooxygenase potentiate cellulose degradation by Neurospora crassa. *ACS chemical biology*, 6 (12): 1399-1406.

Pollard, T. D. (2010). A guide to simple and informative binding assays. *Molecular biology of the cell*, 21 (23): 4061-4067.

Quinlan, R. J., Sweeney, M. D., Leggio, L. L., Otten, H., Poulsen, J.-C. N., Johansen, K. S., Krogh, K. B., Jørgensen, C. I., Tovborg, M. & Anthonsen, A. (2011). Insights into the oxidative degradation of cellulose by a copper metalloenzyme that exploits biomass components. *Proceedings of the National Academy of Sciences*, 108 (37): 15079-15084.

Ryan, K. C., Johnson, O. E., Cabelli, D. E., Brunold, T. C. & Maroney, M. J. (2010). Nickel superoxide dismutase: structural and functional roles of Cys2 and Cys6. *JBIC Journal of Biological Inorganic Chemistry*, 15 (5): 795-807.

Sameni, J., Jaffer, S. A., Tjong, J. & Sain, M. (2020). Advanced Applications for Lignin Micro-and Nano-based Materials. *Curr Forestry Rep*.

Scheller, H. V. & Ulvskov, P. (2010). Hemicelluloses. *Annual review of plant biology*, 61.

Schmermund, L., Jurkaš, V., Özgen, F. F., Barone, G. D., Büchsenschütz, H. C., Winkler, C. K., Schmidt, S., Kourist, R. & Kroutil, W. (2019). Photo-biocatalysis: Biotransformations in the presence of light. *ACS Catalysis*, 9 (5): 4115-4144.

Silveira, R. L., Stoyanov, S. R., Gusarov, S., Skaf, M. S. & Kovalenko, A. (2013). Plant biomass recalcitrance: effect of hemicellulose composition on nanoscale forces that control cell wall strength. *Journal of the American Chemical Society*, 135 (51): 19048-19051.

Terashima, N. & Fukushima, K. (1989). Biogenesis and structure of macromolecular lignin in the cell wall of tree xylem as studied by microautoradiography. In *Plant Cell Wall Polymers*: ACS Publications.

Vaaje-Kolstad, G., Horn, S. J., van Aalten, D. M., Synstad, B. & Eijsink, V. G. (2005). The non-catalytic chitin-binding protein CBP21 from Serratia marcescens is essential for chitin degradation. *Journal of Biological Chemistry*, 280 (31): 28492-28497.

Vaaje-Kolstad, G., Westereng, B., Horn, S. J., Liu, Z., Zhai, H., Sørlie, M. & Eijsink, V. G. (2010). An oxidative enzyme boosting the enzymatic conversion of recalcitrant polysaccharides. *Science*, 330 (6001): 219-222.

Vaaje-Kolstad, G., Forsberg, Z., Loose, J. S., Bissaro, B. & Eijsink, V. G. (2017). Structural diversity of lytic polysaccharide monooxygenases. *Current opinion in structural biology*, 44: 67-76.

van den Brink, J. & de Vries, R. P. (2011). Fungal enzyme sets for plant polysaccharide degradation. *Applied microbiology and biotechnology*, 91 (6): 1477.

Van Erven, G., De Visser, R., De Waard, P., Van Berkel, W. J. & Kabel, M. A. (2019). Uniformly 13C Labeled Lignin Internal Standards for Quantitative Pyrolysis− GC− MS Analysis of Grass and Wood. *ACS Sustainable Chemistry & Engineering*, 7 (24): 20070-20076.

Voshol, G. P., Vijgenboom, E. & Punt, P. J. (2017). The discovery of novel LPMO families with a new Hidden Markov model. *BMC research notes*, 10 (1): 105.

Weng, J.-K., Li, X., Bonawitz, N. D. & Chapple, C. (2008). Emerging strategies of lignin engineering and degradation for cellulosic biofuel production. *Current opinion in biotechnology*, 19 (2): 166-172.

Weng, S., Pei, Z., Zheng, Z., Hu, J. & Liu, P. (2013). Exciton-free, nonsensitized degradation of 2-naphthol by facet-dependent BiOCl under visible light: novel evidence of surface-state photocatalysis. *ACS applied materials & interfaces*, 5 (23): 12380-12386.

Westereng, B., Cannella, D., Agger, J. W., Jørgensen, H., Andersen, M. L., Eijsink, V. G. & Felby, C. (2015). Enzymatic cellulose oxidation is linked to lignin by long-range electron transfer. *Scientific reports*, 5 (1): 1-9.

8. Appendices

Appendix A

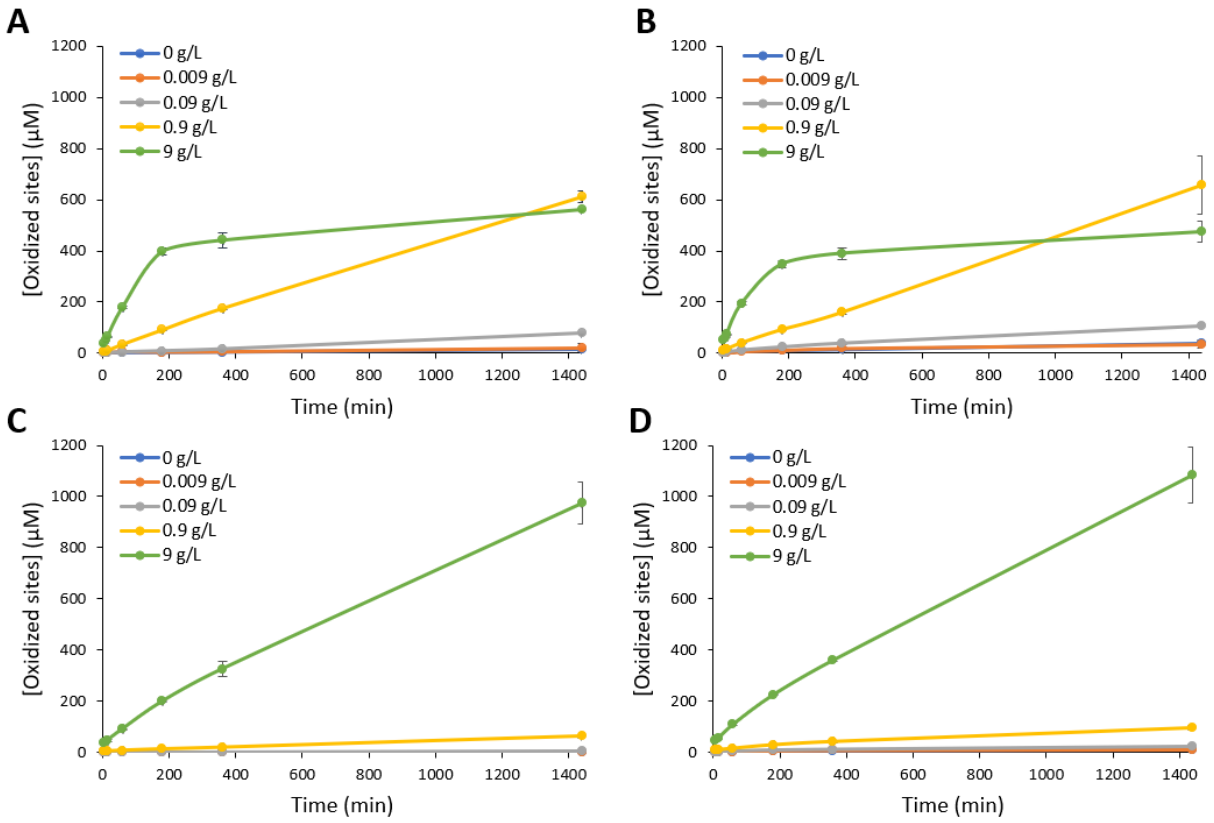

Figure A1. The impact of lignin on photobiocatalytic activity of *Sc*AA10C. The figure shows product formation for up to 24 h in reactions with *Sc*AA10C and Avicel that were exposed **(A, B)** or not exposed **(C, D)** to visible light (I = 10 % of I_{max}, approximately 16.8 W.cm^{-2}) and did **(B, D)** or did not **(A, C)** contain AscA (20 µM). The concentration of *Sc*AA10C was 0.5 µM in all reactions. Reactions were performed in 50 mM sodium phosphate buffer pH 7.0 with 10 g/L Avicel and various concentrations of Kraft lignin (0, 0.009, 0.09, 0.9, 9 g/L), at 40°C, for 24 h, with magnetic stirring. Soluble products, of varying degrees of polymerization were treated with endoglucanase, *Tf*Cel5A, to yield oxidized products with a degree of polymerization of 2 (GlcGlc1A) or 3 (Glc_2Glc1A), which were analyzed by HPAEC-PAD and quantified, to yield the total amount of solubilized oxidized sites. Reactions were performed in duplicates and the standard deviations are shown as error bars.

Appendix B

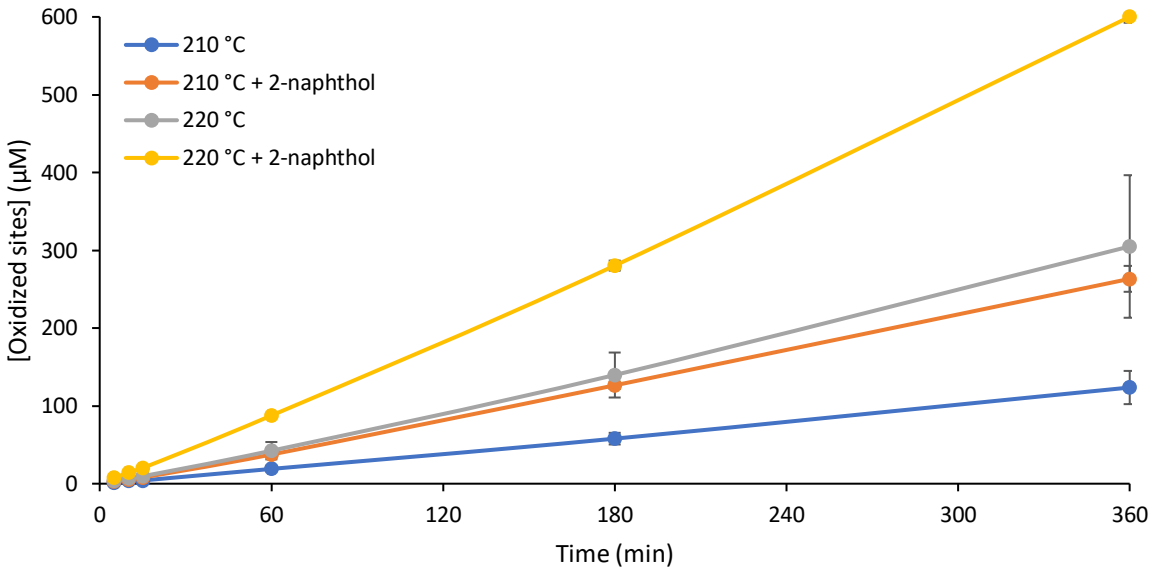

Figure B1. The influence of differently pretreated Spruce-wood lignin on *Sc*AA10C photobiocatalytic activity. The figure shows the influence of lignins from Spruce-wood subjected to various pretreatments on *Sc*AA10C catalytic activity on Avicel. All reactions contained 0.5 µM *Sc*AA10C, 0.9 g/L lignin from the different Spruce-wood lignin samples and were exposed to visible light (I = 10 g% I_{max}, approximately 16.8 $W.cm^{-2}$). The figure displays reactions conducted with lignin from Spruce-wood impregnated with **(orange, yellow)** or without **(blue, grey)** 2-naphthol, and steam-exploded at 210°C **(blue, orange)** or 220°C **(grey, yellow)**. Reactions were performed in 50 mM sodium phosphate buffer pH 7.0 with 10 g/L Avicel, at 40°C, for 6 h, with magnetic stirring. Soluble products, of varying degrees of polymerization were treated with endoglucanase, *Tf*Cel5A, to yield oxidized products with a degree of polymerization of 2 (GlcGlc1A) or 3 (Glc_2Glc1A), which were analyzed by HPAEC-PAD and quantified, to yield the total amount of solubilized oxidized sites. Reactions were performed in duplicates and the standard deviations are shown as error bars.

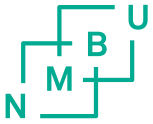

Norges miljø- og biovitenskapelige universitet
Noregs miljø- og biovitskapelege universitet
Norwegian University of Life Sciences

Postboks 5003
NO-1432 Ås
Norway